Memo

To
Kees Sloff

Date
27 December 2010

Number of pages
66

From
Sanjay Giri

Direct line
+31 (0)88 33 58 471

E-mail
sanjay.giri@deltares.nl

Subject
Study of Dordtsche Kil and Hollands Diep area using Delft3D

1 Introduction

The basic objective of this study is to extend the morphological model of the Merwede branches towards Dordtsche Kil and Hollands Diep, evaluate and improve the hydrodynamic performance of the model including tidal boundaries based on the SOBEK and WAQUA model results. Furthermore, a morphological analysis of Dordtsche Kil has been carried out based on available multi-beam soundings, sediment characteristics as well as geotechnical survey data of river bank and bed characteristics. Sediment transport analysis of the Hollands Diep and Dordtsche Kil area considering mud fraction has been done using Delft3D. Computation of long-term morphological behaviour of Dordtsche Kil has briefly been carried out as well. Model includes two sediment fractions and the mud. The new Van Rijn formula (TR2004/2007) has been used in its original form with default settings. Morphological computation has been carried out for the average upstream discharge condition as well as for a simplified schematization of discharge hydrograph.
Model shows satisfactory performance in terms of the hydrodynamics, particularly the complex tidal flow in Dordtsche Kil area seems to be predicted well by the model in comparison with SOBEK and WAQUA models. In regard to the morphological computation, with such a complex settings that we have used in this model (i.e. complex model area with multiple domains, tidal boundaries, non-uniform sediment with mud fraction, bed and suspended sediment transport, new Van Rijn formulation and so on), it seems to be difficult to conduct morphological calibration of the all branches. Some preliminary long-term morphological computations have been carried out, which give some preliminary impression of the morphological behaviour of the Dordtsche Kil. Nevertheless, the model should be improved to be used for the morphological analysis of the all branches. Moreover, it would be useful to conduct detailed data analysis of the sediment characteristics and morphological features of the whole region (this has already been done to some extent) before conducting detailed morphological calibration.

2 The model

Current Delft3D model of Rijnmaasmonding includes existing three domains of Merwedes branches and newly connected fourth and fifth domains deduced from an old Delf3D model (Kallen et al., 2008) and refined in Dordtsche Kil and Hollands Diep areas (Figure 1). The upstream part of the domains was connected with the Beneden- and Nieuwe-Merwede, and

the downstream was cut at Oude Mass in northern part and at Willemstad in southern part respectively.

The baseline projection was made for the fourth and fifth domains of the current model, which includes weirs and roughness definitions. The roughness definition file was made by using different source of information on roughness codes and parameters. The modified Zee-delta model used by Kallen et al. (2008) does not include the weirs and roughness definition (instead, a constant roughness for each river reach was used in this model).

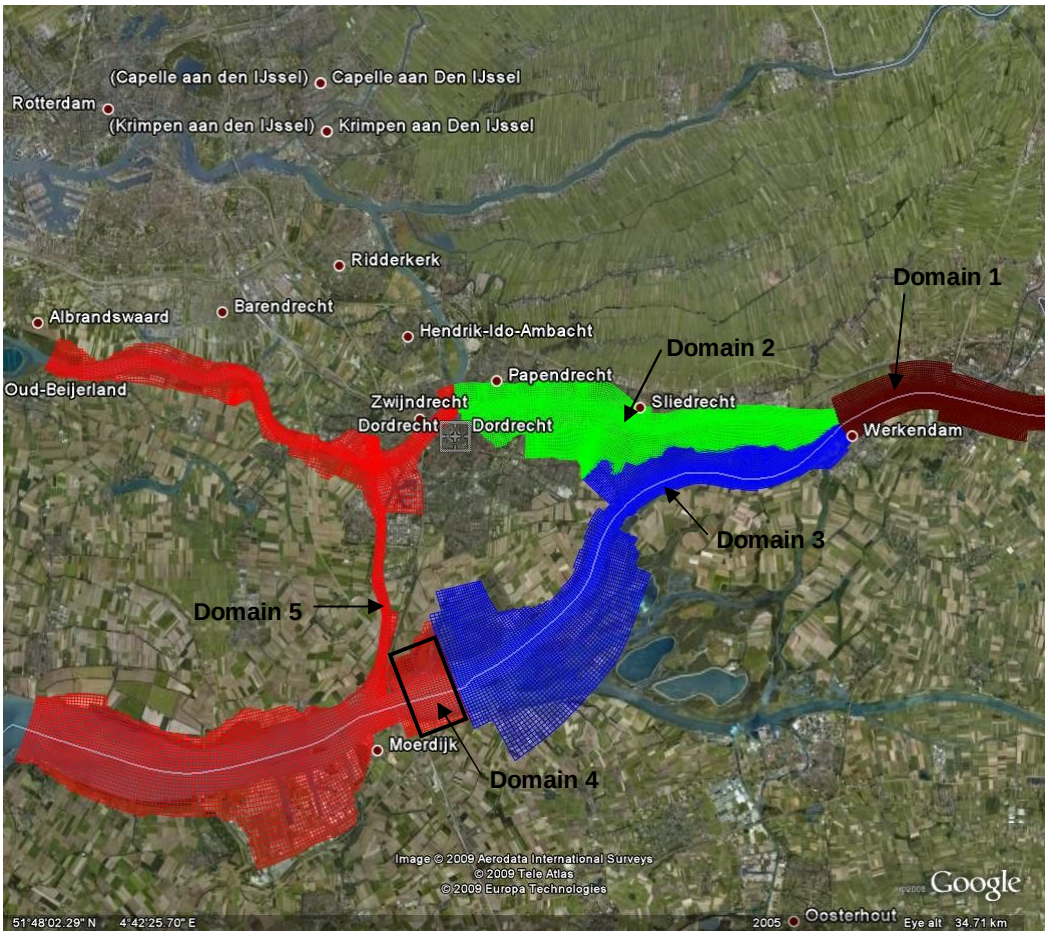

Figure 1 Computational domains

3 Hydrodynamic computation

3.1 Introduction

For the hydrodynamic simulation, first we did computations for low, medium and high flows with tidal boundary using SOBEK model. Then we use a new WAQUA Zee-Delta model and attempted to verify the performance of the Delft3D model with the WAQUA result for an observed situation.

The hydraulic simulation result of these models was used to deduce the boundary condition for the Delft3D model. In SOBEK and WAQUA models, three upstream discharge boundaries at Tiel, Lith and Hagestein respectively and the tidal boundaries at Haringvliets and Hoek Van Holland have been used. Whereas, a time-series discharge boundary at Boven-Merwede (upstream) was deduced from the full model and used as upstream boundary condition in the new model (however, an average discharge has been used for morphological simulation). Likewise, two downstream boundaries were used from the time-series water levels deduced from the full model at locations Oude Mass (KP 993) in the North part and between West Kopperland and Cromstrijn. Besides, since the branch of Noord River was not included in the new model, we attempted to evaluate the discharge insertion/extraction operation and also the time-series of water level boundary at this location, and finally selected the water level boundary as it appeared to be performing better. Also, the discharge coming from Amer River has been taken into account in the domain of Nieuwe Merwede as time-series of discharge insertion/extraction as shown in Figure 2 (this river was not incorporated in the model domain). The amount of inserted/extracted discharge was deduced from the SOBEK model.

Figure 2 Discharge insertion/extraction point near Amer - Nieuwe Merwede confluence

3.2 SOBEK modelling

3.2.1 Hydrodynamic simulation under varying flows (observed during 2003)

At first, we carried out different simulations using SOBEK model of Rijnmaasmonding. The simulations were carried out for an observed varying flow during 2003 (Figure 7) as an upstream boundary, and also observed water levels at Haringvliet and Hoek van Holland (boundary name - ‘Massmond’ in the model) as downstream boundary (Figure 8).
The model results were compared with some available observation data on water levels (discharge data does not seem to be available) as depicted in (Figure 9).

Based on SOBEK simulation result and observation, the boundary conditions for Delft3D simulations were deduced. Following time-series boundary conditions were extracted from the SOBEK model and observation:

(i) Upstream boundary at Boven Merwede: Observed discharge at Tiel.
(ii) Downstream boundary at North branch (in Oude Maas): Deduced from the SOBEK simulation result.
(iii) Downstream boundary at South branch (in Hollandse Diep): Deduced from the SOBEK simulation result.
(iv) Boundary at Noord River entrance: Three options were used, namely discharge boundary, water level boundary and discharge extraction/insertion. All data were deduced from the SOBEK simulation result.
(v) Discharge extraction/insertion from/into Nieuwe Merwede near the confluence with Amer River: Deduced from the SOBEK simulation result.

3.2.2 Hydrodynamic simulation under constant upstream discharge and tidal boundary conditions

SOBEK simulations were made for a range of constant upstream discharges (at Tiel, Lith and Hagestein). The range of constant discharge for each upstream boundary was deduced based on observed data during 1997-2009. For this purpose, all collected observed data of the Tiel were sorted and averaged for the ranges 900-1100 m^3/s, 1500-1700 m^3/s, 3800-4200 m^3/s and 4500-5500 m^3/s, from which the corresponding averaged discharges at Tiel 998 m^3/s, 1590 m^3/s, 3976 m^3/s and 4897 m^3/s respectively were obtained. The corresponding averaged discharges for Lith and Hagestein is shown in Table 1. Yet, the sorted discharges at all three upstream boundaries for each range are depicted in Figure 3 to *Figure 6*. The tidal downstream boundary condition was used (as used in original SOBEK model).

Table 1 Constant discharge boundary conditions for SOBEK model

Discharge boundary conditions	Q_Tiel (m^3/s)	Q_Lith (m^3/s)	Q_Hagestein (m^3/s)
1	998	119	11
2	1590	292	362
3	3976	1006	1055
4	4897	1194	1308

From the SOBEK simulation results for each discharge level, the boundary conditions for Delft3D model were deduced (upstream discharge at Boven Merwede as used in Tiel, north and south downstream boundaries, options for Noord River entrance and discharge extraction/insertion at Amer).

3.2.3 Comparison with Delft3D model

Delft3D computations were carried out for each discharge levels, and the results on tidal-averaged discharge at some key locations were compared with SOBEK results. First, Delft3D simulation results for the observed case during 2003 were compared with SOBEK results that are depicted in Figure 9 - Figure 12.
Furthermore, the comparison was made for the cases with constant upstream boundary with low, medium and high flows and tidal downstream boundaries. Figure 13 shows the discharge distribution (tide-averaged residual flows) at different branches. The magnitude and the direction of residual flow in Dordtsche Kil for different flow level appear to be reproduced by the model reasonably well comparing to the SOBEK result. Result shows also the comparison

between the cases for using different boundary conditions at Noord River, namely water level and discharge.
The discharge distribution between the Nieuwe and Beneden Merwedes shows some discrepancy with the SOBEK result. Delft3D shows the division of 55%-45% for all levels, whereas SOBEK shows mostly 60%-40%. This might explain the under-estimation of the discharge in Hollands Diep area by Delft3D comparing to the SOBEK.

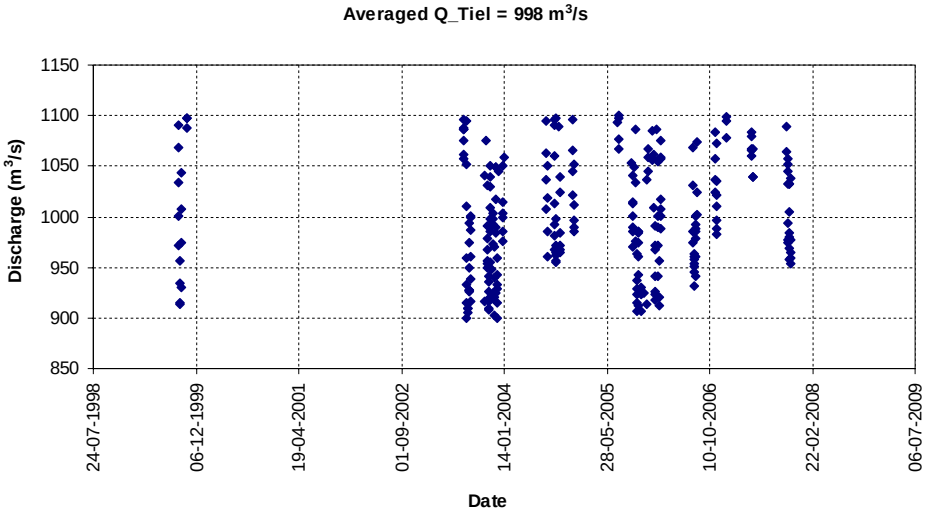

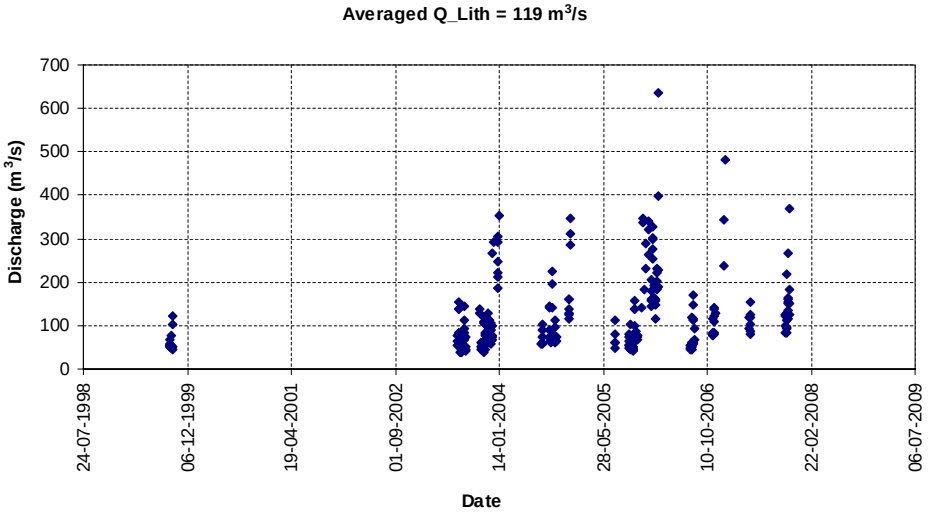

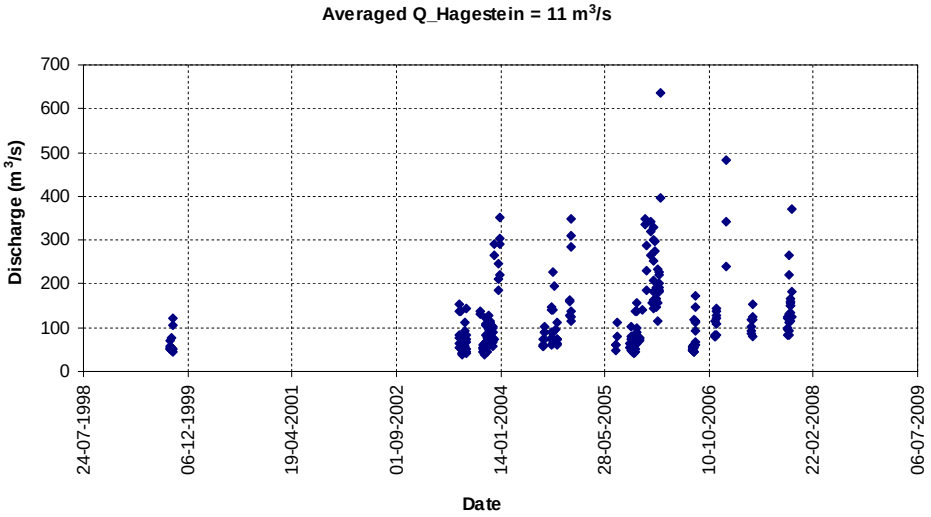

Figure 3 Observed discharge sorted for the range 900-1100 m^3/s

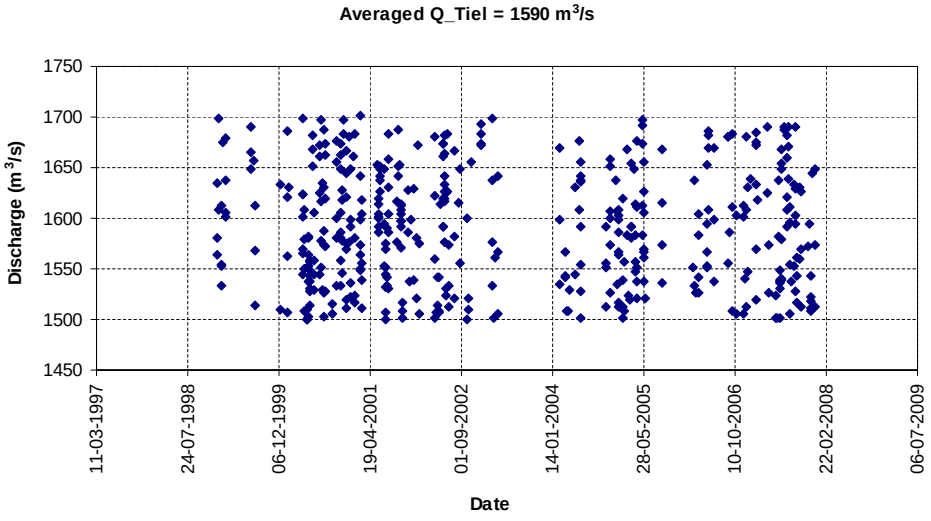

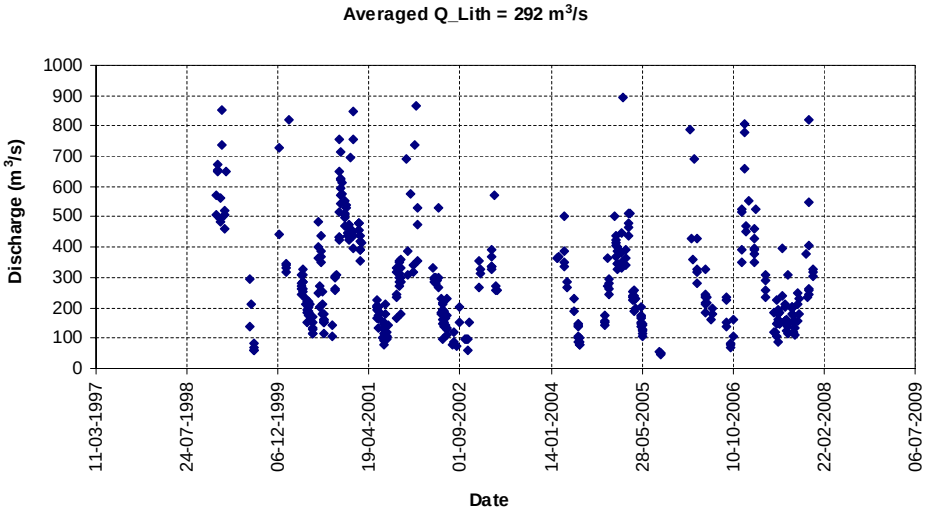

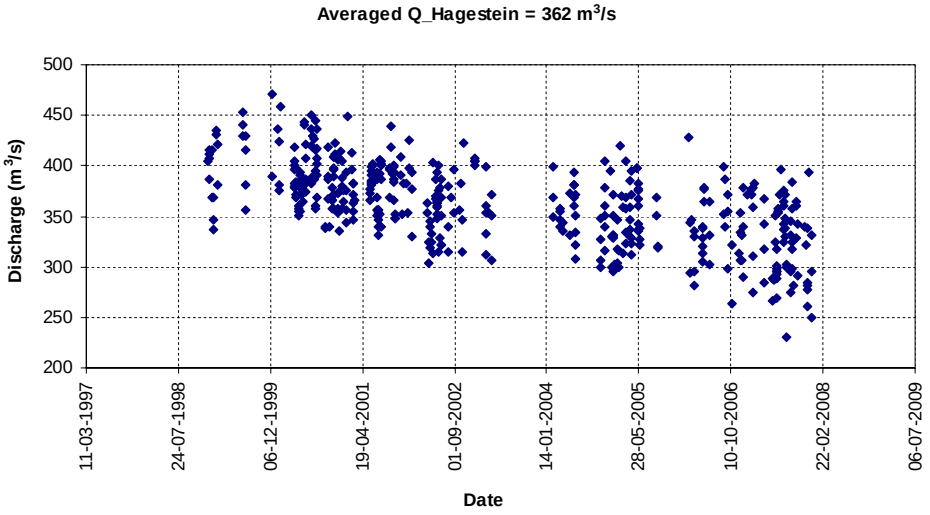

Figure 4 Observed discharge sorted for the range 1500-1700 m^3/s

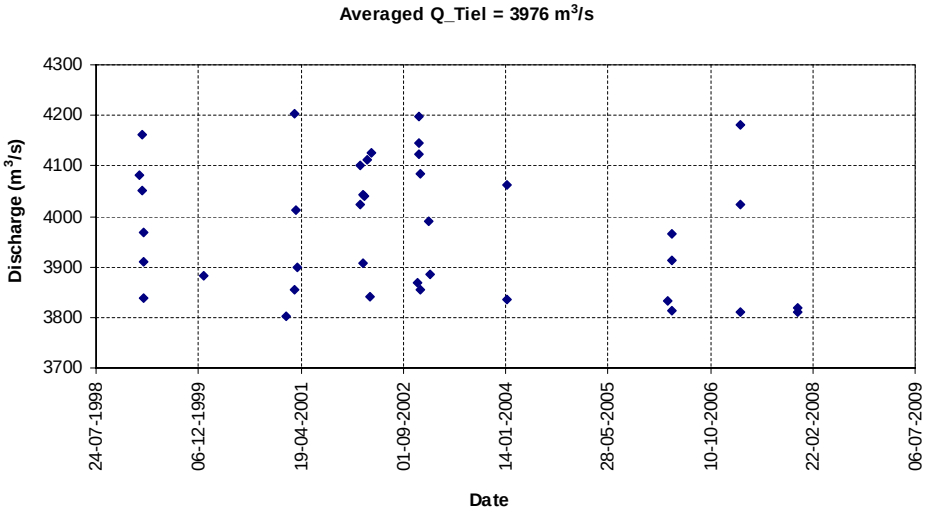

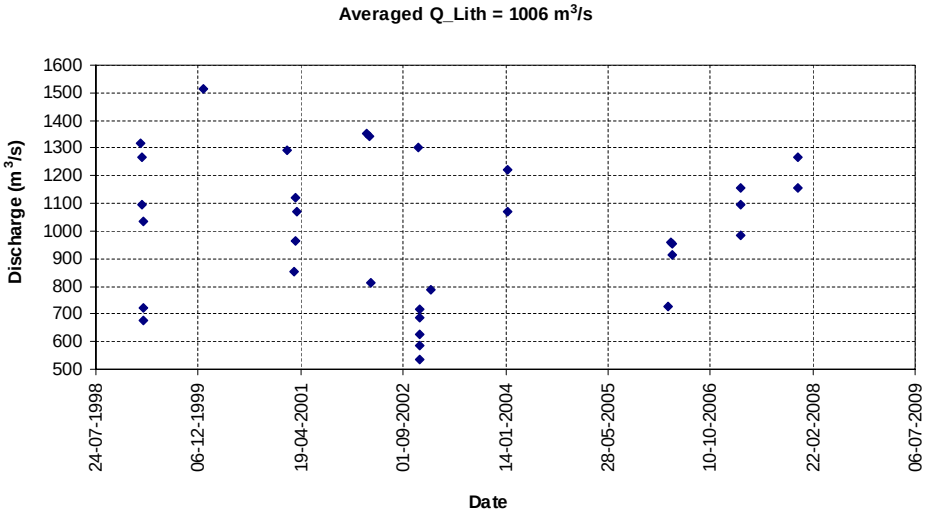

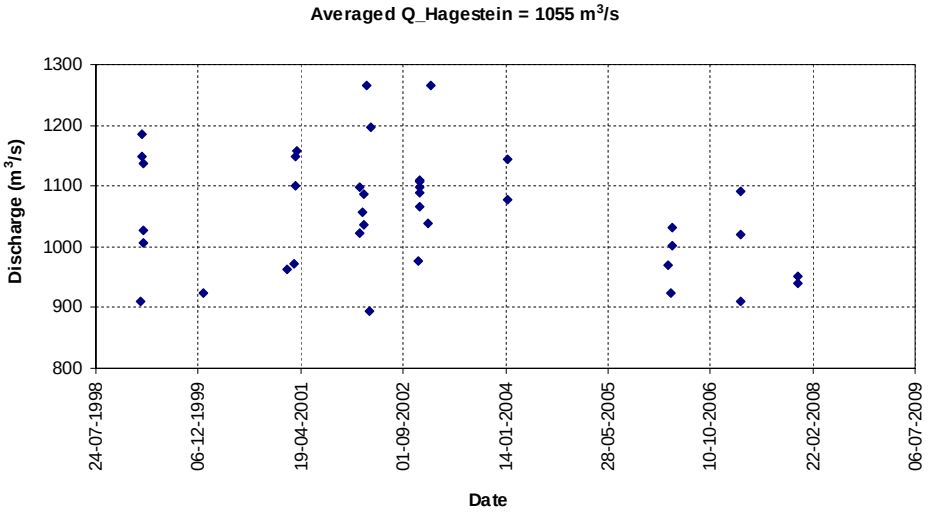

Figure 5 Observed discharge sorted for the range 3800-4200 m^3/s

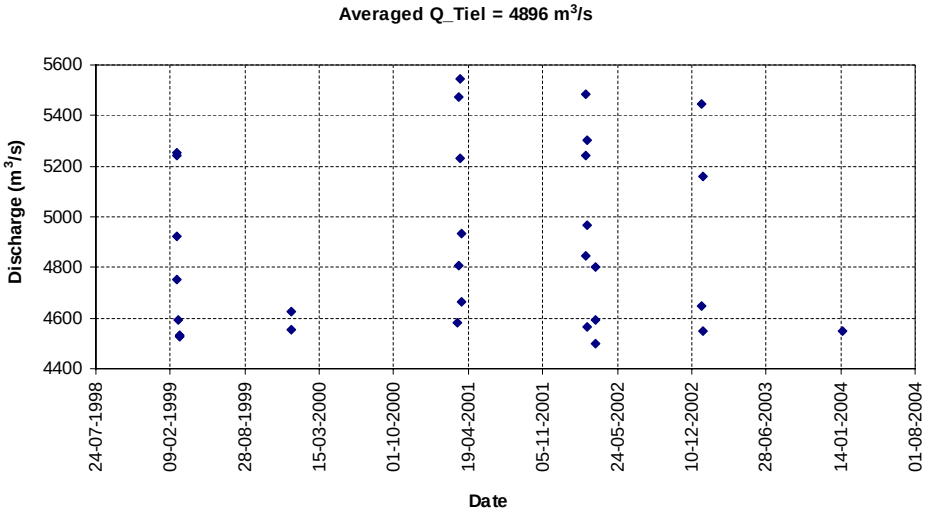

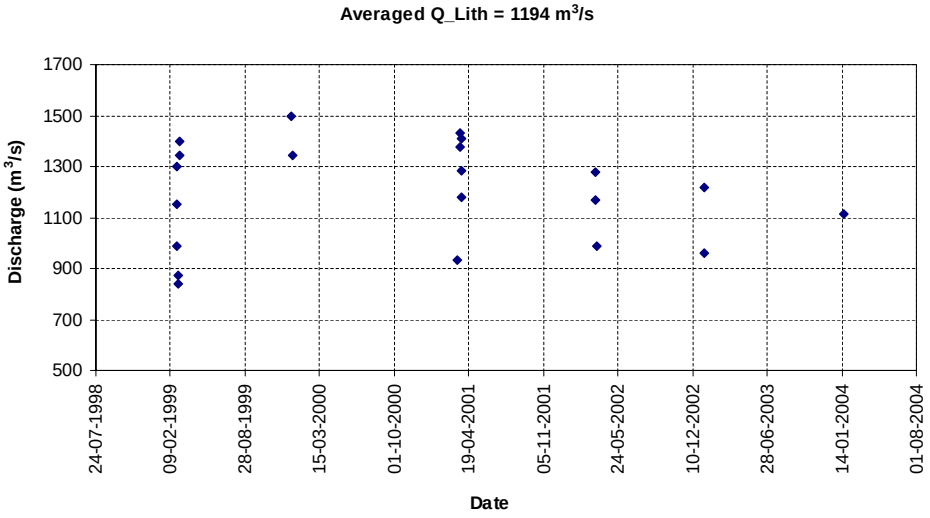

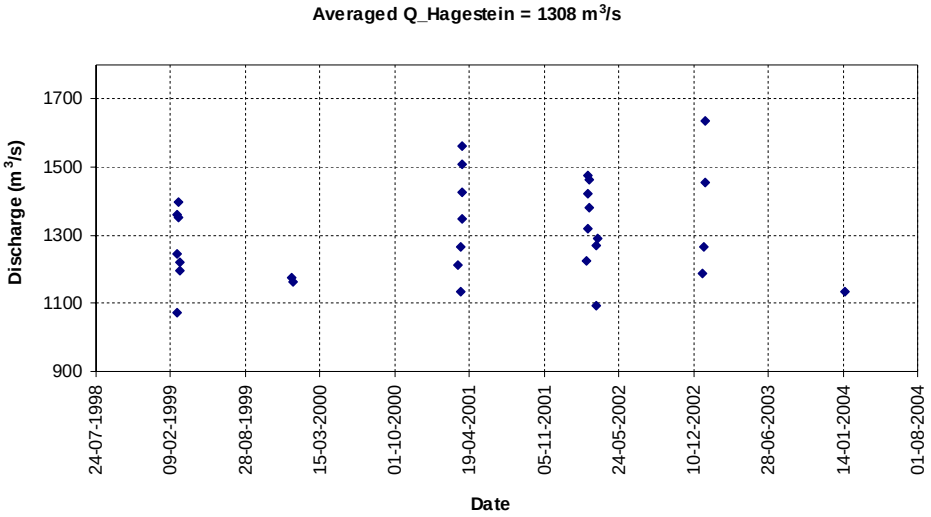

Figure 6 Observed discharge sorted for the range 4500-5500 m3/s

Figure 3 to Figure 6 can be moved to APPENDIX!!!!

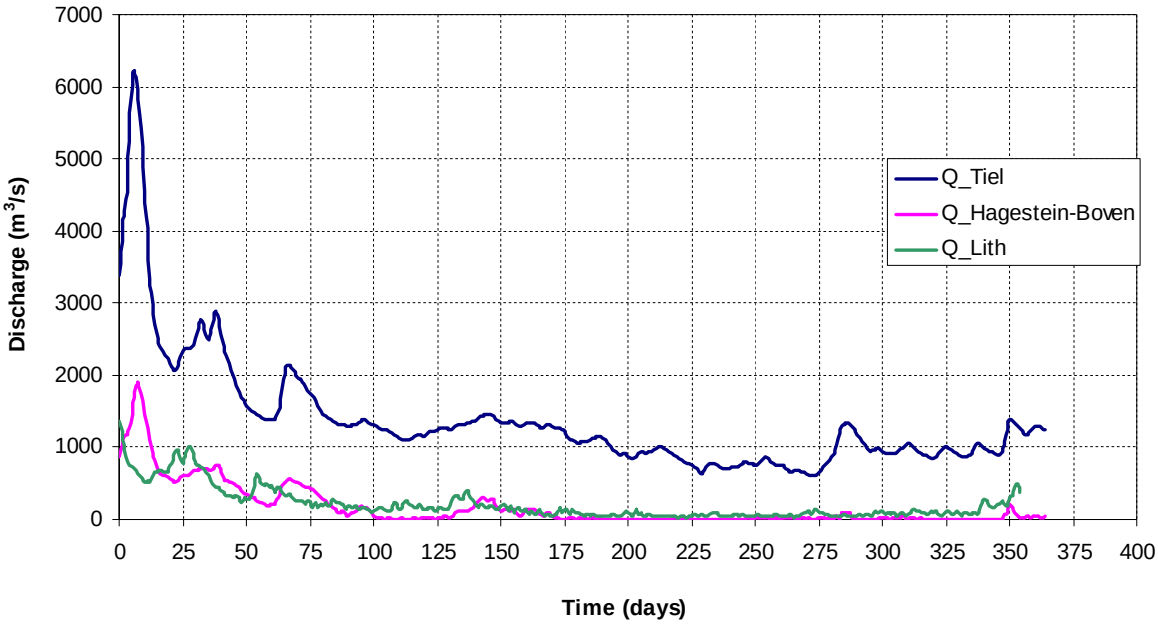

Figure 7 Upstream boundary conditions for SOBEK model (based on observed data of 2003)

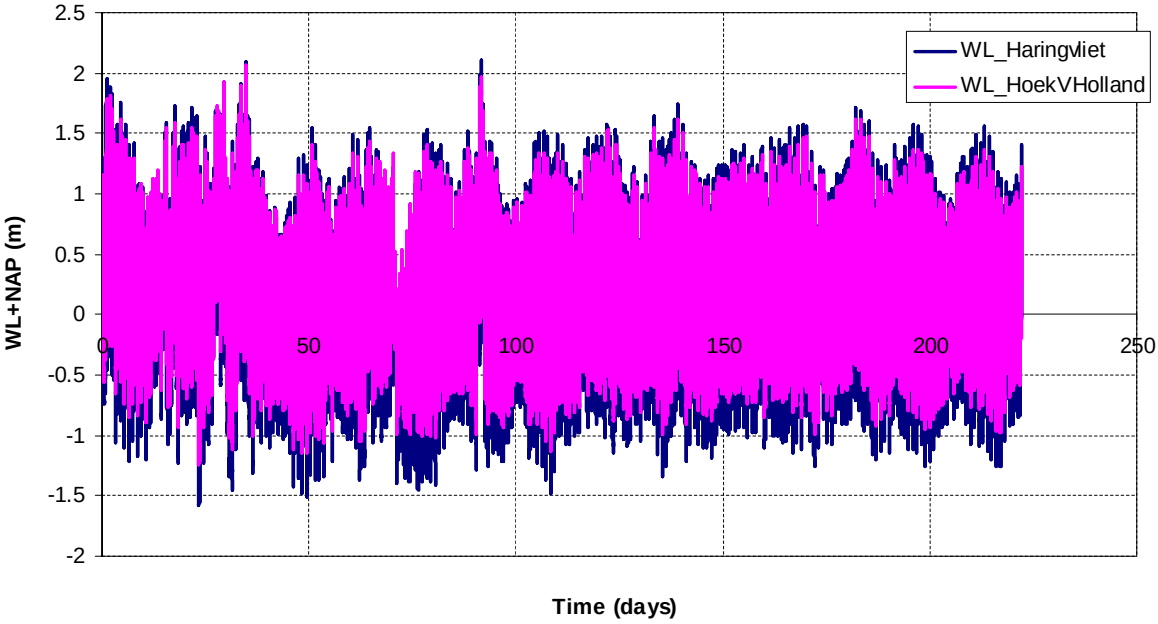

Figure 8 Downstream boundary condition for SOBEK model (based on observed data of 200)

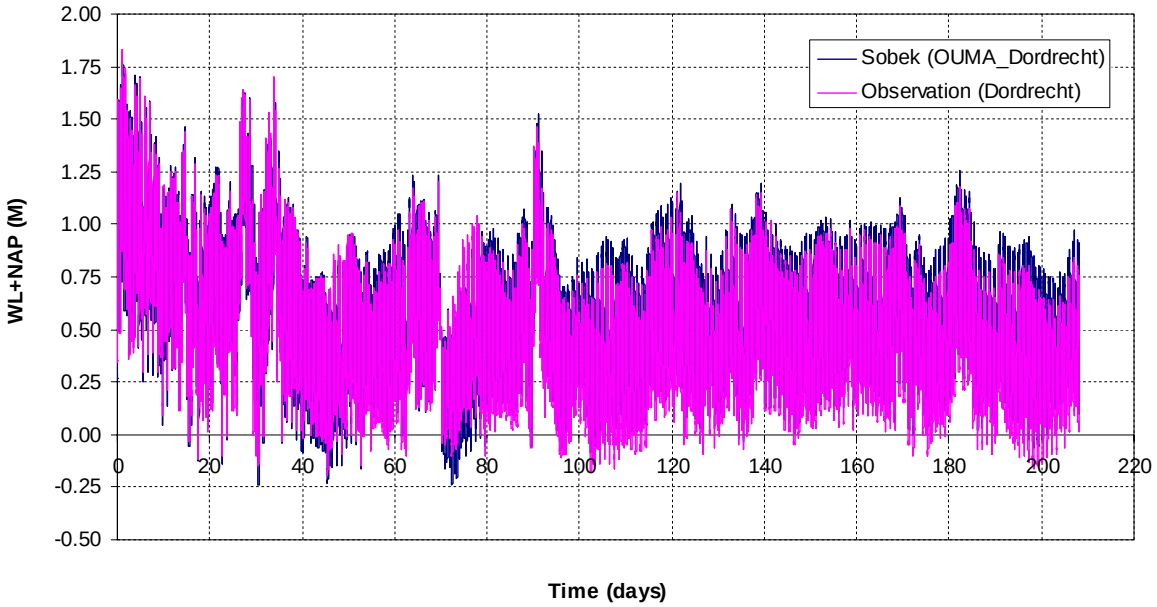

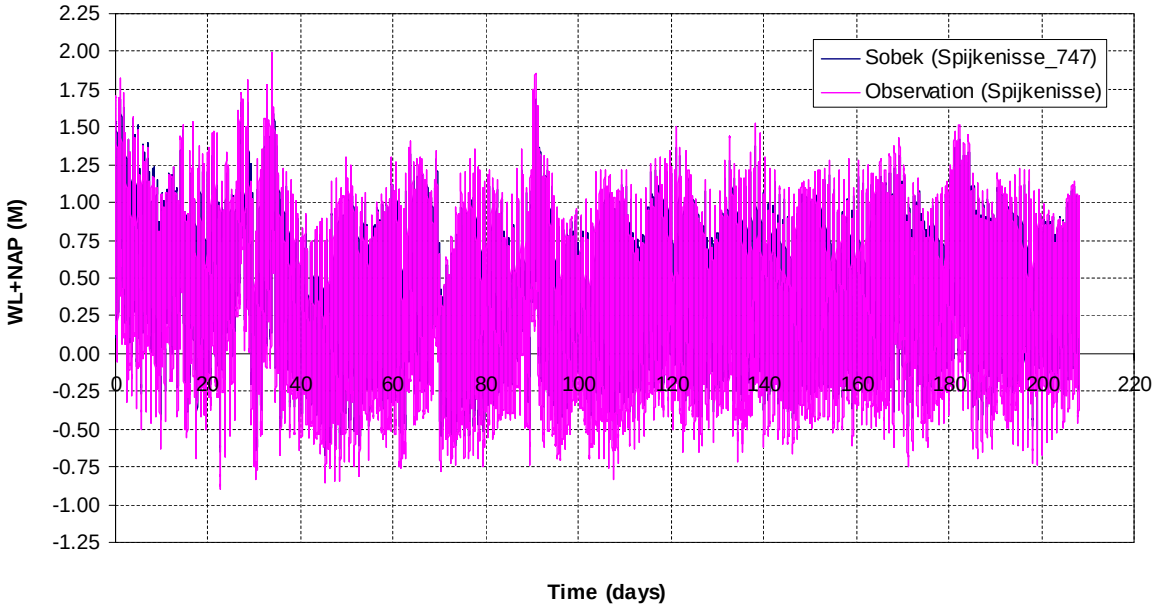

Contd. next page

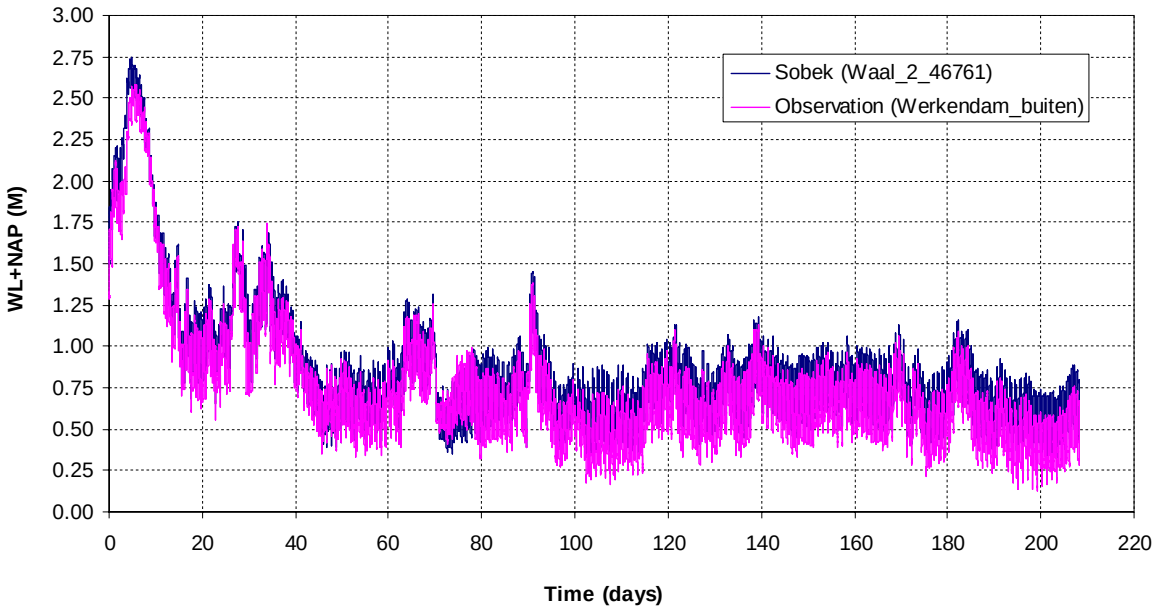

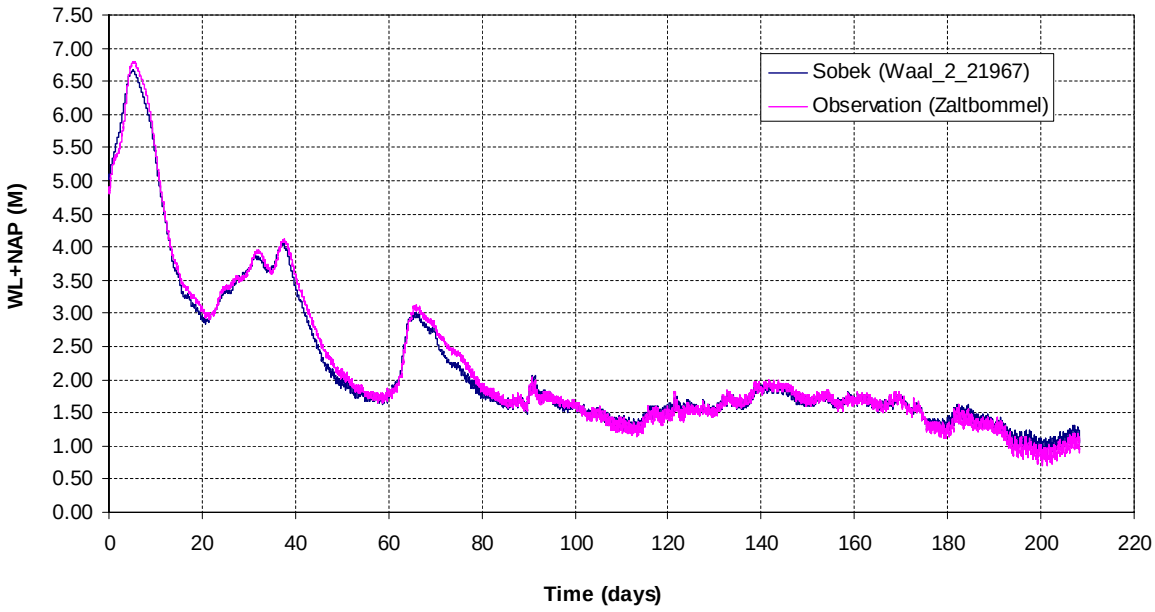

Figure 9 Comparison of SOBEK results with some observation (year 2003)

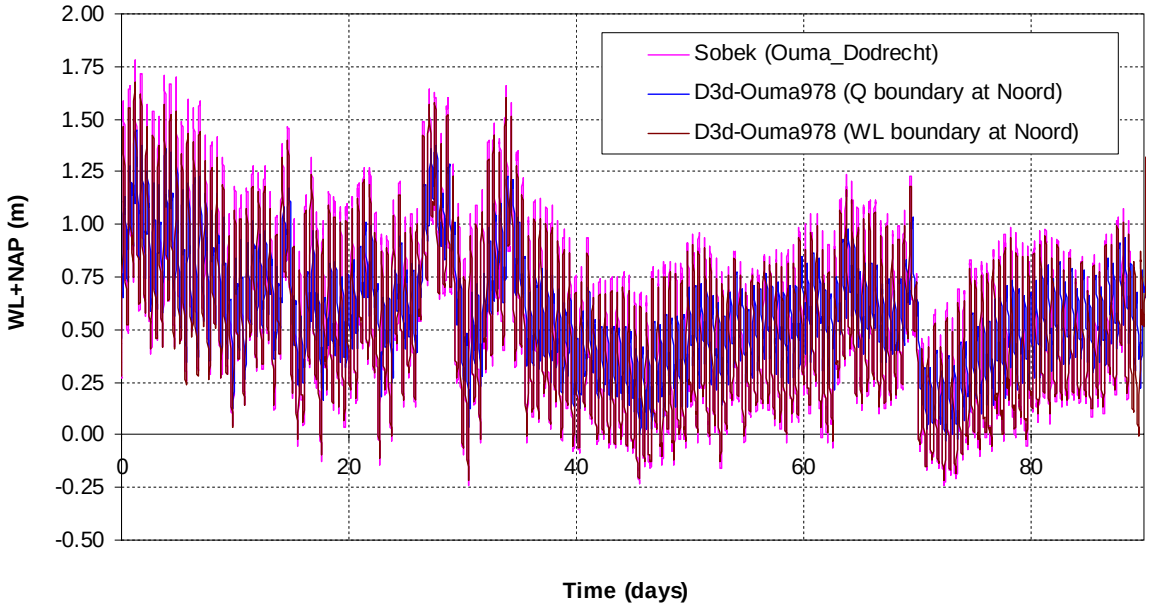

Figure 10 Comparison between Delft3D and SOBEK models (Water levels at Dodrecht)

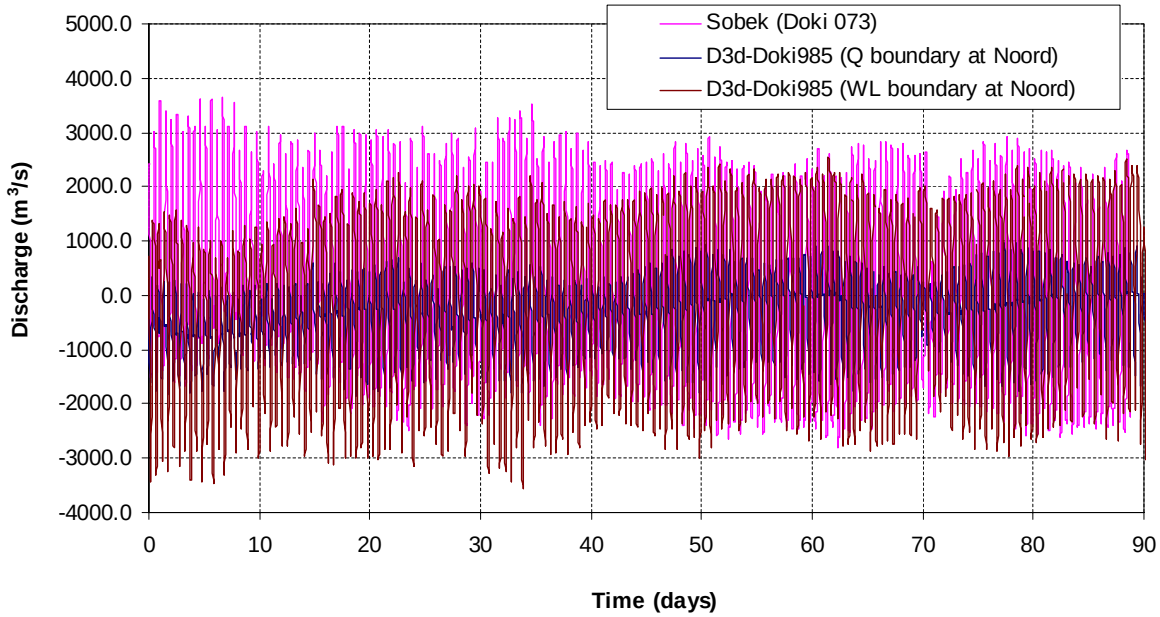

Figure 11 Comparison between Delft3D and SOBEK models (Discharges at Dordtse Kil)

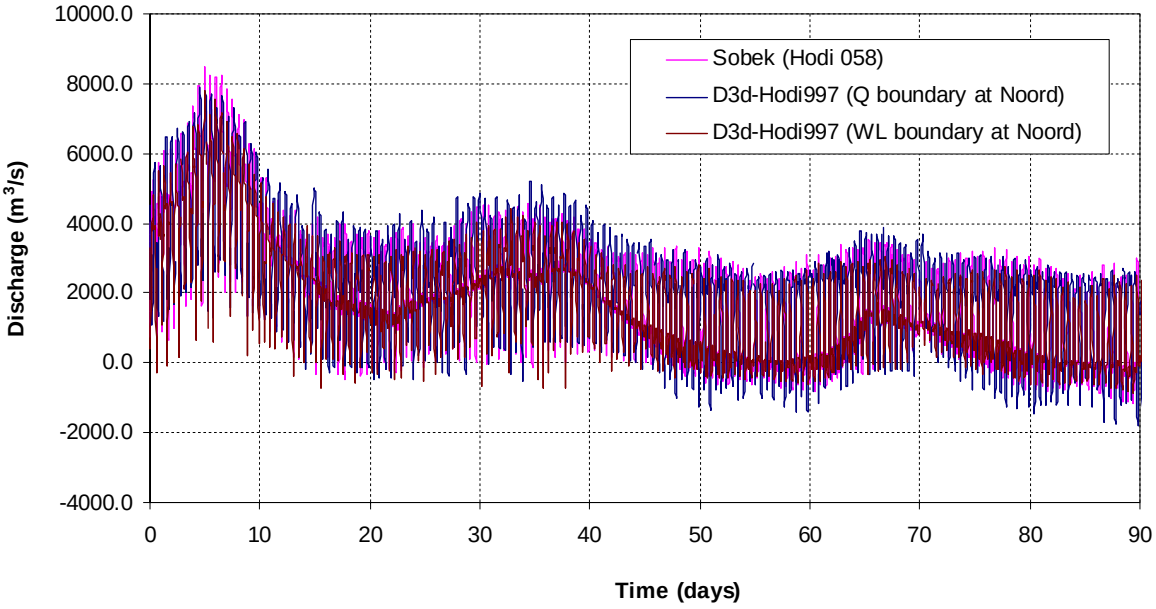

Figure 12 Comparison between Delft3D and SOBEK models (Discharges at Hollands Diep)

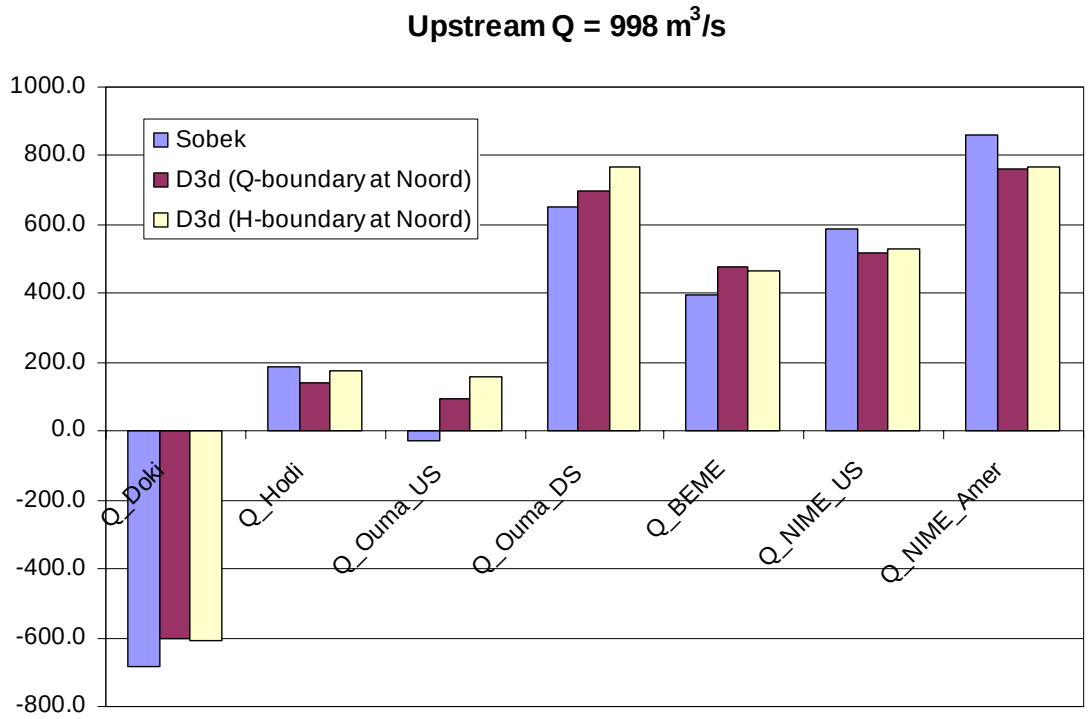

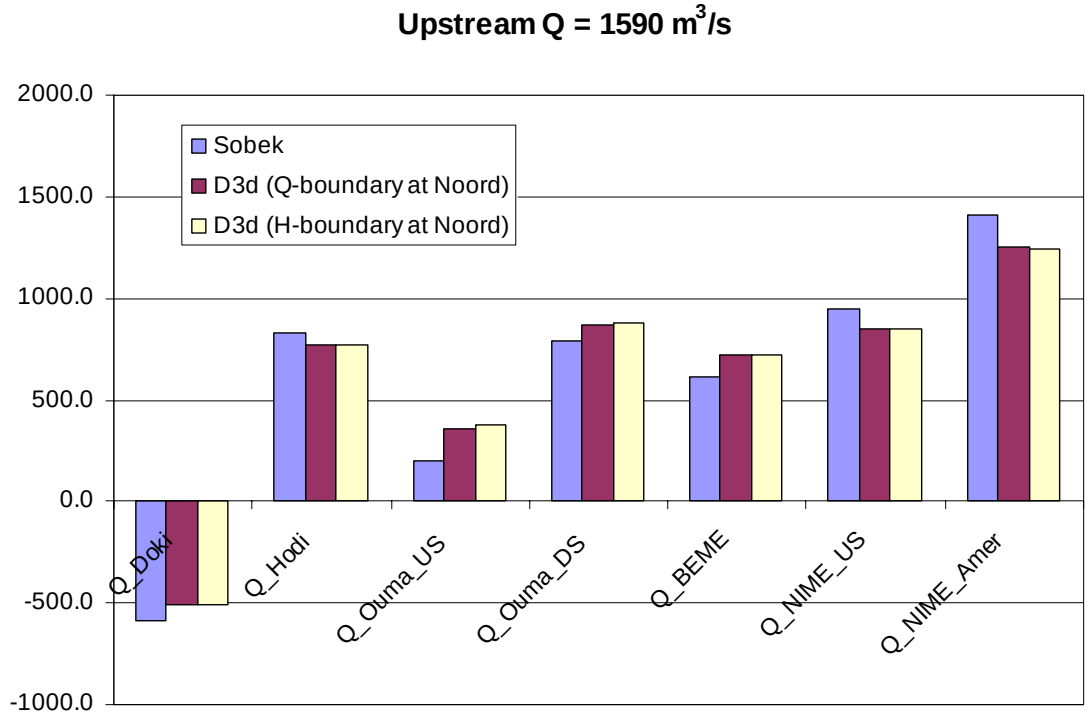

Contd. next page

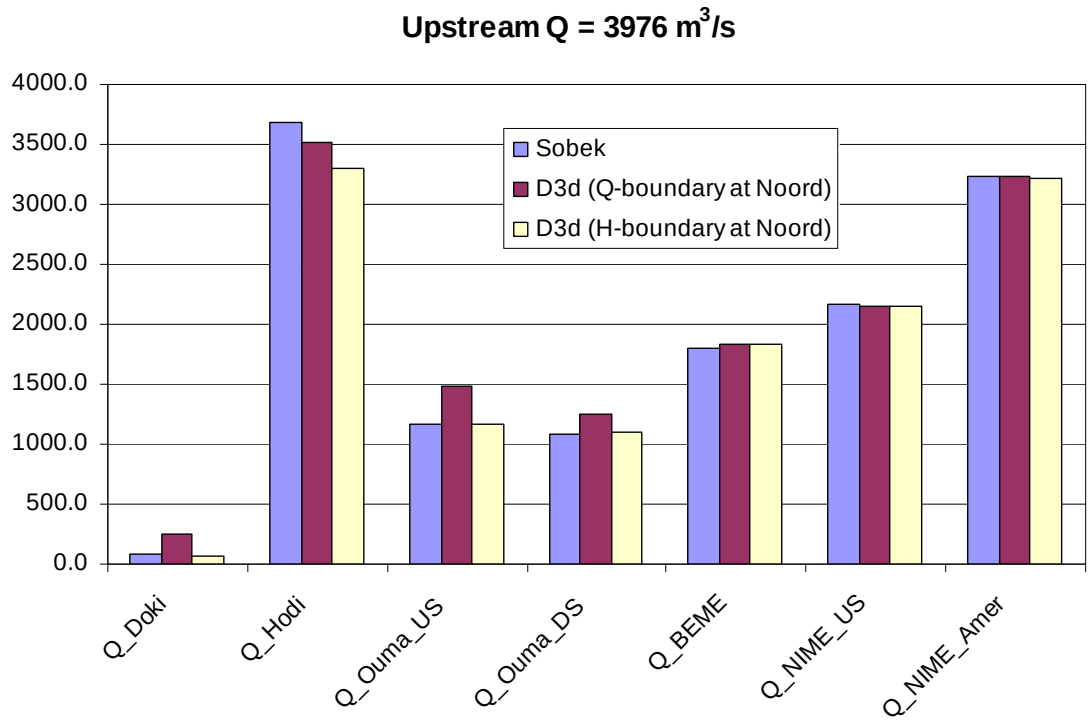

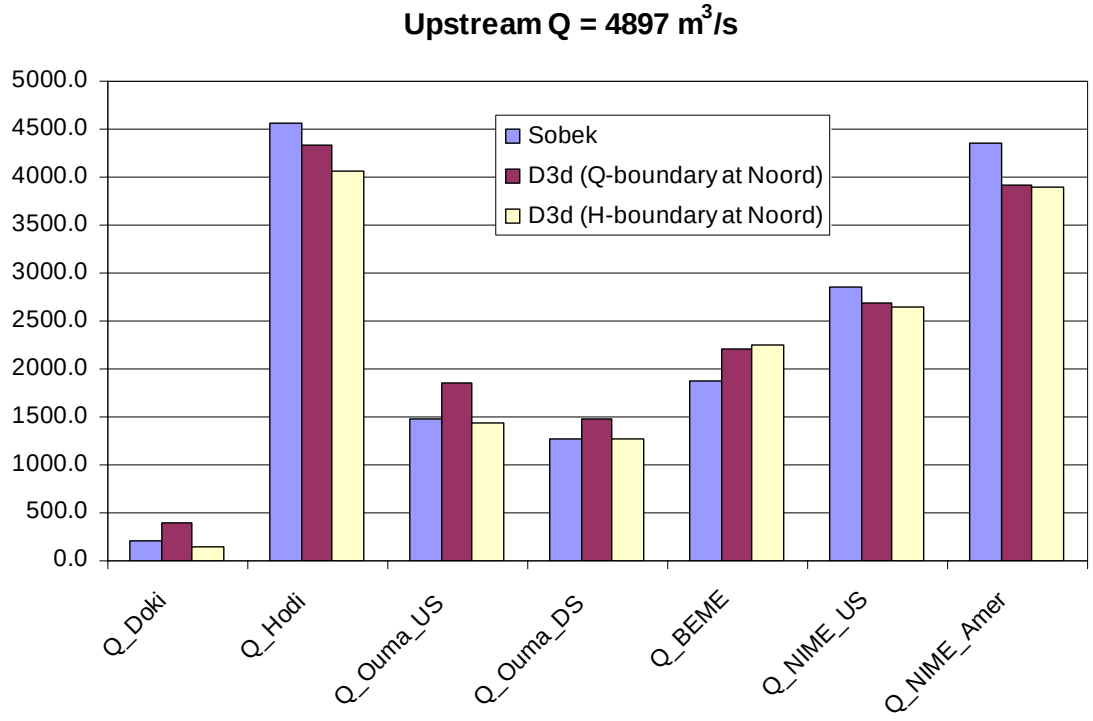

Figure 13 The comparison between tidal averaged discharges simulated by SOBEK and Delft3D model for some key locations (negative sign for Q_Doki denotes the residual flow towards south)

3.3 Delft3D- WAQUA comparison

3.3.1 WAQUA simulation

We have used the simulation results of WAQUA model of Rinmaasmonding that was made for observed period of about 3 months (1 August '98 to 14 November '98). We have compared the Delft3D simulation for the similar case as in WAQUA study by deducing the Delft3D boundary conditions from the larger WAQUA model. The boundary conditions, deduced from WAQUA model and used for the Delft3D model, are depicted in Figure 14 - Figure 16.

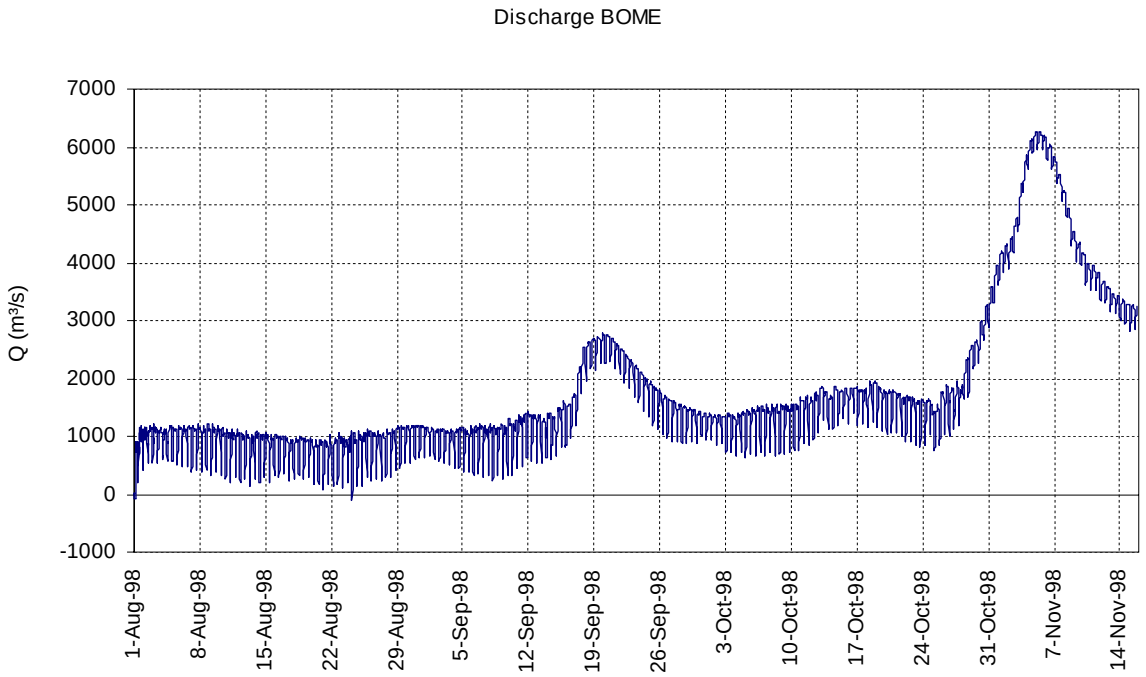

Figure 14 Upstream discharge boundary deduced from WAQUA

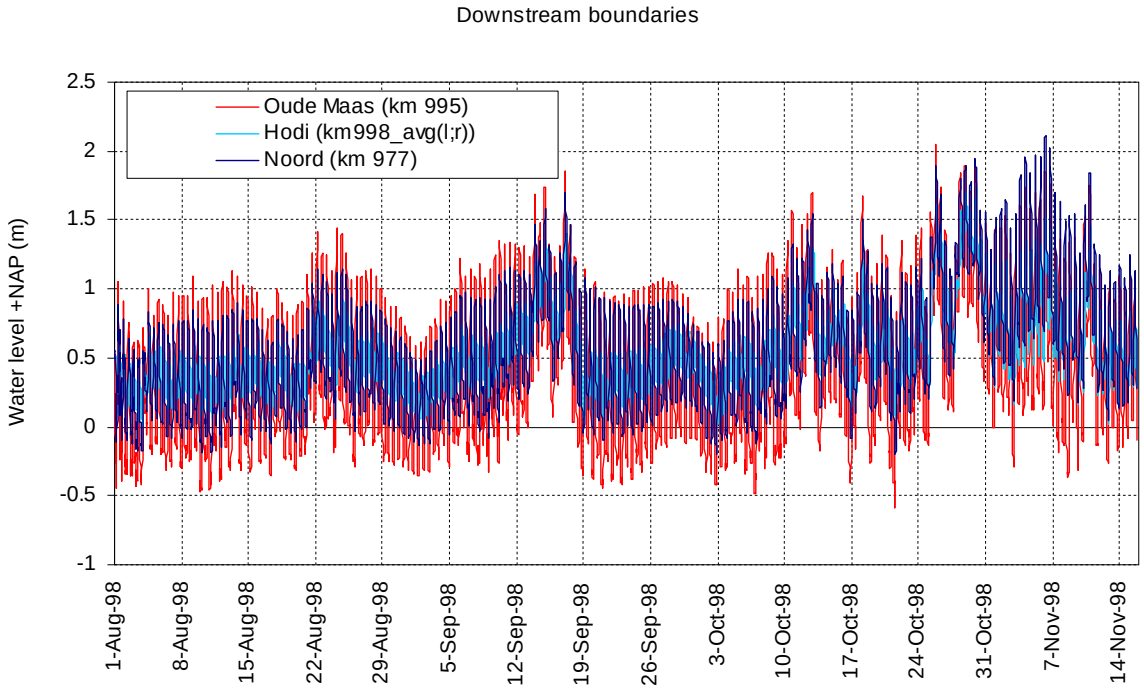

Figure 15 Downstream waterlevel boundaries, deduced from WAQUA

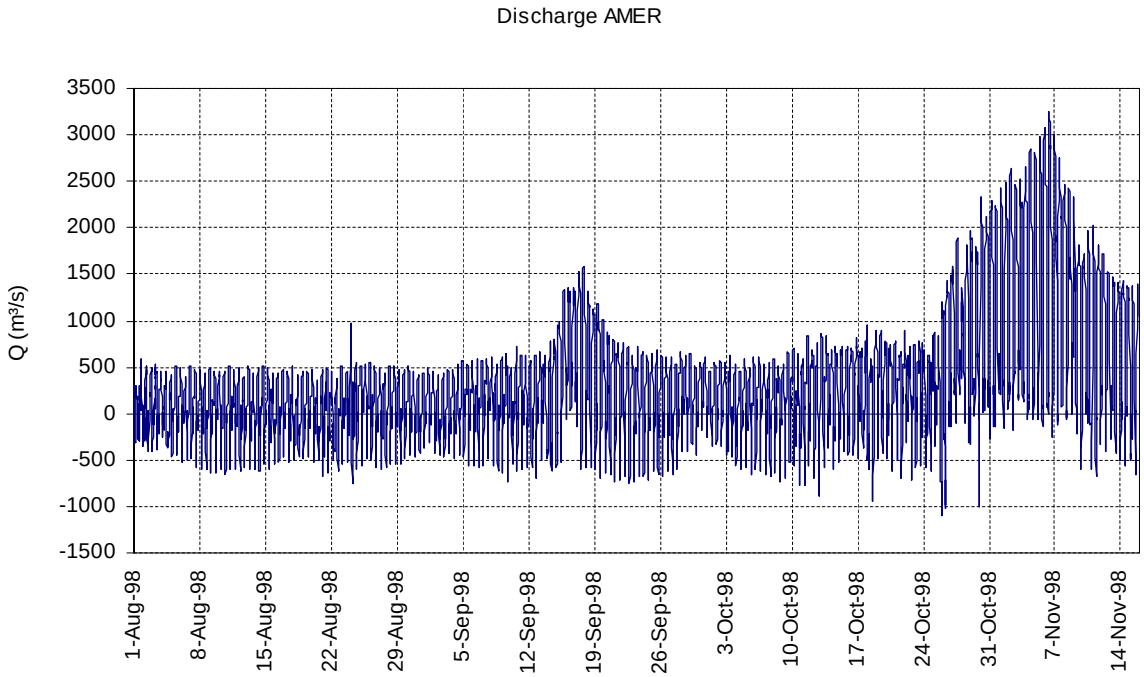

Figure 16 Discharge insertion/extraction at AMER, deduced from WAQUA

3.3.2 Delft3d simulation and comparison with WAQUA results

Delft3D computational results have been compared with WAQUA results for some key locations (as per availability of output data in the WAUA model). Figure 17 to Figure 27 provide a detailed impression of Delft3D model performance comparing to the WAQUA model, which shows that the result is reasonably consistent.

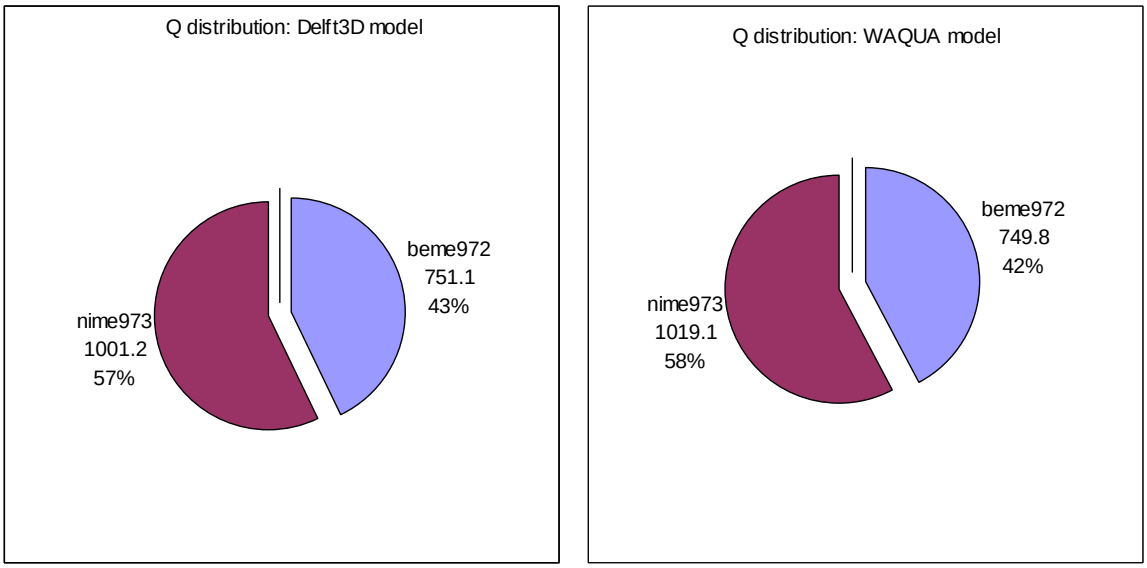

Figure 17 Comparison on averaged discharge distribution at Merwedes branches

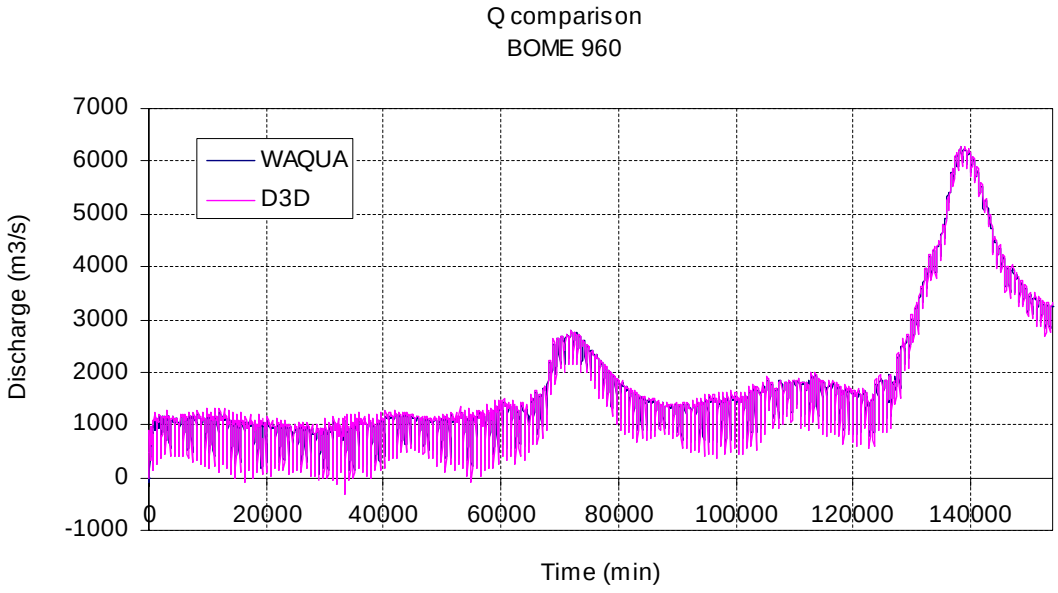

Figure 18 Comparison on discharge variation at BOME (for the whole simulation period)

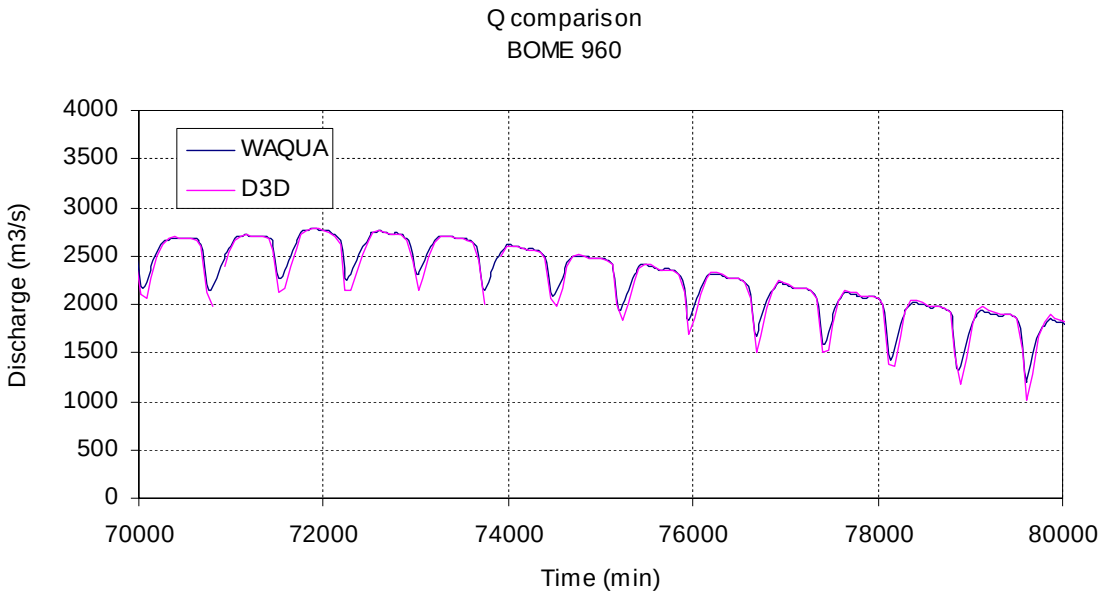

Figure 19 Comparison on discharge variation at BOME (for a selected shorter time-span for clarity)

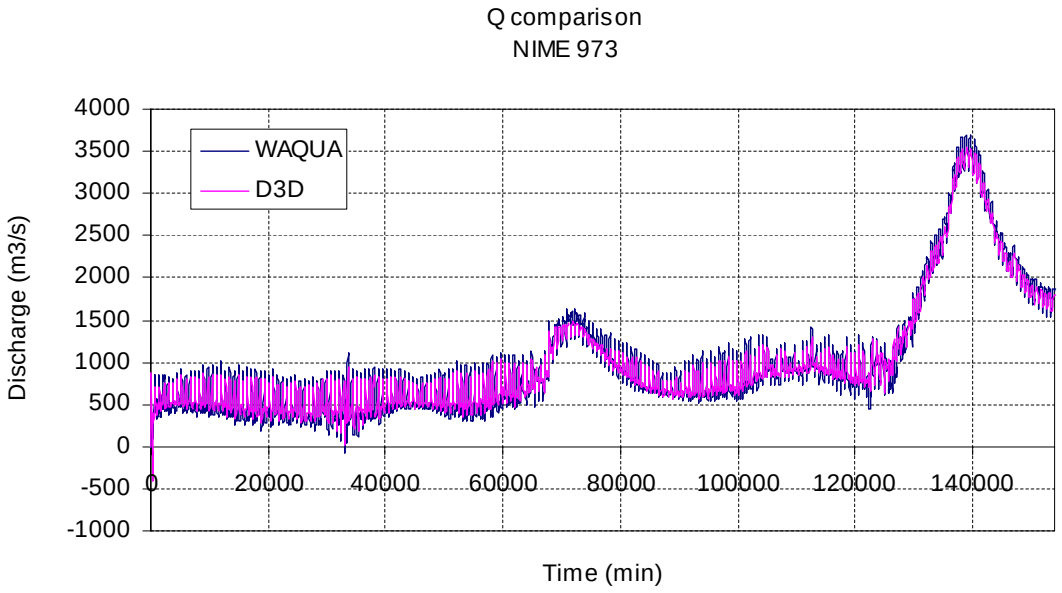

Figure 20 Comparison on discharge variation at NIME (for the whole simulation period)

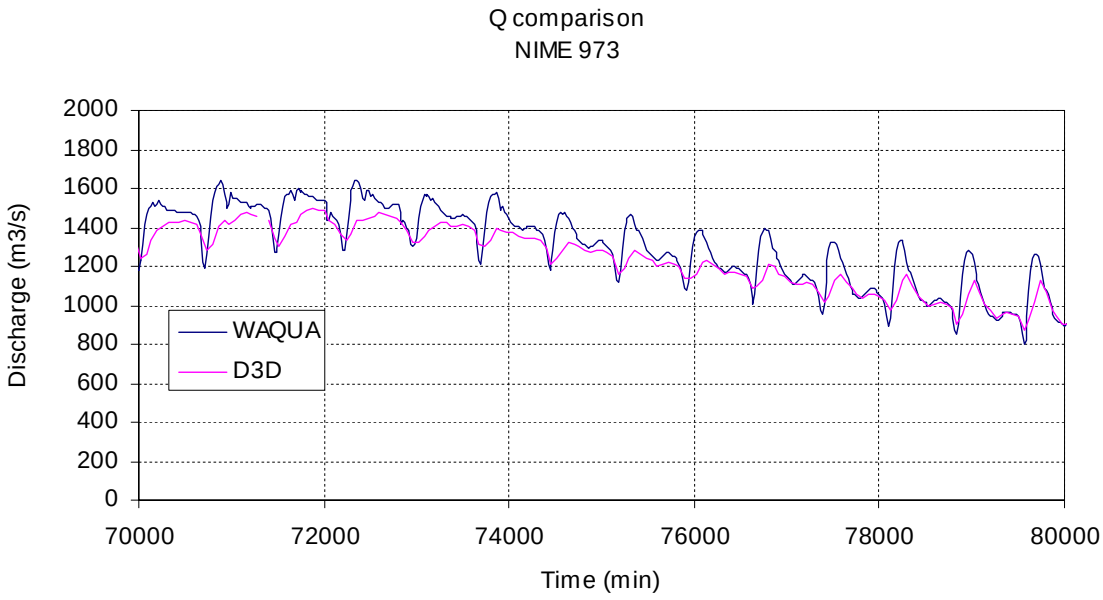

Figure 21 Comparison on discharge variation at NIME (for a selected shorter time-span for clarity)

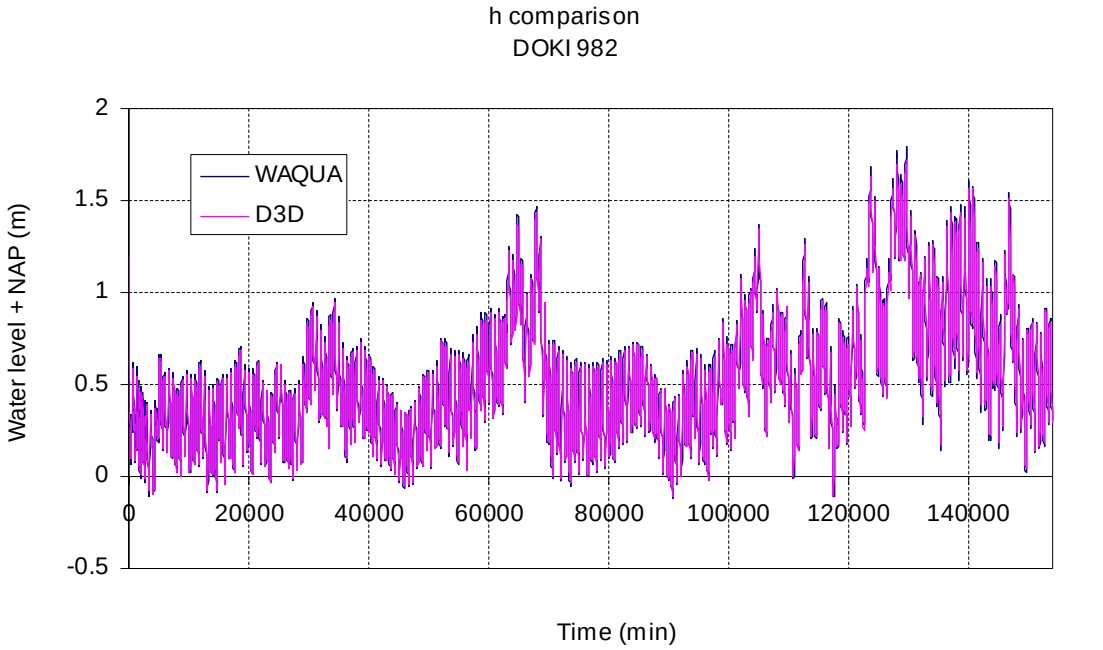

Figure 22 Comparison on water level variation at Dordtsche Kil (for the whole simulation period)

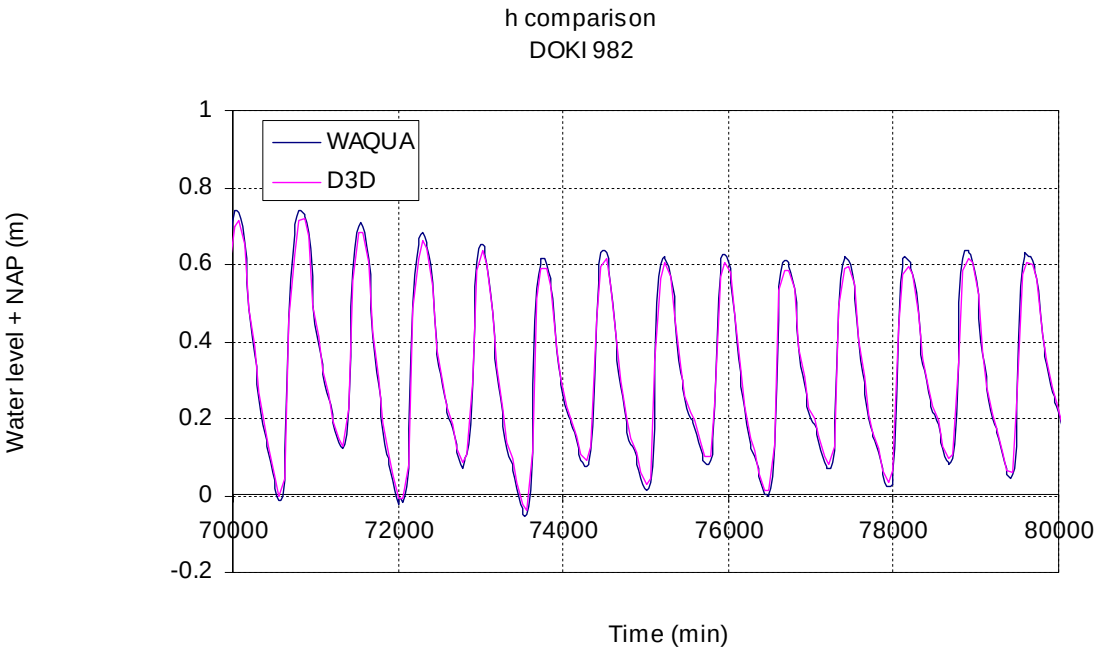

Figure 23 Comparison on water level variation at Dordtsche Kil (for a selected shorter time-span for clarity)

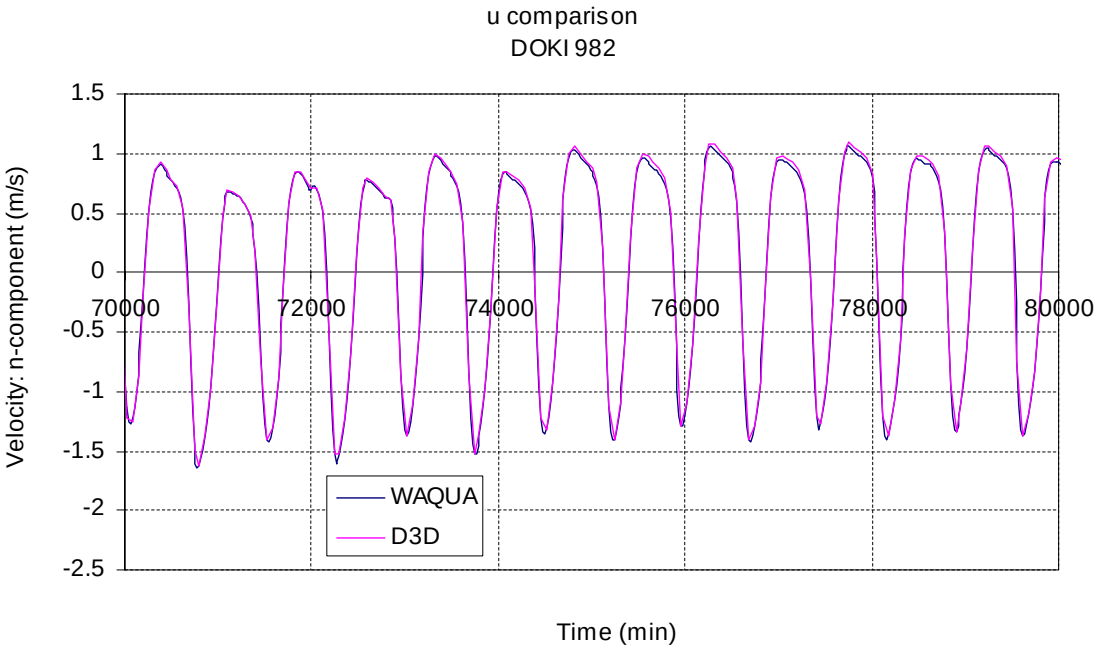

Figure 24 Comparison on variation of velocity (n-component) at Dordtsche Kil (for a selected shorter time-span for clarity)

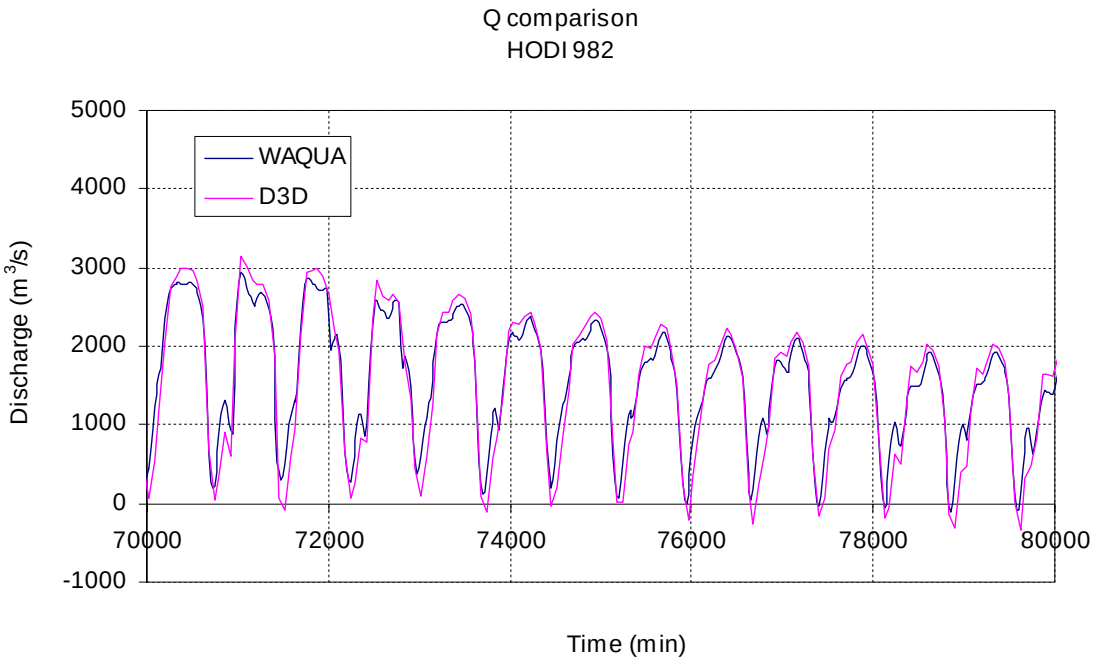

Figure 25 Comparison on discharge variation at Hollands Diep (for a selected shorter time-span for clarity)

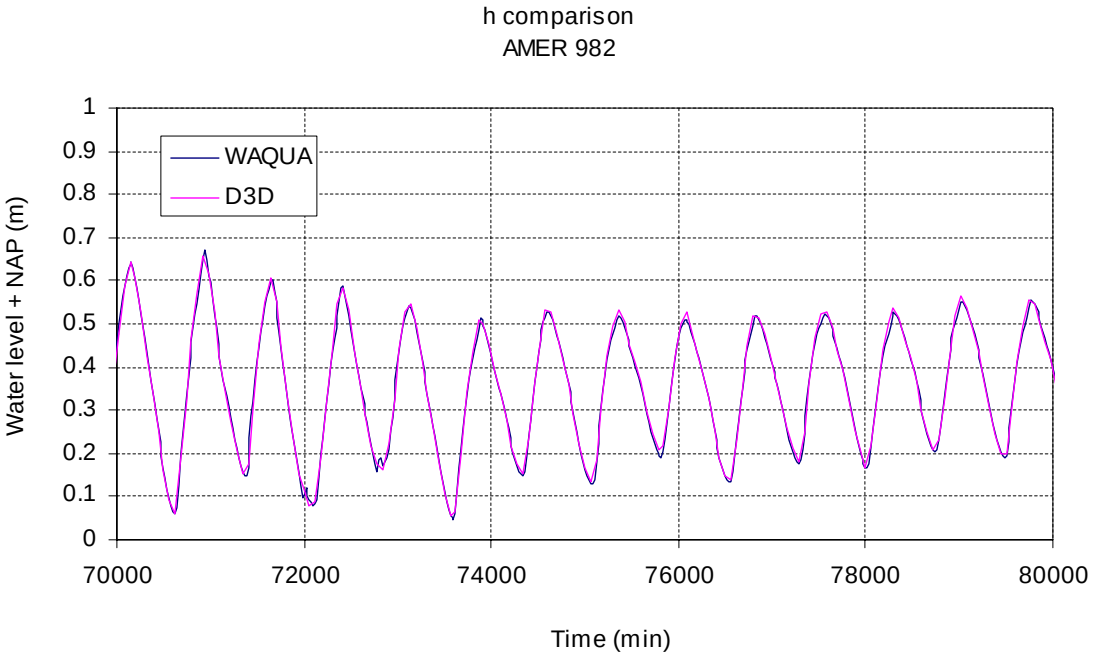

Figure 26 Comparison on water level variation at Amer (for a selected shorter time-span for clarity)

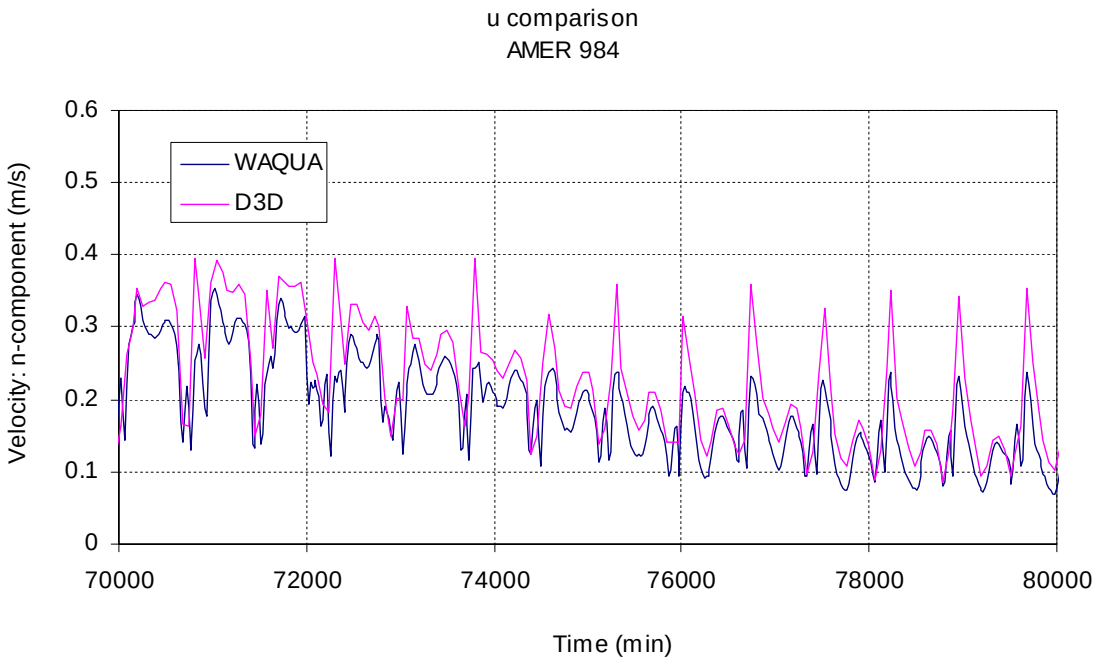

Figure 27 Comparison on variation of velocity at Amer (for a selected shorter time-span for clarity)

4 Sediment Transport and Morphology at Dordtsche Kil – Hollands Diep

4.1 Data Analysis

Based on the available soundings, the morphological behaviour as well as the bed feature (particularly, the non-erodible area, fixed layers and deep pits) at Dordtsche Kil and Hollands Diep area can somewhat be identified. Furthermore, a brief analysis of geotechnical survey data of the river bank and bed of the Dordtsche Kil including the data of sediment characteristics has been made that can be used to specify the active and non-erodible layers as well as understanding morphodynamic behaviour. A brief analysis of characteristics of all branches has been made to define the fraction content in each domain in a simplified manner.

4.1.1 Some impression of the multi-beam measurement

The multi-beam soundings for Dordtsche Kil (2009), Hollands Diep (2008) and Oude Maas (2009) has been presented in figures below **(**Figure 28 to Figure 30**; see APPENDIX for additional images**), from which different characteristics of bed feature can be seen, e.g. non-erodible clay layers, artificial fixed layers, deep pits with apparently sandy material, bed forms etc.
The northern part of Dordtsche Kil appears to be mainly non-erodible bed with clay with some sandy pits. The southern part includes bed forms with sandy material. It can be seen that the bed level with bed forms is deeper than the level of fixed layer on HSL tunnel in both south and north direction. Further south to HSL towards Hollands Diep, the bed level is higher and bed forms look like ripples with fine sediment and also some sand waves can be seen inside the navigation channel (Figure 30).
From the longitudinal profiles of multi-beam soundings for 2005 and 2009 (Figure 31 to Figure 33), it can be seen that the bed is eroding and the amplitude of the micro-scale features appear to be decreasing. The erosion appears to be more severe towards the northern part, and even more pronounced along the east part of the river axis (i.e., along the outer bend, Figure 33). Since, under the averaged flow condition, the residual flow and thereby transport appears to be towards north (as shown by our hydrodynamic computation, verified with SOBEK model). It is to be noticed that the erosion seems to be more pronounced in outer bend of the north part of HSL tunnel. However, this might also be attributed to the dredging activities (at least partly as there were some dredging activities during 2007 and 2008, namely ~ 56,000 and 106,000 m^3 respectively, although we have no information on the location of dredging activities).

The comparison on longitudinal profiles in other parts is depicted in Figure 34 - Figure 35, which shows that the north part with non-erodible layers contain few deep pits, and do not show any noticeable bed level changes (Figure 34). Deep pits in both side of the fixed layer at Kil tunnel can be seen from this plotting, though they seem to be stable. Whereas, the middle part with sand bed shows the sign of degradations as can be seen in Figure 35 (this might be attributed to the dredging activities as well).

4.1.2 Sediment characteristics

For Merwedes branches, the non-uniform grain-size was used as reported in previous studies (Sloff et al., 2007), and simplified it to only two fractions. Based on the analysis of data for all branches, we simplified the amount of sediment fractions so as to get a unified characteristic for the entire computational domain including the mud fraction. The amount of the mud fraction corresponds to the sediment diameter less than 63 μ.
The grain-size variation within Dordtsche Kil is depicted in Figure 36. From the variation of the D50, D84 and D16, it can be seen that the sediment is rather uniform and coarser (i.e., ~300-400 μ, D50 averaged over the reach,) than other part. It appears to be much finer and non-uniform towards the Hollands Diep (within the area of navigation channel) with significant clay content (Figure 37). This leads to the fact that the locally eroded coarse material in Dordtsche Kil (area with bed forms) does not seem to be transported towards the Hollands Diep.

The grain-size distribution curve for Oude Maas is depicted in Figure 38, which also shows non-uniform material with fine sediment and mud fraction. Based on these data information, the fraction content for the each domain (and even each part of the 5th domain that includes Dordtsche Kil, Hollands Diep and Oude Maas) has been defined, which is depicted in Figure 39 and Figure 40. As it can be seen, the variation in sediment characteristics in different areas appears to have sharp transition which might be a problem for morphological simulation.

4.1.3 Geotechnical observation at Dordtsche Kil

Since the evaluation of bed changes at Dordtsche Kil is the main focus of this study, we try to define the bed characteristics of the Dordtsche Kil based on the geotechnical survey data along the west and east banks. Such analysis would be useful to define the active or movable as well as non-erodible layers. There are a number of fixed/non-erodible layers in Dordtsche Kil that can be identified analysing the multibeam data as well as geotechnical survey data. We have analyzed the geological survey data to identify the movable layer and specify the sediment layer thickness (Figure 41 and Figure 42). The geotechnical characteristics are available up to the depth -20 + NAP, and the material below -10 + NAP can be considered as river bed material.

Analyzing the longitudinal profile of 2009 multi-beam data (Figure 31 to Figure 35), we can see that the bed level in the south part (~km 984 to ~km 988) appears to be within the range of ~ -12 m +NAP to ~ -13.5 m +NAP (except for the level of fixed layer over HSL tunnel, which is ~-10 m +NAP). Whereas, the bed level at the north part (~km 983 to ~km 980) seems to be at the level of ~-10 m +NAP with few deep pits (the absolute depth of which varies from ~5 m to ~ 9 m). Now, if we look at the geotechnical characteristics along this reach (along both west and east banks as shown in Figure 41 and Figure 42), a course sediment layer can be seen within -10 m+NAP to -15 m+NAP in the south part. Also, from above-mentioned sediment analysis (Figure 36), it can be concluded that the bed level in this part lies within this layer with coarse sediment. The erosion in southern part (between ~km 987 and ~km 988) of the fixed layer at HSL appears to be approaching towards the non-erodible layer (sandy clay), and even almost hitting this layer just before km 988 (at km 988, there is a big layer of non-erodible sandy clay as can be seen in Figure 41). This non-erodible layer appears to be preventing the erosion progression towards Hollnads Diep. In the north part (~km983 to km 980), the bed level seems to lie on a non-erodible layer with sandy clay; whereas the deep pits have already reached the level below coarse sands (i.e., up to the layer with silty/sandy clay).

There is no continuation of the map towards the Hollands Diep area; nevertheless, it can be inferred from the bed level, sediment size and the soil characteristics near km 988 of Dordtsche Kil that the bed material in this area (where the navigation channel has been made) is comprised of clay with fine sand and silt.

From the geotechnical map, it is evident that the movable layer in the river bed at Dordtsche Kil is within the limit of 5 m in southern part containing the medium to coarse sediment; whereas the northern part is comprised of non-erodible (semi-erodible) layers with peat and clay material. However, in northern part, coarse sand seems to be evident below the elevation of about -13 m + NAP (up to -20 m +NAP). Figure 43 gives an impression of river bed characteristic along the Dordtsche Kil.

Based on these observations and analyses, we will define the fixed layer and the layer thickness of the mobile sediment in this reach (to be described in next sections).

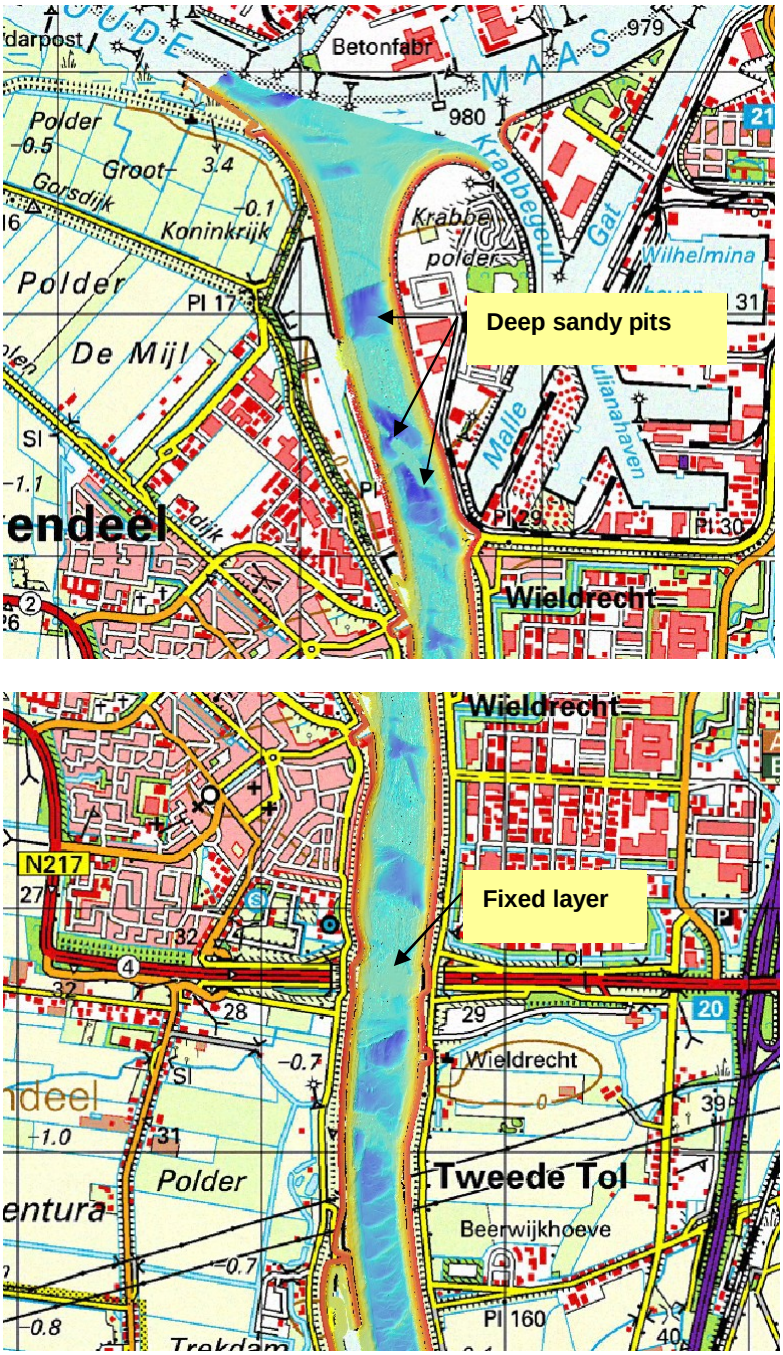

Figure 28 Northern part of Dordtsche Kil with non-erodible layers and deep pits with sandy materials

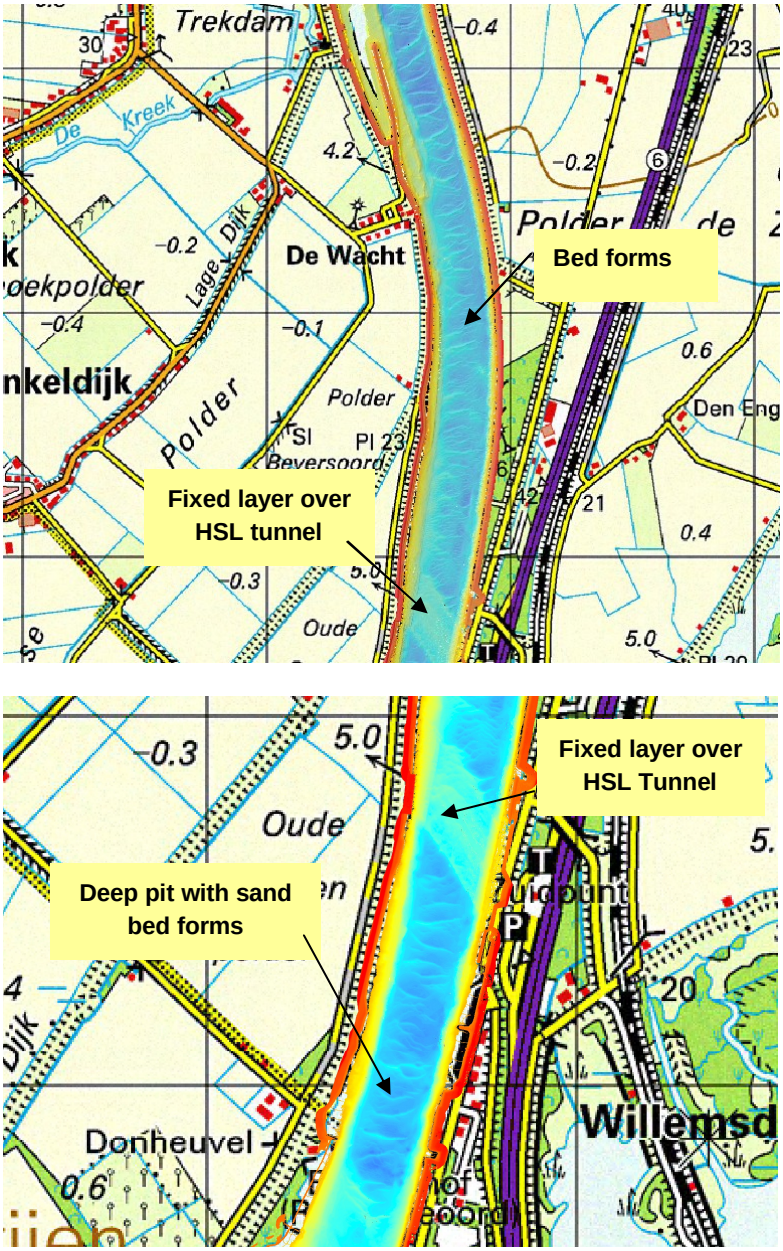

Figure 29 Middle and southern part of Dordtsche Kil with HSL tunnel

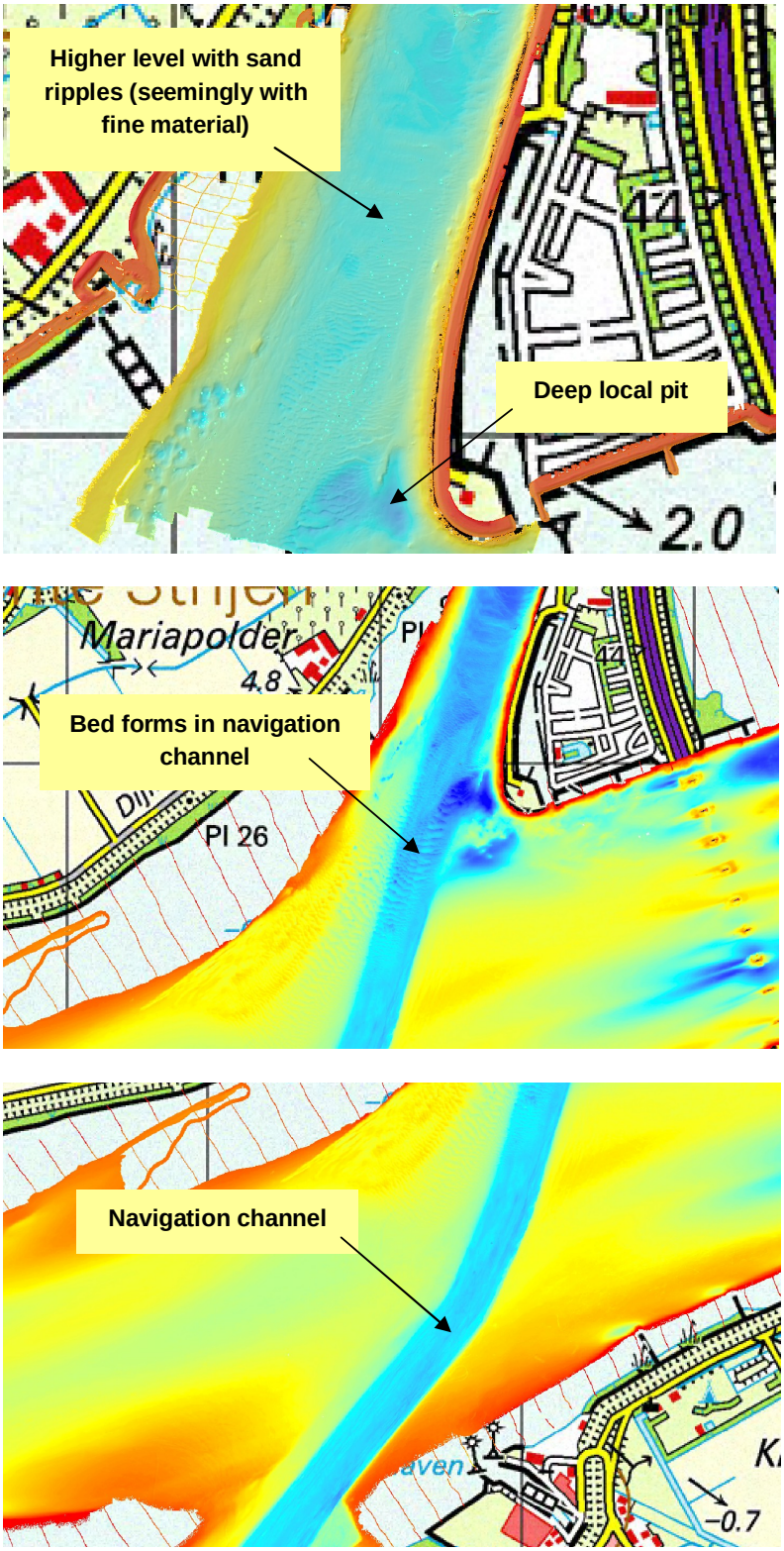

Figure 30 Junction of Dordtsche Kil and Hollands Diep with navigation channel

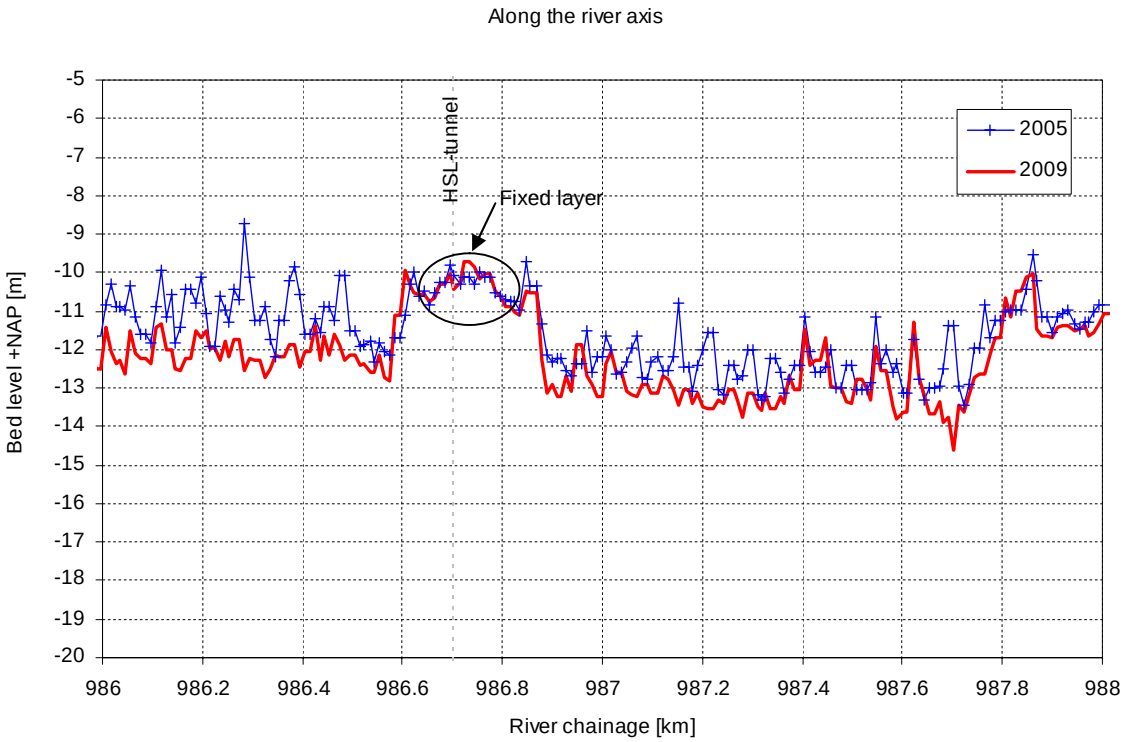

Figure 31 Comparison of longitudinal profile along the river axis near HSL tunnel

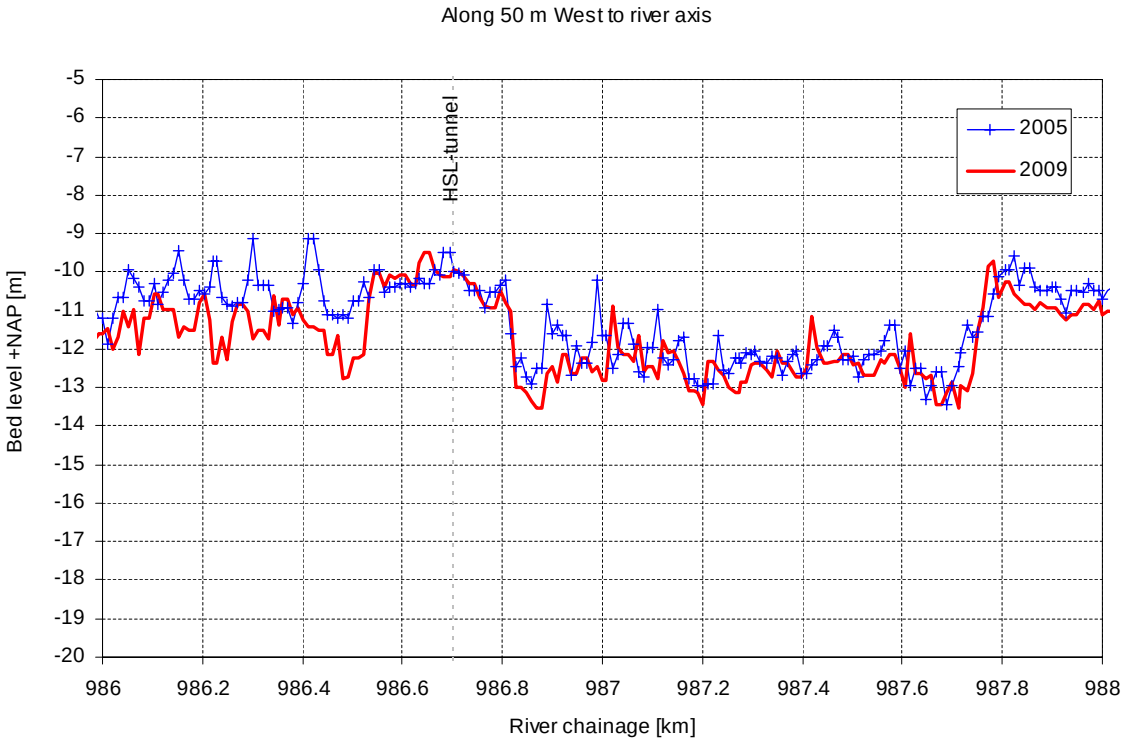

Figure 32 Comparison of longitudinal profile along the 50 m west to the river axis near HSL tunnel

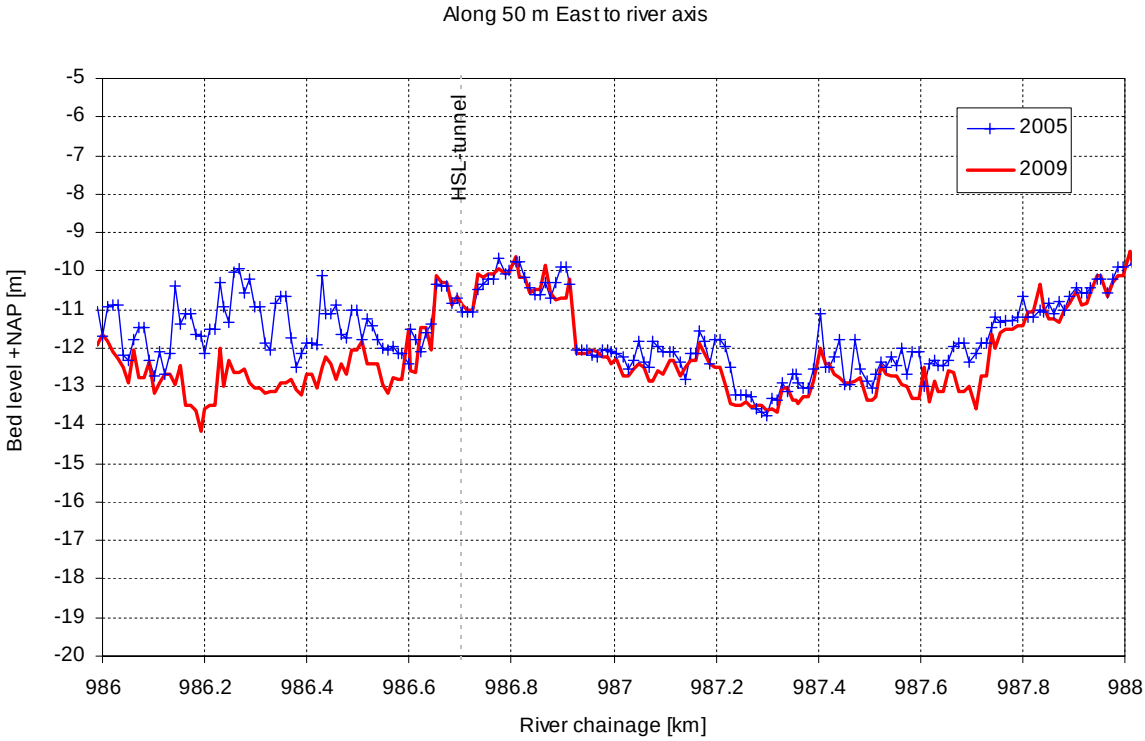

Figure 33 Comparison of longitudinal profile along the 50 m east to the river axis near HSL tunnel

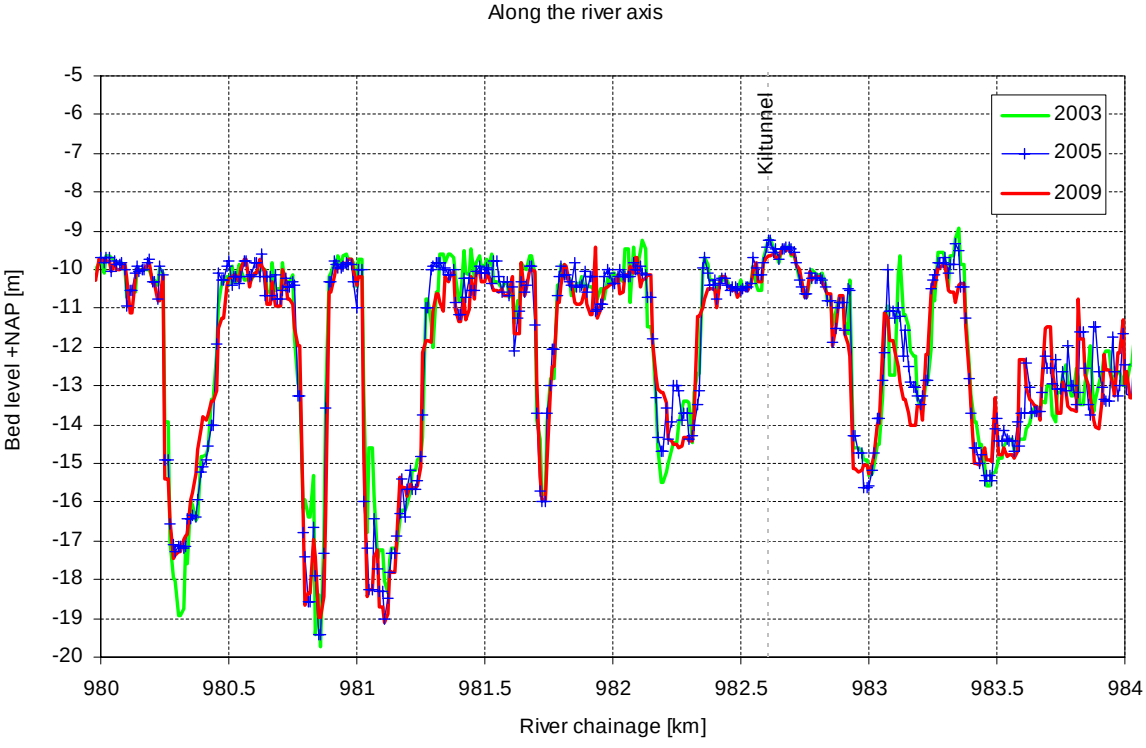

Figure 34 Comparison of longitudinal profile along the river axis in Northern part of Dordtsche Kil

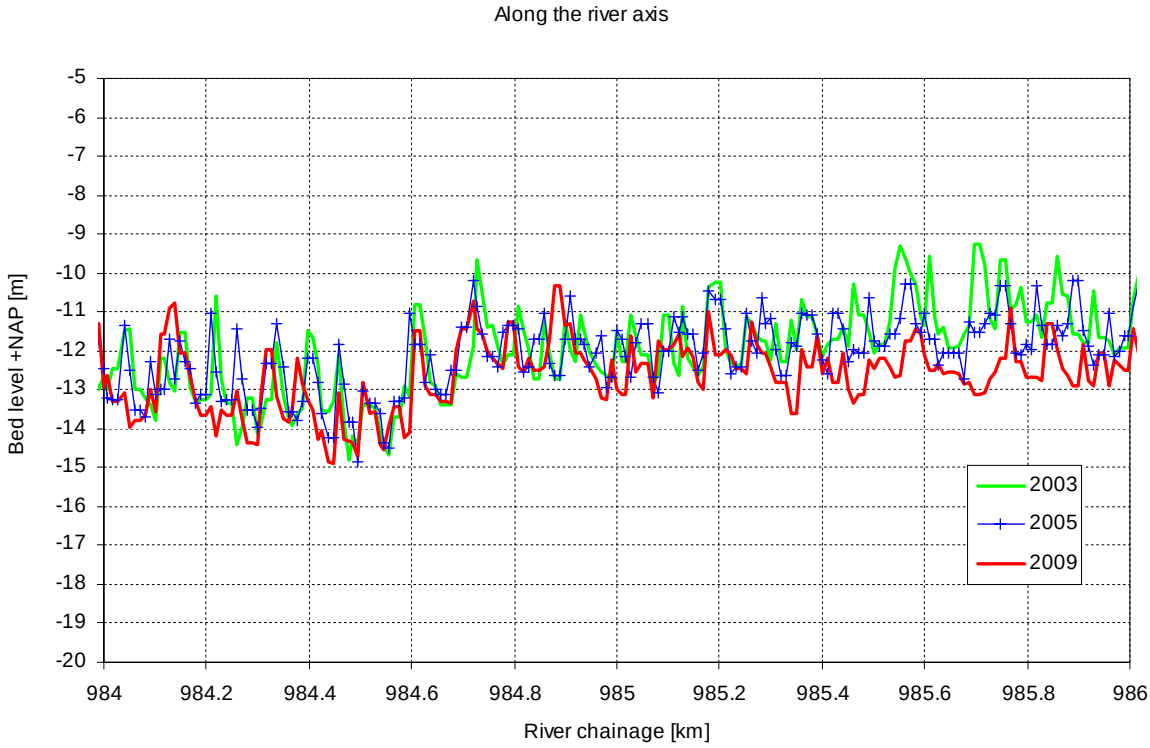

Figure 35 Comparison of longitudinal profile along the river axis in the middle part of Dordtsche Kil

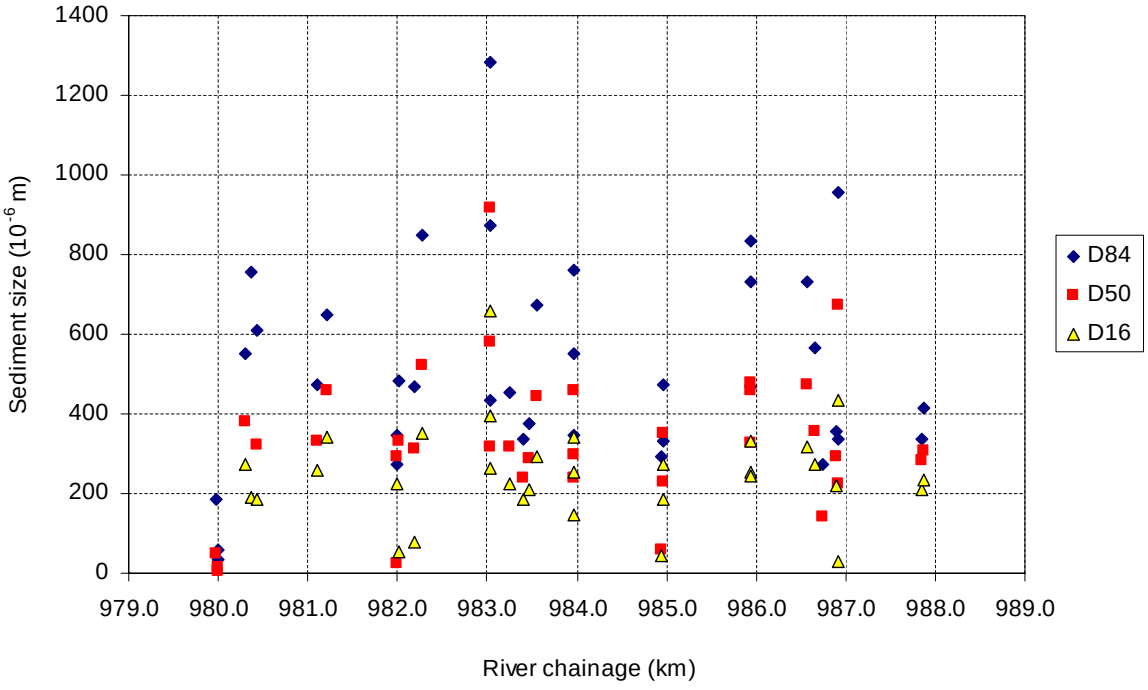

Figure 36 Variation of sediment characteristic along the Dordtsche Kil (sampling seems to be made at different spots in some cross-sections, i.e. left, middle and right)

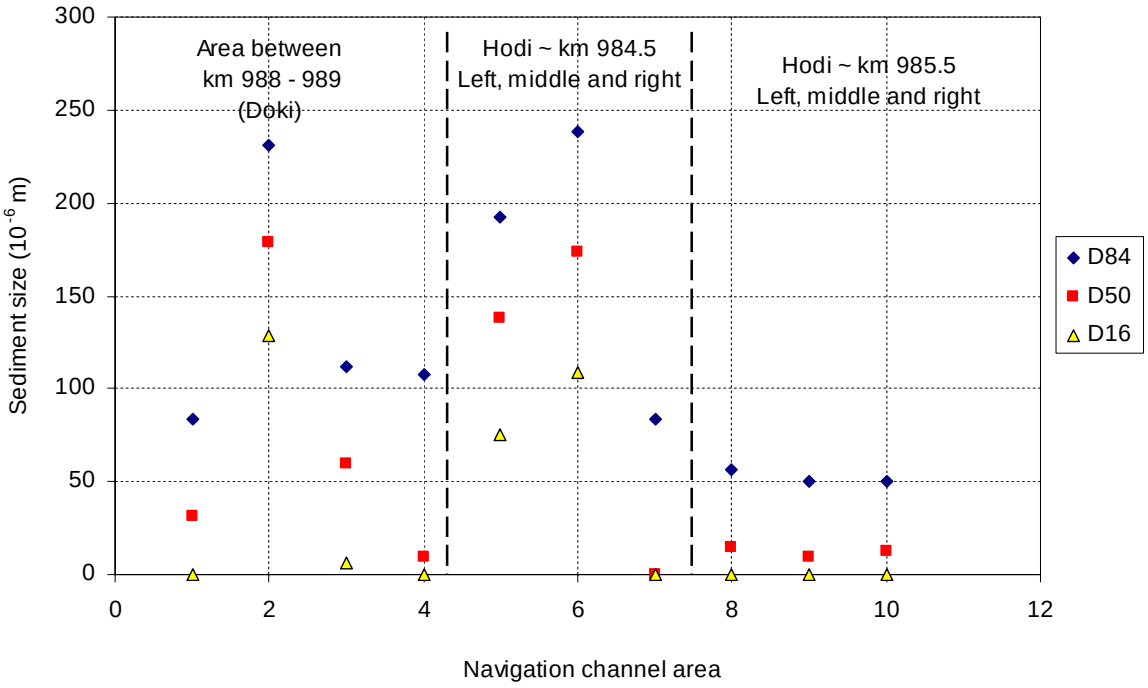

Figure 37 Sediment characteristics at the Dordtsche Kil-Hollands Diep area in the navigation channel

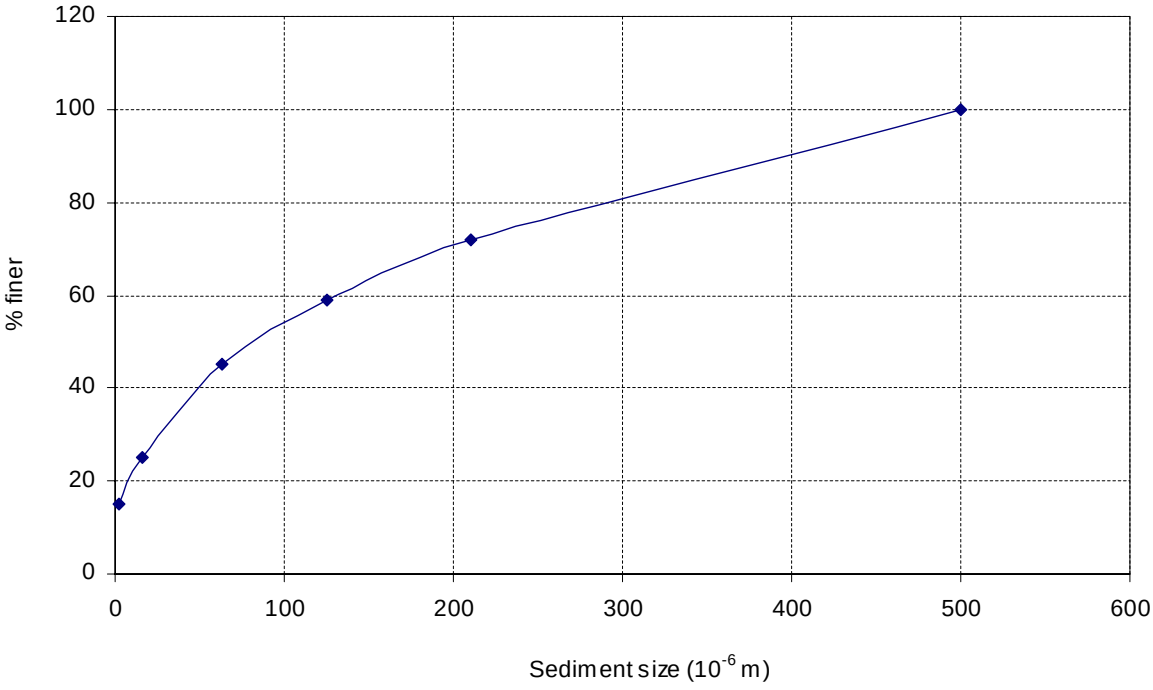

Figure 38 Grain-size distribution at Oude Maas

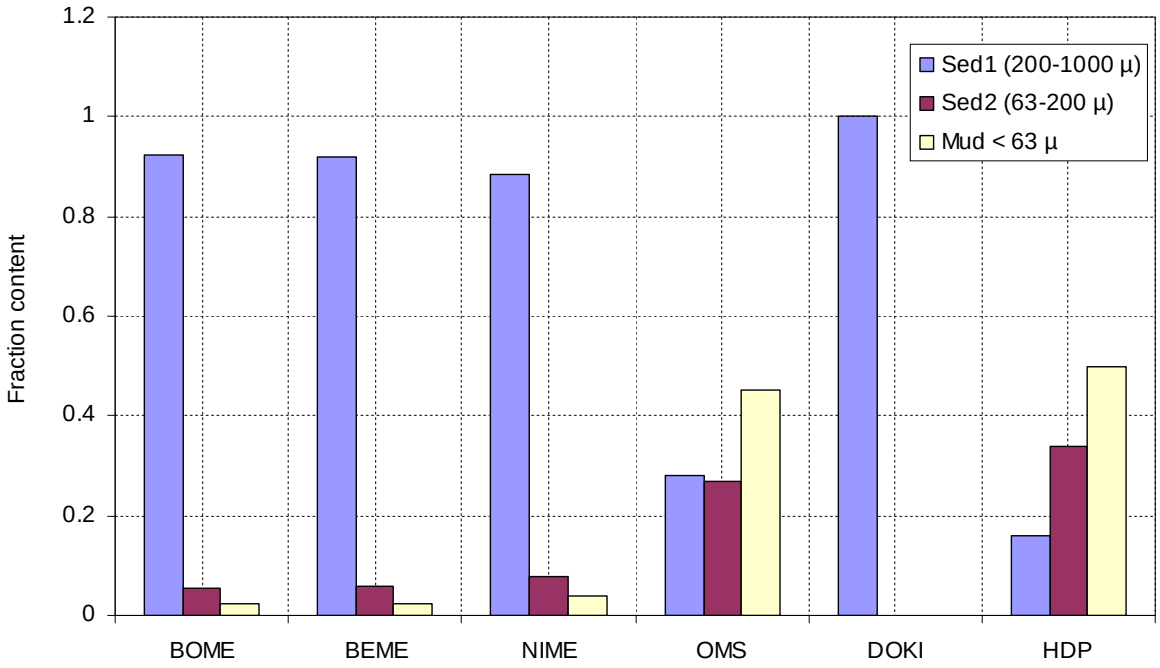

Figure 39 Faction content in each computational domain (HDP contains two domains, i.e. hdp and mw4 and fraction content OMS DOKI and HDP has been used for 5th domain, see Figure 40)

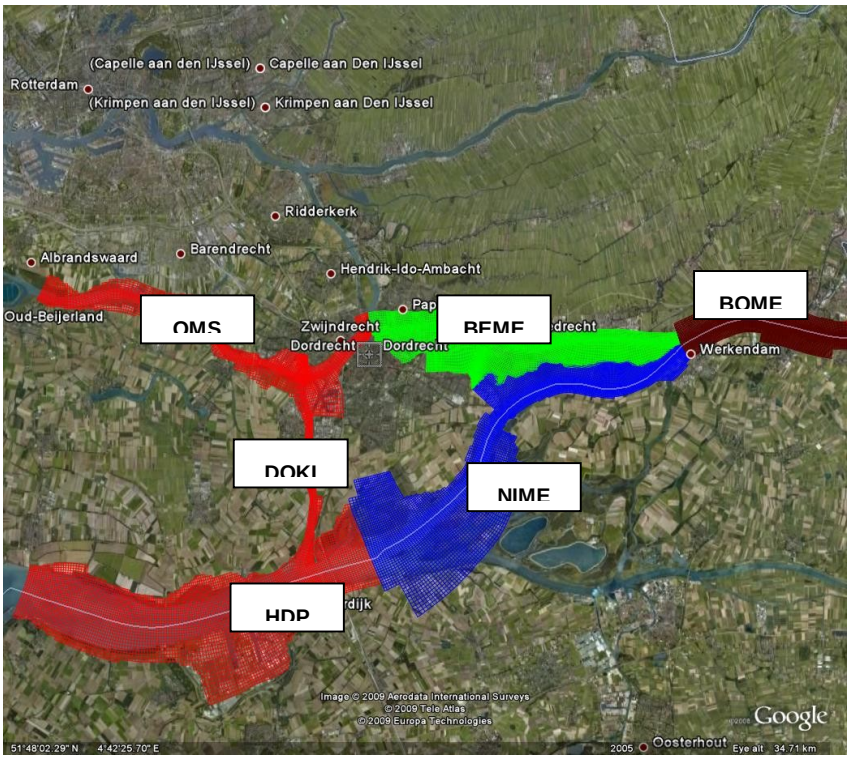

Figure 40 Domain location for different sediment distribution

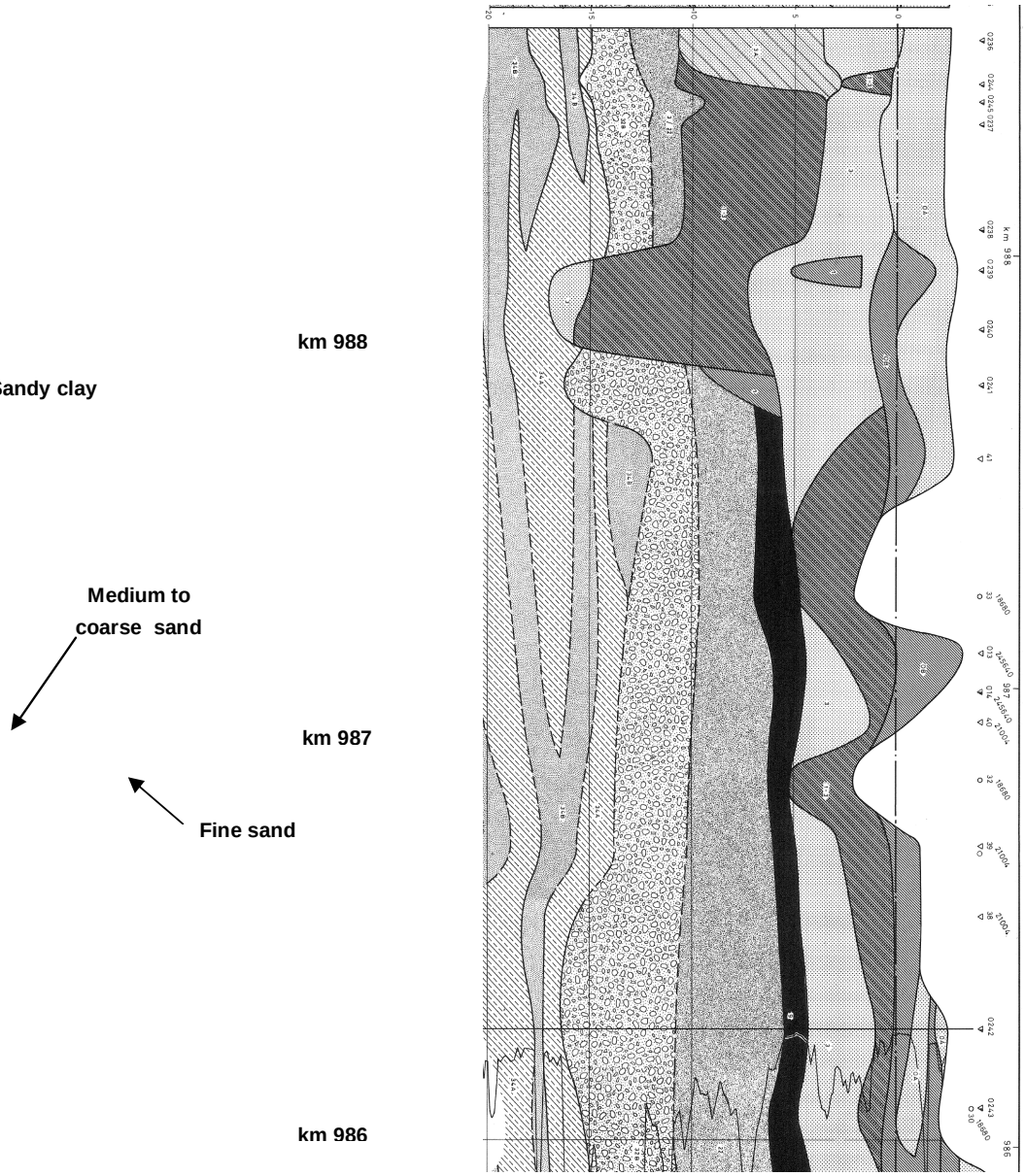

Figure 41 Geological survey along the west (left plot) and east (right plot) banks of Dordtsche Kil (south part in the region of HSL tunnel)

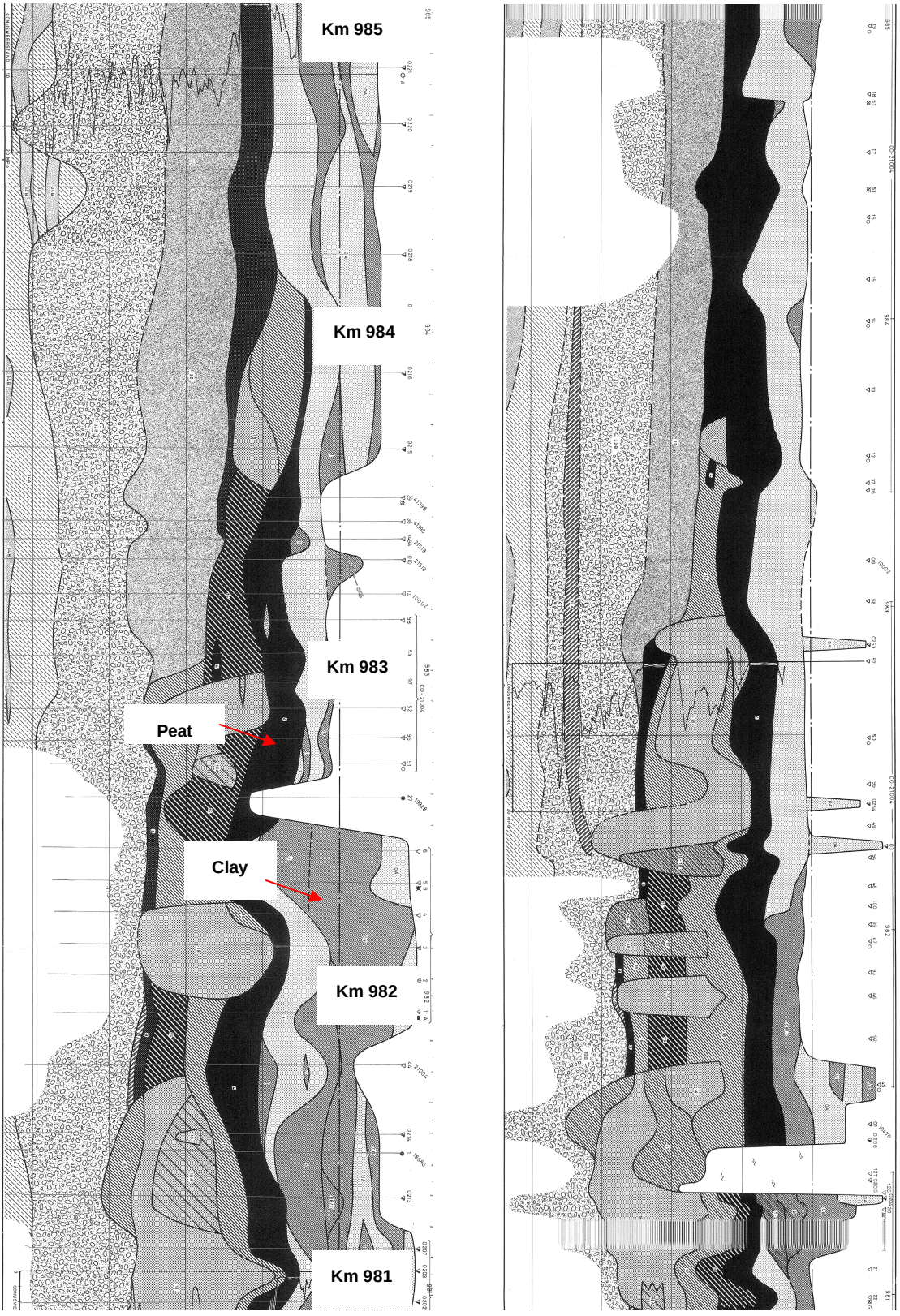

Figure 42 Geological survey along the west (left plot) and east (right plot) banks of Dordtsche Kil (middle and north part near Kil tunnel)

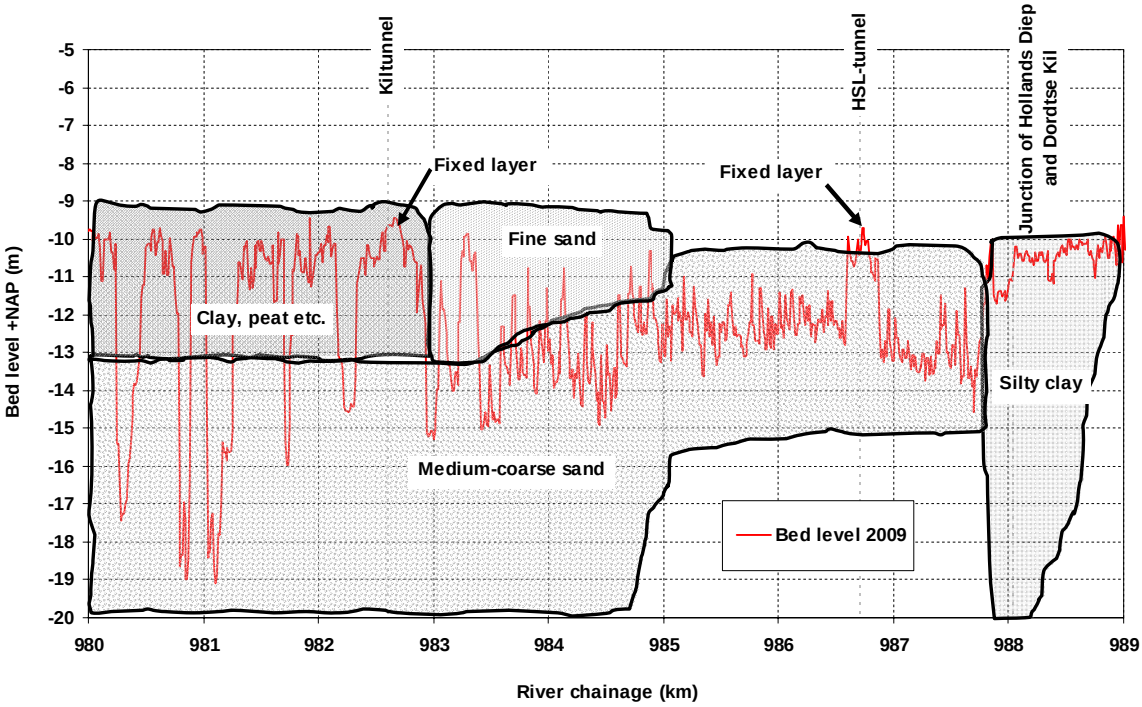

Figure 43 An approximate sketch of river bed characteristics along Dordtsche Kil (Bed level is depicted along the river axis)

4.2 Sediment transport

4.2.1 Transport formulation for bed load and suspended load considering mud fraction

In this computation, the formula of Van Rijn (TR2004/2007) with some new features (2007) has been used, which includes the suspended sediment transport (considering advection-diffusion of sediment concentration). The formula has been developed as a unified for both wave and currents. However, this study concerns only current part.

The bed load transport formulation reads as follows:

$$q_b = \gamma \rho_s f_{silt} d_{50} D_*^{-0.3} \left(\frac{\tau_b^{'}}{\rho} \right)^{0.5} \left[\left(\frac{\tau_b^{'} - \tau_{b,cr}}{\tau_{b,cr}} \right) \right]^{\eta} \qquad (1.1)$$

with,

$$\tau_b^{'} = 0.5 \rho f_c^{'} U_\delta^2 \qquad (1.2)$$

$$f_c^{'} = 8g \left[18 \log \left(\frac{12h}{k_{s,grain}} \right) \right]^{-2} \qquad (1.3)$$

$$D_* = d_{50} \left[\frac{(s-1)g}{\nu^2} \right]^{1/3} \qquad (1.4)$$

in which, $\tau_b^{'}$ = instantaneous grain-related bed-shear stress; $f_c^{'}$ = grain friction coefficient due to current; U_δ = instantaneous current velocity; $\tau_{b,cr}$ = critical shear stress; D_* = dimensionless

particle size; f_{silt} = silt factor = d_{sand}/d_{50} (f_{silt}= 1 for $d_{50} > d_{sand}$); γ = calibration coefficient (= 0.5); η = exponent (= 1, calibrated value).

Earlier, Van Rijn (1993) proposed the approximated simplified form that reads as:

$$q_b = \alpha_b \rho_s u h \left(d_{50} / h \right)^{1.2} M_e^{\eta} \qquad (1.5)$$

with

$$M_e = \frac{u - u_{cr}}{\left[(s-1) g d_{50} \right]^{0.5}} \qquad (1.6)$$

in which, h = flow depth; u = depth-averaged flow velocity; and u_{cr} = critical depth-averaged velocity.

Current Van Rijn formulation incorporates some new features, e.g. the effect of mud fraction on the critical shear stress of the sand particle that reads as follows:

$$\tau_{b,cr} = (1 + p_{mud})^3 \tau_{b,cr,0} \qquad (1.7)$$

in which, $\tau_{b,cr,0}$ = critical bed shear stress for pure sand; p_{mud} = fraction of mud (≤0.3).

However, mud fraction does not interact with the bed, and only affects the mobility of sand.

The main (changes) features of new Van Rijn formula (related to currents only) are as follows:

- The bed roughness is calculated as a sum of the roughness due to ripples, mega ripples and dunes.

  $$k_{s,c} = \left(k_{s,c,r}^2 + k_{s,c,mr}^2 + k_{s,c,d}^2 \right)^{0.5} \qquad (1.8)$$

- Different option for calculation of suspended sediment diameter.

  Based on following expressions:

  $$d_s = \max\left[d_{10}\left(1 + 0.0006\left(\frac{d_{50}}{d_{10}} - 1\right)(\psi - 550)\right) d_{50} \right] \quad for\ \psi < 550$$
  $$d_s = d_{50} \quad for\ \psi \geq 550\ and\ d_{50} > d_{silt} \qquad (1.9)$$
  $$d_s = d_{50} \quad for\ d_{50} < d_{silt}$$
  $$d_s = 0.5 d_{silt} \quad for\ d_{50} < 0.5 d_{silt}$$

  User-defined option:
  $d_s = fact * d_{50}$ (1.10)
  in which, fact = user-defined multiplication factor

- Shields criteria for fine sand

  $\theta_{cr} = 0.115 * D_*^{-0.5}$ *for* $1 < D_* \leq 4$ (1.11)
  $\theta_{cr} = 0.14 * D_*^{-0.64}$ *for* $4 < D_* \leq 10$

$\theta_{cr} = 0.04*D_*^{-0.1}$ *for* $10 < D_* \leq 20$
$\theta_{cr} = 0.013*D_*^{0.29}$ *for* $20 < D_* \leq 150$
$\theta_{cr} = 0.055$ *for* $1 < D_* \leq 4$

- Reference level (reference height) for current case

$a = max\ (0.5*k_{s,c,r}\ ;\ 0.01)$ (1.12)

For the non-uniform sediment case, d_i (diameter of each sediment fraction) is used instead of d_{50} in all formulations.

Also, the suspended sediment transport has been considered in this study.
For computing suspended sediment transport, a depth-integrated model of Galappatti (1983) has been implemented in Delft3d, which is based on the 2D advection-diffusion equation (in a vertical plane) with a boundary condition near the bed. This approach does not consider the non-uniform flow (i.e. spatial variation of concentration in streamwise and transverse directions is zero), but considers the unsteadiness (it is variable with time). The first order form for the depth-averaged concentration reads as follows:

$$c_a = c(t) + T_A \frac{dc}{dt} \quad (1.13)$$

where c_a = equilibrium concentration; T_A = adaptation time

The characteristic time scale (adaptation time), T_A, is calculated as:

$$T_A = \frac{\gamma_1}{\gamma_0}\frac{h}{w_s} \quad (1.14)$$; in case of imposed concentration at reference level

$$T_A = \frac{\gamma_1 + 1}{\gamma_0}\frac{h}{w_s} \quad (1.15)$$; in case of imposed vertical concentration gradient at reference level (i.e. Neumann boundary condition)
where, γ_1 and γ_0 = shape factors; h = flow depth; w_s = settling velocity.

The reference concentration is calculated by using Van Rijn formula:

$$c_a = 0.015(1 - p_{clay})f_{silt}\frac{d_{50}}{a}\frac{T^{1.5}}{D_*^{0.3}} \quad (1.16)$$

a = reference height.

Then, the suspended sediment load can be calculated as:

$$q_{s,c} = \int_a^h ucdz \quad (1.17)$$

Or, the bed level change due to sediment concentration can be calculated directly using entrainment or deposition flux.

A simplified formula of Van Rijn for suspended sediment transport under steady flow reads as follows:

$$q_s = \alpha_s \rho_s u d_{50} M_e^{\eta} D_*^{-0.6} \quad (1.18)$$

with α_s = 0.012 and η = 2.4

However, this formulation was not used herein (possible to use simplified Van Rijn formula instead of using advection-diffusion????)!!!

4.2.2 Flow and sediment boundary condition

Sediment transport analysis has been carried out for the average flow condition with a constant upstream discharge (=1590 m^3/s), since the flow appears to be mainly driven by downstream tidal flow. The downstream boundaries including Noord River are time-series water depth, i.e. tidal boundary (Figure 44). In addition, the time series of discharge extraction-insertion at Nieuwe Merwede (at the junction with Amer) has been extracted from the SOBEK simulation (Figure 45).

The equilibrium sediment transport has been assigned at the boundaries.

4.2.3 Computation of bed and suspended sediment transport without morphological update

We have attempted to compute the sediment transport, particularly with an emphasis on the Dordtsche Kil and Hollands Diep to get some impression on instantaneous transport of bed and suspended load and the effect of tide on residual transport at Dordtsche Kil.

Computational result on instantaneous transport through different river sections has been depicted in Figure 46 -Figure 52. From these results, the residual transport in Dordtsche Kil appears to be towards north. The bed load component is low in comparison to suspended sediment. On the other hand, total transport capacity at the upstream part of the Hollands Diep and Amer near the Nieuwe Merwede appears to be comparatively low (almost twice; Figure 51 and Figure 52). Moreover, the bed load is almost negligible in comparison with suspended sediment in Hollands Diep area, which means that the suspended sediment transport under the tidal effect is more pronounced (given the computational condition and transport formulation, used in this study)..
It appears that no sediment is transported from upstream part towards the Hollands Diep area (under the given averaged flow and sediment condition). This can also be seen from the result of the sediment availability (Figure 53), where we have traced the sediments and mud faction coming from upper part of Hollands Diep (i.e. domain ‘mw4’). The available mud fraction at the junction of the Hollands Diep and Dordtsche Kil is only locally available sediment mass, and there is hardly any transport from the upstream part. This requires a careful study of the upstream branches with this sediment transport formulation.

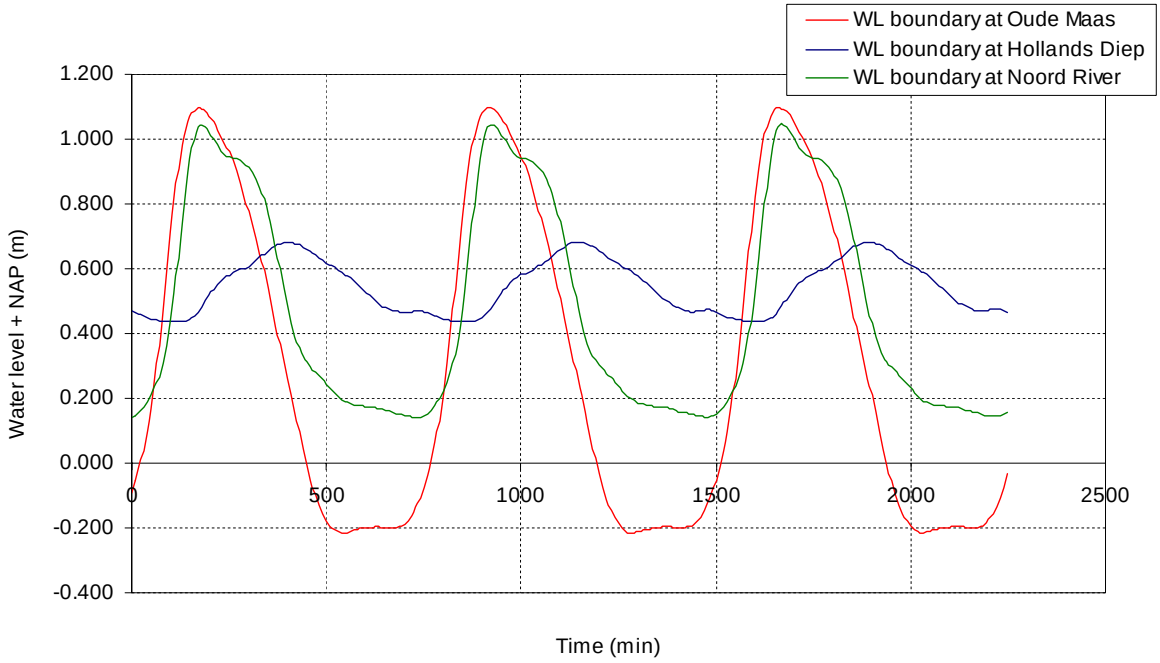

Figure 44 Tidal boundaries at the downstream (only a fragment)

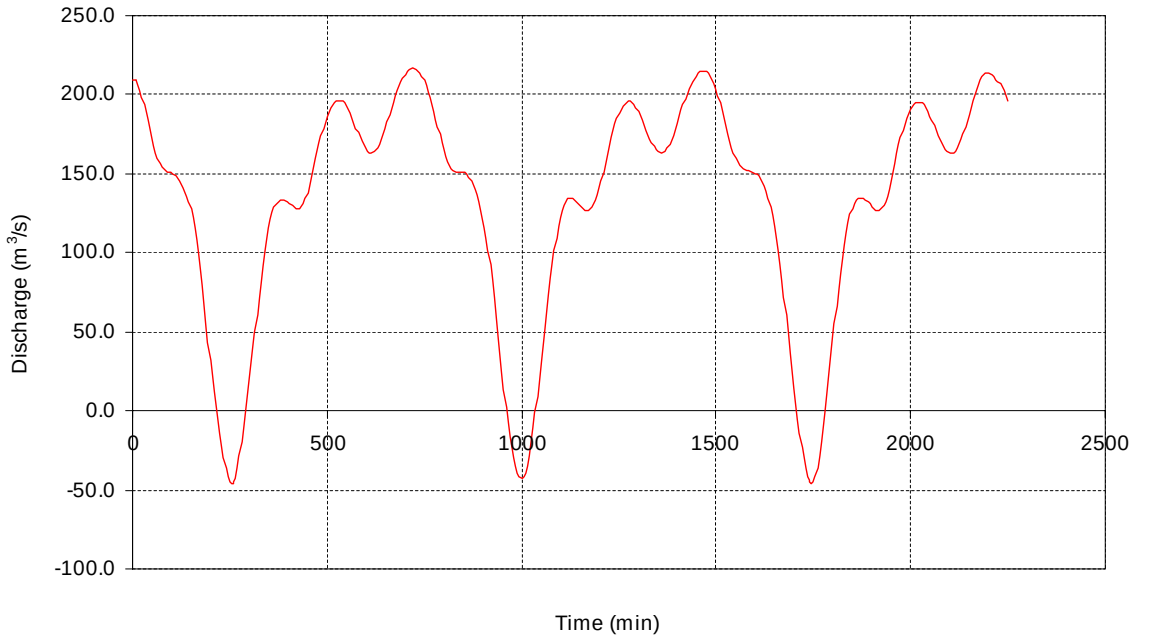

Figure 45 Discharge extraction/insertion at the Nieuwe Merwede near the junction with Amer (only a fragment)

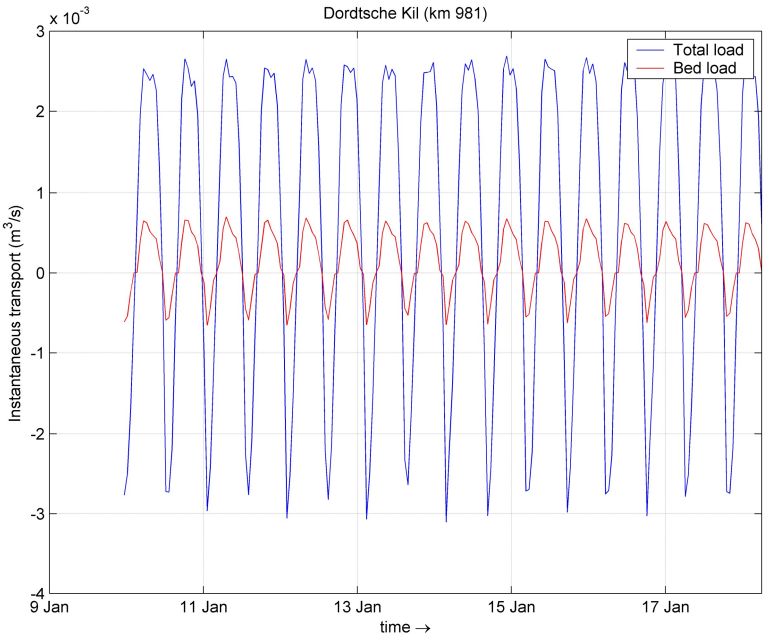

Figure 46 Instantaneous transport (bed load and total load) through the observation point at km 981 (Dordtsche Kil)

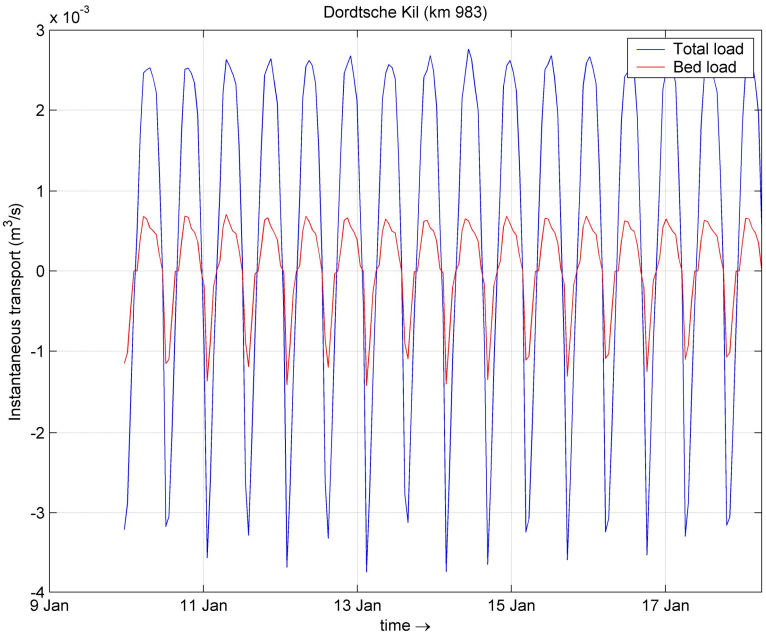

Figure 47 Instantaneous transport (bed load and total load) through the observation point at km 983 (Dordtsche Kil)

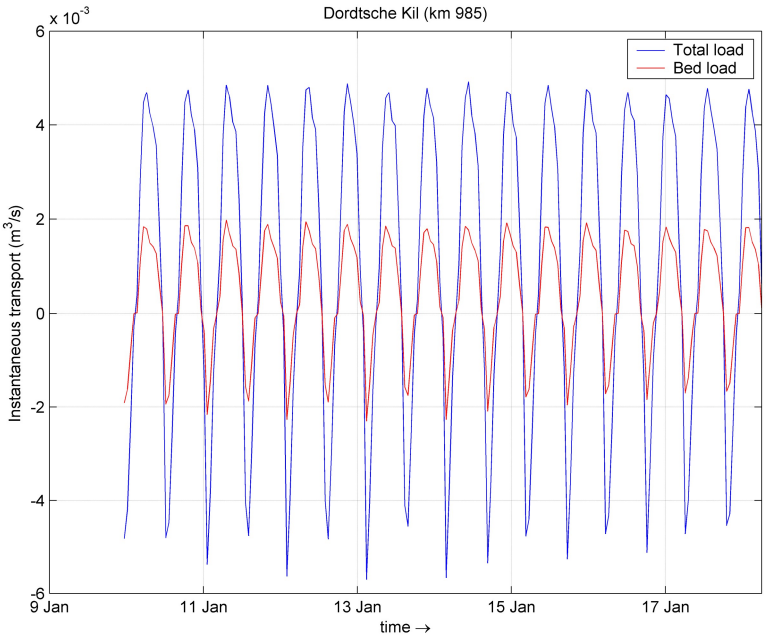

Figure 48 Instantaneous transport (bed load and total load) through the observation point at km 985 (Dordtsche Kil)

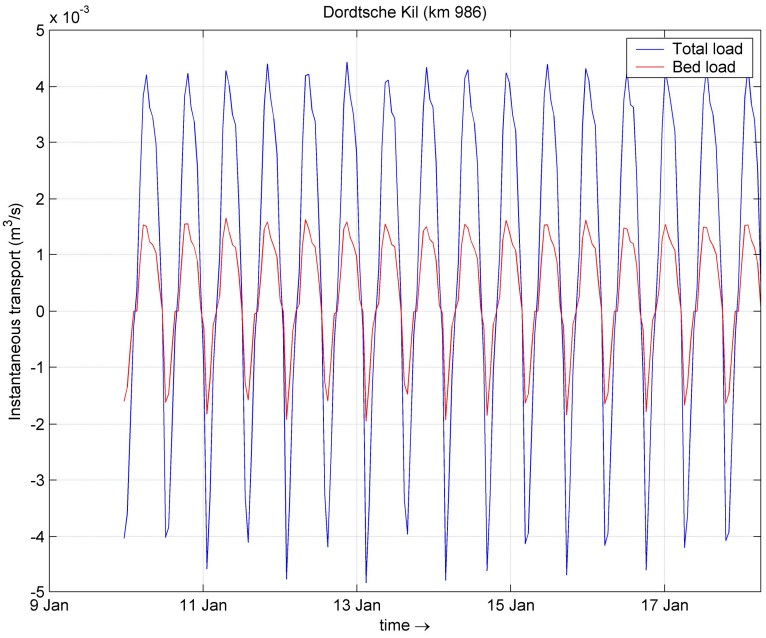

Figure 49 Instantaneous transport (bed load and total load) through the observation point at km 986 (Dordtsche Kil)

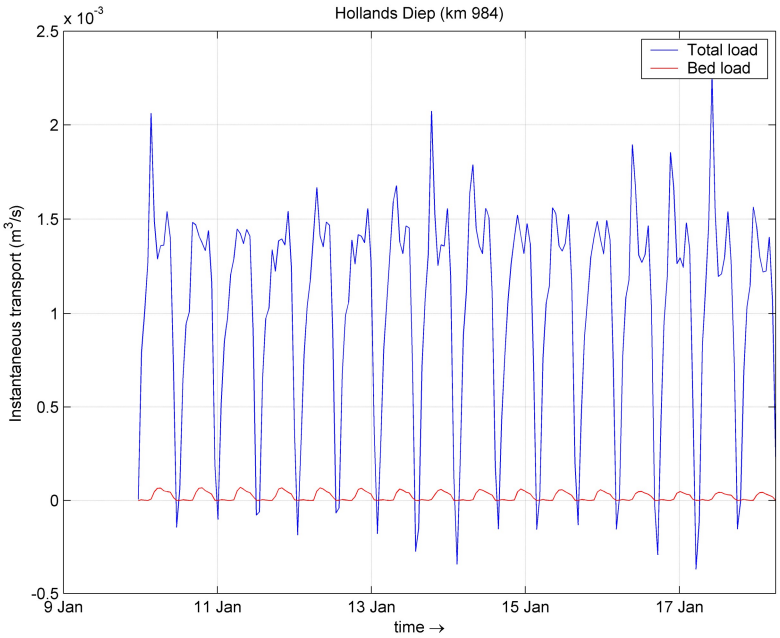

Figure 50 Instantaneous transport (bed load and total load) through the observation point at km 984 (junction of Hollands Diep and Dordtsche Kil)

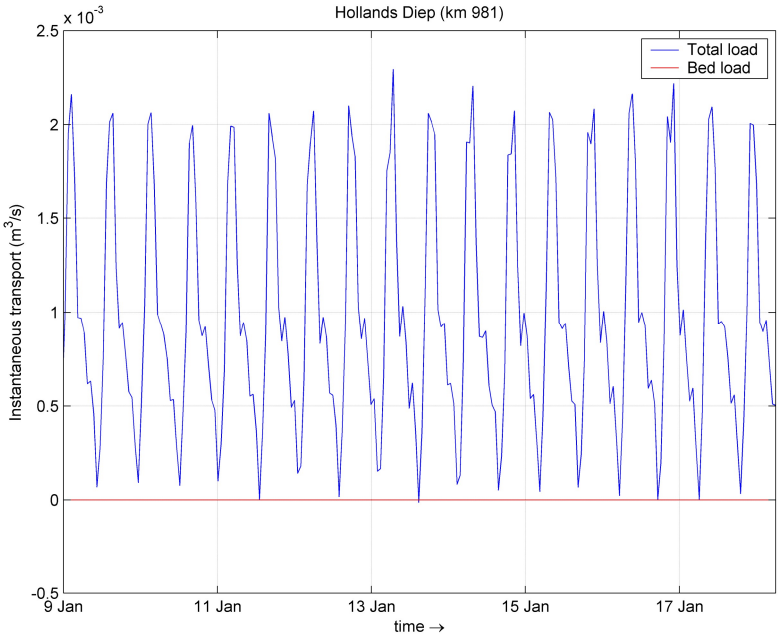

Figure 51 Instantaneous transport (bed load and total load) through observation point at km 981 (Hollands Diep; model domain 'mw4')

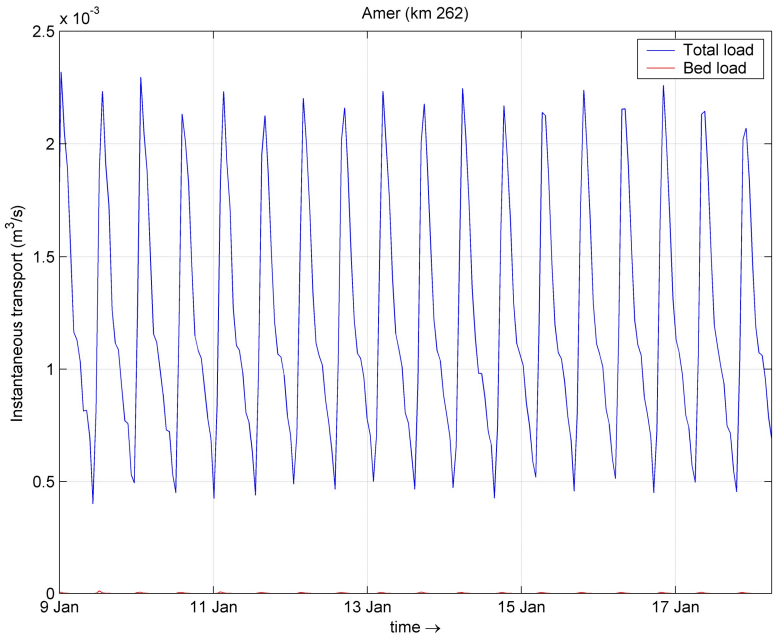

Figure 52 Instantaneous transport (bed load and total load) through observation point at km 262 (junction of Amer and Nieuwe Merwede)

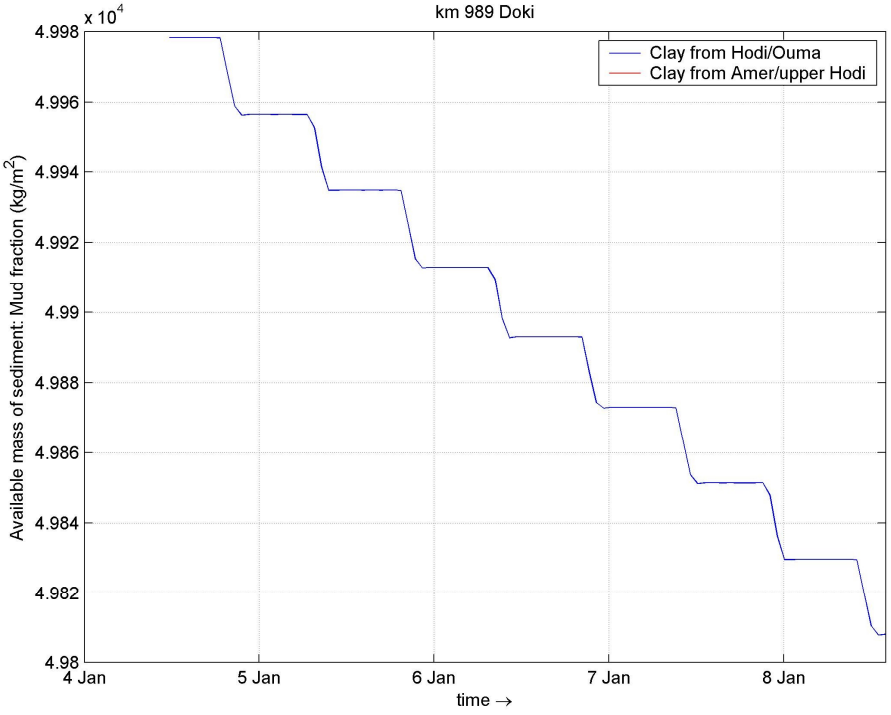

Figure 53 Variability of the available mass of mud fraction at the junction of Dordtsche Kil and Hollands Diep (km 989)

4.3 Morphological computation

4.3.1 General consideration

Some preliminary morphological computations have been carried out to test the model performance. Detailed calibration has not been performed, and this study has mainly been focused on replicating the morphological behaviour at Dordtsche Kil. Also, the morphology of other upstream branches as well as Oude Maas was not checked, and even bed level was not updated in some simulations. So far, the upstream models have been used for uniform sediment with DVR settings of Van Rijn transport formulation, and still not fully calibrated. In this study, the approach is somehow new with non-uniform transport considering mud fraction and transport formulation of Van Rijn with some new features.

After having a number of preliminary simulations, it has been decided to consider only Dordtsche Kil area as a mobile part (South part of the Dordtsche Kil, which contains the coarse sediment) within the scope of this study. We have attempted to put emphasis on the bed development in the area of fixed layer over HSL tunnel that seems to be an important issue.

4.3.2 Flow and morphological boundary conditions

For the average flow condition, the same boundary condition has been used as described in previous section. The morphological analysis of Dordtsche Kil has been performed for 10 years (morphological time) of simulation. In addition, a couple of test simulations have been conducted for a schematised annual hydrograph that includes a low and a high discharge levels in addition to the average condition (Figure 54). The downstream boundaries and time-series of discharge extraction/insertion have been extracted from SOBEK simulation for each discharge levels (Figure 55 to Figure 58).

Morphological factor of 50 has been used for averaged flow condition; whereas for schematised discharge case, the value of 10, 25 and 25 has been used for the discharges of 3930 m^3/s, 1590 m^3/s and 998 m^3/s respectively. We try to keep morfac as small as possible so as to include properly the tidal effect on sediment transport and morphology, and at the same time somehow keep the reasonable computational time.

4.3.3 Sediment fractions and fixed/non-erodible layers

The fraction content for each domain and region has been mentioned earlier (Figure 39 and Figure 40). As it has already been pointed out, the problem is that the median diameter based on these fraction contents seems to have sharp transition from one domain to another, e.g. quite coarse in Beneden and Nieuwe Merwede and Dordtsche Kil, whereas fine bed material in Oude Maas and Hollands Diep. This appears to be somewhat problematic for morphologic study. For the accuracy, it is necessary to include more fractions. Also, in earlier studies the upstream models include calibrated Van Rijn formulation for uniform sediment. So, in this study, we have not made use of these fraction contents, and basically did not deal with the morphology of other branches rather than Dordtsche Kil.

Fixed layers in the area of Kil Tunnel and HSL tunnel are easy to identify. Besides, there are number of non-erodible/ semi-erodible layer in the Dordtsche Kil area that has to be included in the model.

Based on the data analysis, that has been done in previous section, the fixed layer and sediment thickness has been defined in Dordtsche Kil as shown in Figure 59. Since, this part of the Dordtsche Kil contains uniform fraction, the active layer contains only one sediment fraction (the layer thickness of other fractions are simply zero). The river bed in northern part of Dordtsche Kil has been made mostly non-erodible except some places where presence of some sandy pits can be seen from the data analysis.
On the other hand, Oude Maas and Hollands Diep area contains all fractions including mud. So, the layer thickness of each fraction is depicted in Figure 60 - Figure 61. Number of places in Oude Maas has been made fixed as well; though the morphological analysis has not been done in this study (the preliminary analysis shows large erosion in movable parts of the Oude Maas, so for the modelling it is necessary to define the precise active layer thickness). In most simulations, we have simply made all part of the river bed fixed except for Dordtsche Kil.

The bed level in the alluvial part, deduced from Baseline projection, has been replaced with 2008-2009 multibeam data (it is to be noted that no dredging activities appear to have been taken place after 2008).

4.3.4 Preliminary results

Our analysis is confined within Dordtsche Kil in present study.

The morphological development in the HSL region shows erosion in both south and north of the tunnel. Temporal variation of reach-averaged erosion in north of HSL (from km 986.6 to km 983.5) appears to be slower than in south part (from km 988 to km 987). It should be noted that the erosion starts to grow faster in north part of HSL once erosion reaches the non-erodible layers in south part. This implies that the supply-limited condition at the south part leads to more active erosion at north part (Figure 62). It appears that the erosion in south part is triggered by not only fixed layer on HSL tunnel, but also a clay layer with sand and silt in the region of km 988 that appears to behave like a non-erodible layer (as can be seen in Figure 41 - Figure 42). So, the fast erosion rate might be attributed to the combined effect of fixed layer and non-erodible layer. However, comparing the multi-beam data of 2005 and 2009, north of HSL tunnel also reveals large erosion (part of this might be attributed to the dredging; **we have to check the exact locations of dredging activities at Dordtsche Kil**).

Furthermore, in our numerical simulation, the deep erosion can be seen right after this non-erodible layer in the region of km 988, which seems to be growing until it reaches non-erodible layer (Figure 63). Comparing the longitudinal profiles of 2005 and 2009 also reveals the similar trend as shown in data analysis. On the other hand, long-term computational result shows the filling up of the deep pits near Kiltunnel in the north part of Dordtsche Kil (Figure 63). The result is same for the case of simulation with schematized hydrograph. However, this is not evident from the multi-beam data (comparing the 4 years of bed development). In the model, the deep pit appears to be filling up by the sediment transported from the south part. A 2D plot is depicted in Figure 64.
It is still difficult to precisely conclude whether this may occur in reality or is a model artefact. There is large velocity gradient apparently caused by sudden depth change due to the deep pit, which leads to the sedimentation inside the pit. It is also possible that in reality there is not much movable layer available in the south part (we have defined about 2 m of mobile sediment in this area). In this case, not much sediment would be available to be transported towards the

deep pits. This has to be analyzed more carefully in future work (also in terms of how good new transport formulation works for this case).

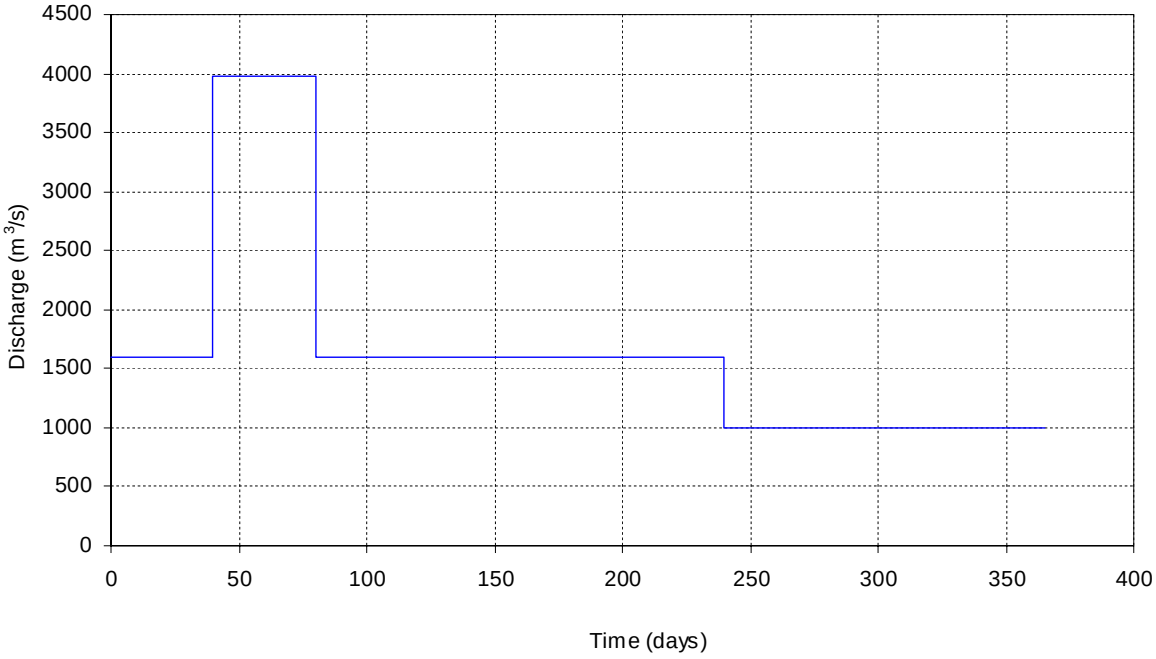

Figure 54 Schematised annual hydrograph for a test simulation

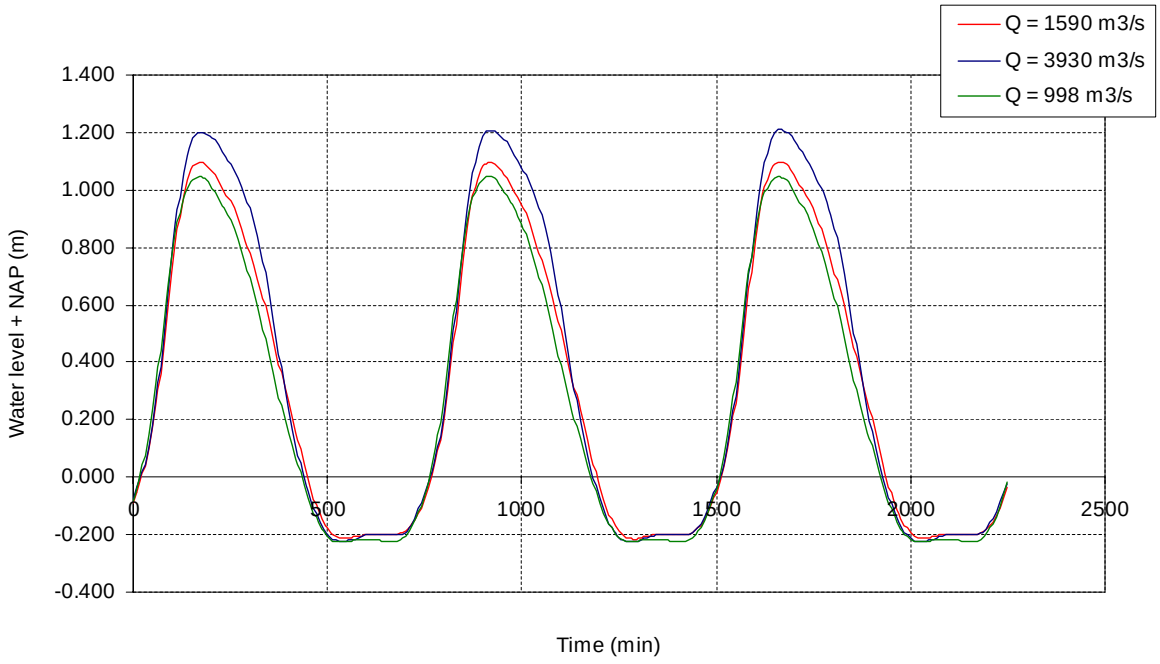

Figure 55 Water level boundary at Oude Maas for each discharge level

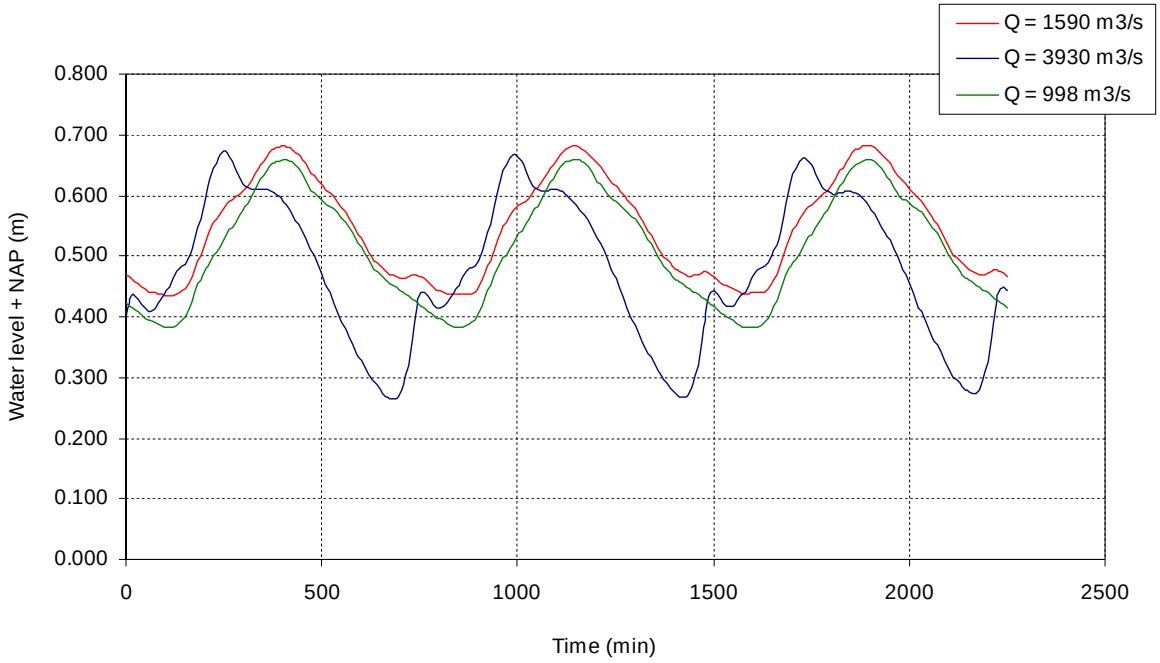

Figure 56 Water level boundary at Hollands Diep for each discharge level

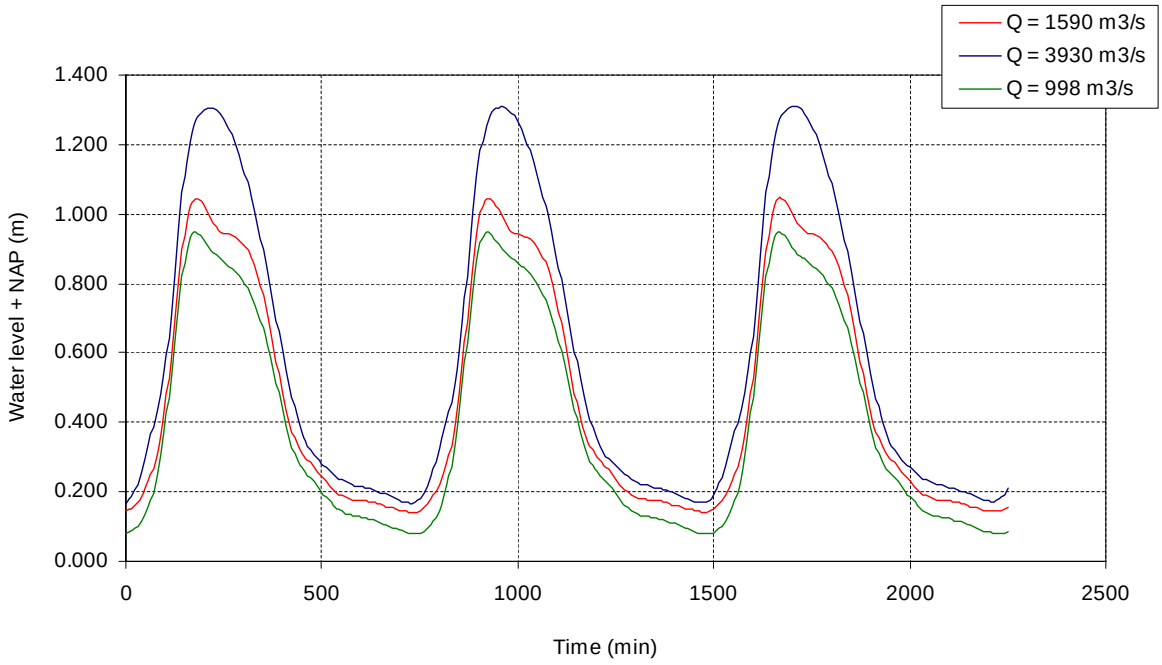

Figure 57 Water level boundary at Noord River

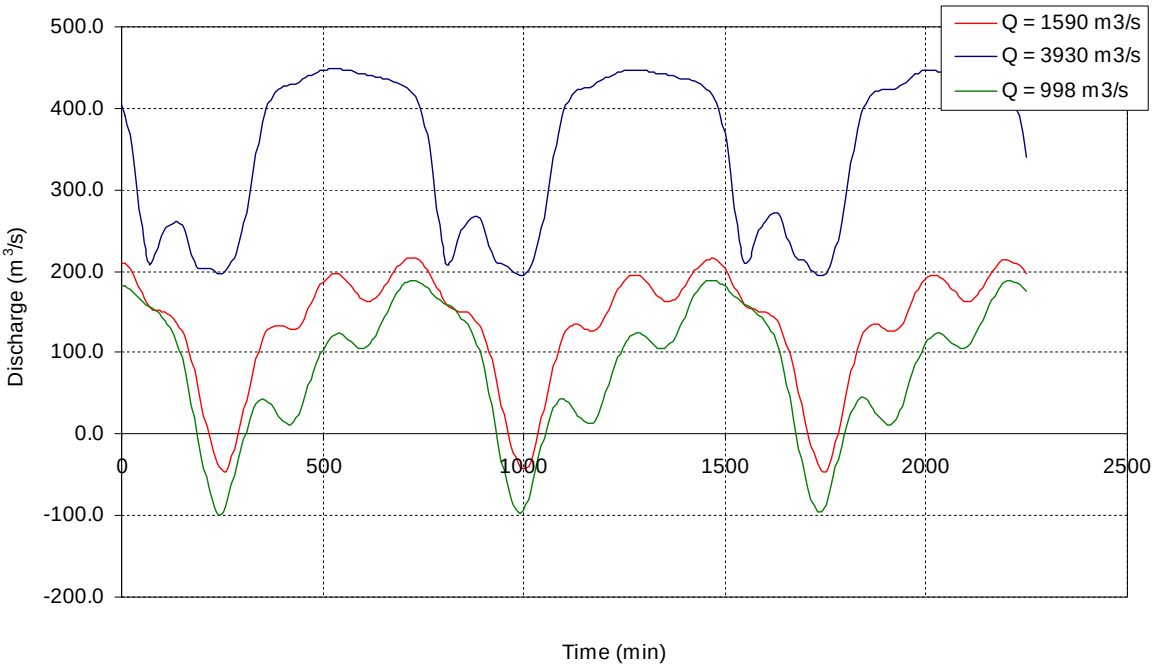

Figure 58 Discharge extraction/insertion at the junction of Nieuwe Merwede and Amer

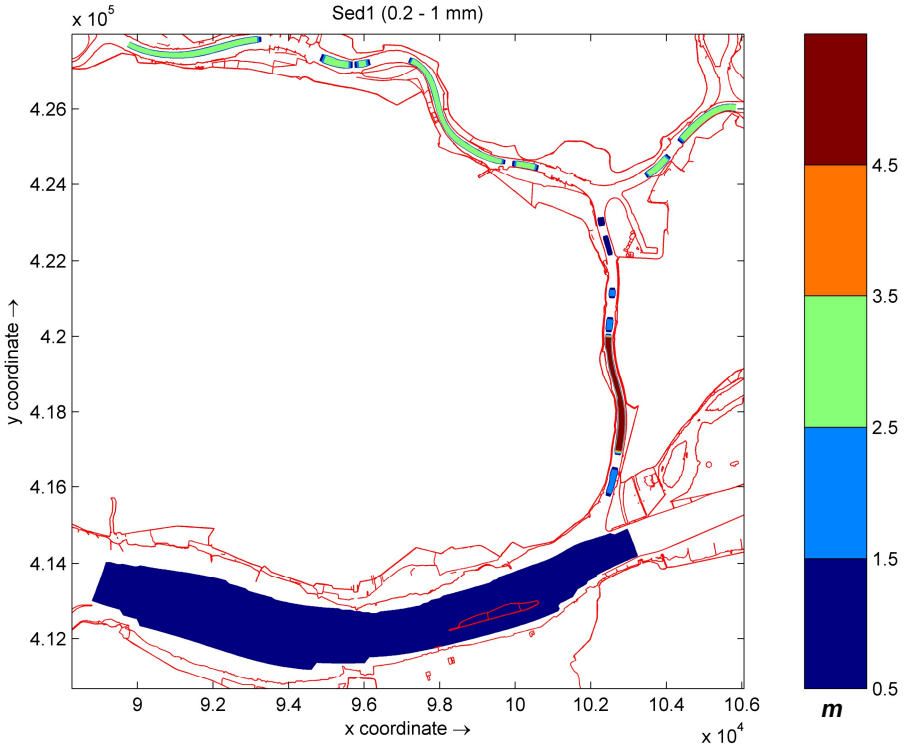

Figure 59 Thickness of active layer for fraction Sed1 (0.2 – 1 mm) in Dordtsche Kil (white parts denotes region with no sediment availability, i.e. fixed/non-erodible layer)

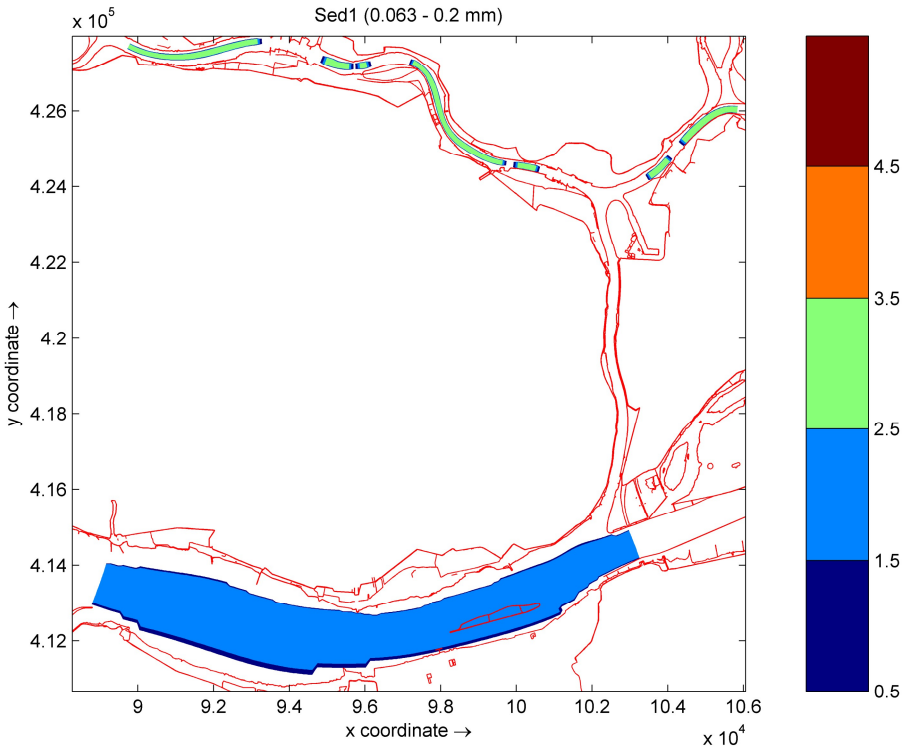

Figure 60 Thickness of active layer for fraction Sed1 (0.063 – 0.2 mm) in Dordtsche Kil

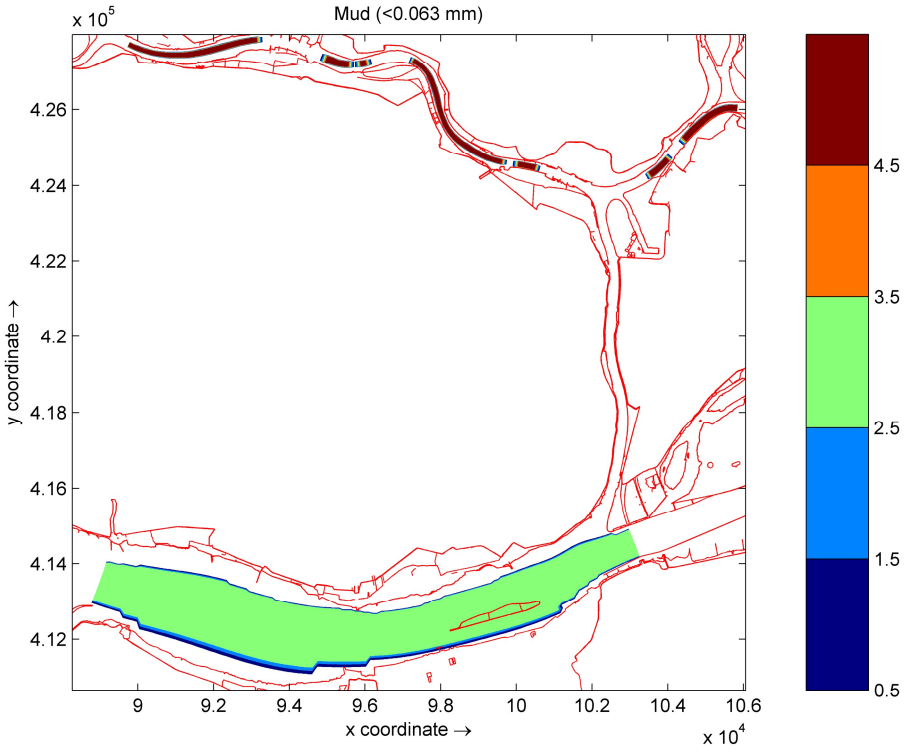

Figure 61 Thickness of active layer for fraction mud (< 0.063 mm)

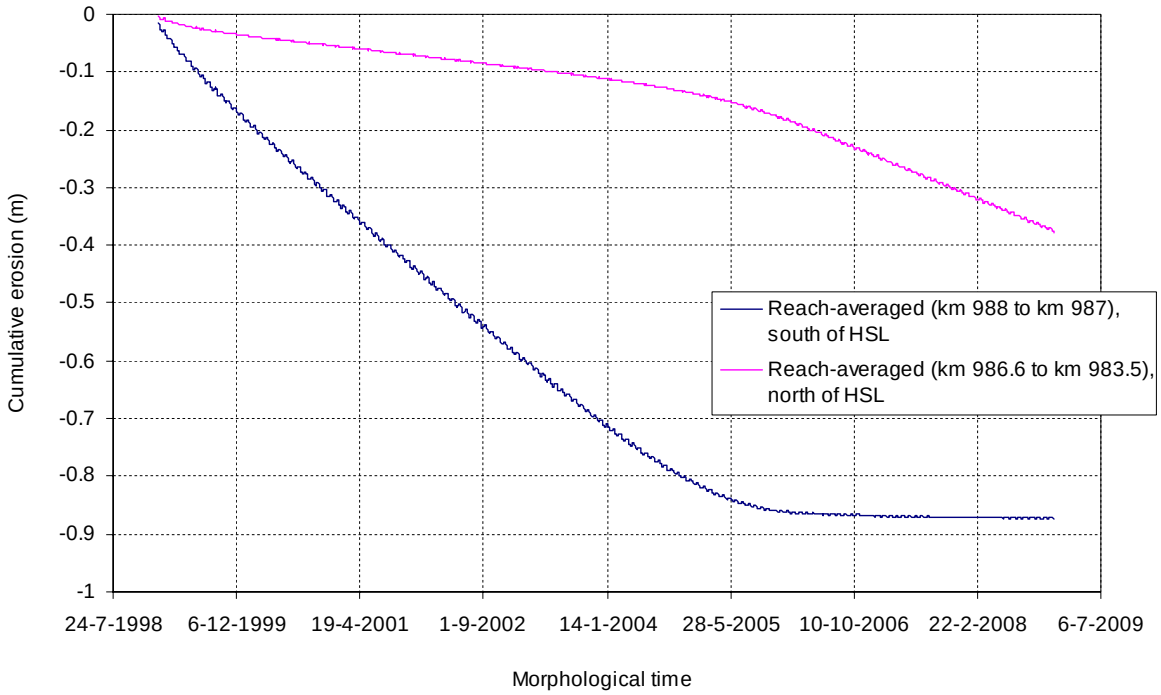

Figure 62 Temporal variation of reach-averaged erosion in south and north part of HSL tunnel

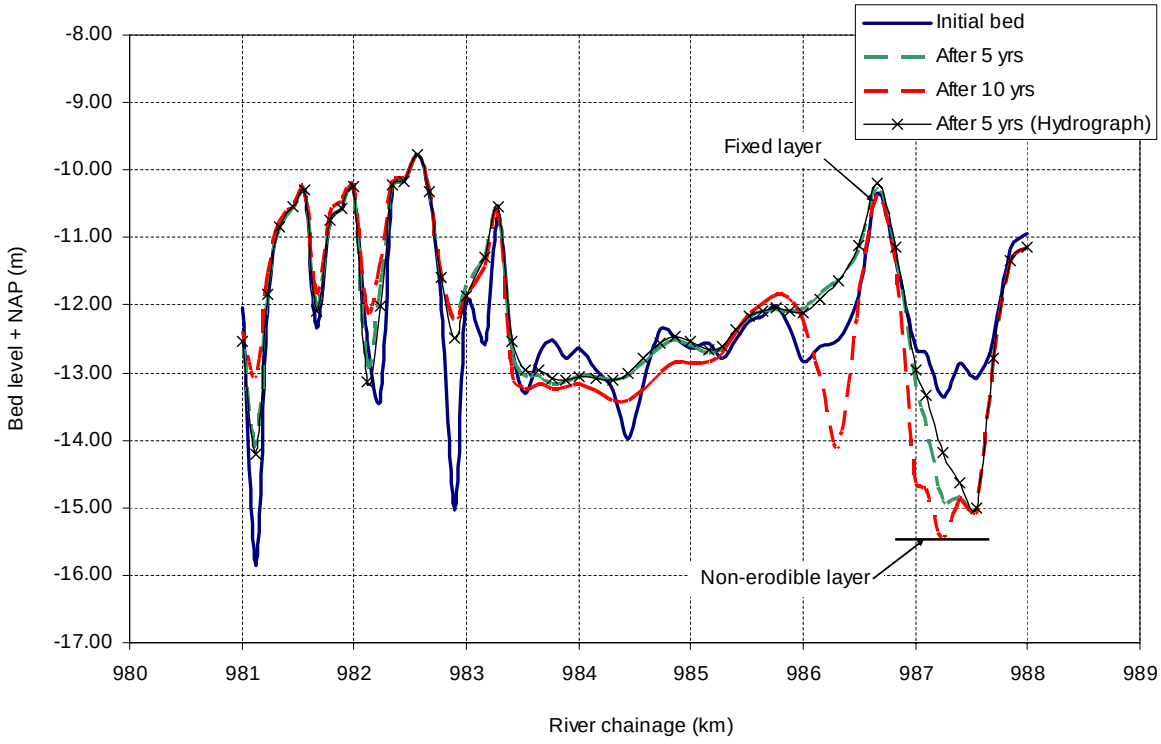

Figure 63 Longitudinal bed profile along the middle of Dordtsche Kil (n = 56), simulated by Deflt3D

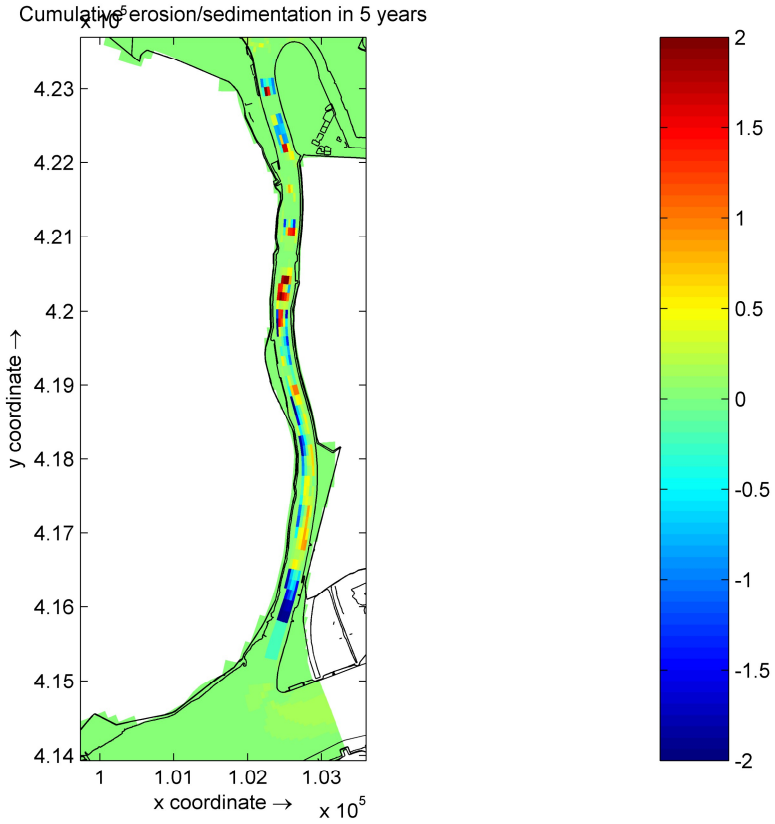

Figure 64 Cumulative erosion/sedimentation in Dordtsche Kil area after 5 years of morphological simulation

5 Summary and preliminary conclusions

The summery of this study and some preliminary conclusions can be outlined as follows:

- Based on an extensive hydrodynamic study, it can be inferred that the performance of the model is satisfactory. Model can reproduce the tidal-driven as well as residual flow characteristics in different branches in more or less consistent manner as SOBEK and WAQUA models. This does not necessarily imply the absolute correctness of the result, since even SOBEK and WAQUA results have not been verified for number of locations, e.g. for Dordtsche Kil, due to the absence of observed time-series data.

- Dordtsche Kil is the focal point of this study. It should be emphasized that the residual flow under averaged condition was found to be towards North, which is consistent with the previous studies.

- From the bed level comparison of 2005 and 2009 at Dordtsche Kil, it can be seen that the bed is eroding and the amplitude of the micro-scale features appear to be decreasing. The erosion appears to be more severe towards the northern part of the HSL tunnel, and even more pronounced along the east part of the river axis (i.e., along the outer bend, Figure 33). However, this might also be attributed to the dredging activities in this area (at least partly as there were some dredging activities during 2007 and 2008, namely ~ 56,000 and 106,000 m^3 respectively; but we have no information on the dredging locations).

- The comparison on longitudinal profiles is depicted in Figure 34 - Figure 35, which shows that the north part with non-erodible layers contain few deep pits, and do not show any noticeable bed level changes (Figure 34). Deep pits in both side of the fixed layer at Kil tunnel can be seen from this plotting, though they seem to be stable. Whereas, the middle part with sandy bed shows the sign of degradations as can be seen in Figure 35 (this might be attributed to the dredging activities as well).

- From the geotechnical survey result, it is evident that the movable layer in the river bed at Dordtsche Kil is within the limit of 5 m in southern part containing the medium to coarse sediment; whereas the northern part is comprised of non-erodible (semi-erodible) layers with peat and clay material. However, in northern part, coarse sand seems to be evident below the elevation of about -13 m + NAP (up to -20 m +NAP). Figure 43 gives an approximate quantitative impression of river bed characteristic along the Dordtsche Kil.

- The residual transport in Dordtsche Kil appears to be towards north. The bed load component is low in comparison to suspended sediment. On the other hand, total transport capacity at the upstream part of the Hollands Diep and Amer near the Nieuwe Merwede appears to be comparatively low (almost twice; Figure 51and Figure 52). Moreover, the bed load is almost negligible in comparison with suspended sediment in Hollands Diep area, which means that the suspended sediment transport under the tidal effect is more pronounced (given the computational condition and transport formulation, used in this study).

- The model does not reproduce any sedimentation in the junction of Dordtsche Kil and Hollands Diep area where the dredged navigation channel is located (i.e., the silting of in this region could not be reproduced by the model). There is no sediment being transported from the upstream, and the available mud fraction in this area is only locally available sediment mass. Since the major part of the bed material is mud, the transport mechanism appears to be more complex to be reproduced by using formulations for non-cohesive materials that we have used in this study. Moreover, a careful study of the all branches with Van RIjn (2007) sediment transport formulation should be done in future. The values of different parameters (e.g. calibration coefficients, reference concentration, settling velocity etc.) should be tested. In this study, we have used the original (default) settings.

- Computational result on the morphological development near the HSL region shows erosion in both south and north of the tunnel. Temporal variation of reach-averaged erosion in north of HSL (from km 986.6 to km 983.5) appears to be slower than in south part (from km 988 to km 987). It should be noted that the erosion starts to grow faster in north part once erosion reaches the non-erodible layers in south part. This implies that the supply-limited condition at the south part leads to more active erosion at north part (Figure 62). However, comparing the multi-beam data of 2005 and 2009, north of HSL tunnel also reveals large erosion (part of this might be attributed to the dredging; **we have to check the exact locations of dredging activities at Dordtsche Kil**).

- Computational result shows deep erosion right after the non-erodible layer in south part of HSL tunnel near km 988, which seems to be growing until it reaches non-erodible layer (Figure 63). Comparing the longitudinal profiles of 2005 and 2009 also reveals the similar trend (shown in data analysis).

- Long-term computational result (5-10 years) shows the filling up of the deep pits near Kiltunnel in the north part of Dordtsche Kil (Figure 63). The result is same for the case of simulation with schematized hydrograph. However, this is not evident from the multi-beam data (comparing the 4 years of bed development). In the model, the deep pit appears to be filling up by the sediment transported from the south part. It is still difficult to precisely conclude whether this may occur in reality or is a model artefact. There is large velocity gradient apparently caused by sudden depth change due to the deep pit, which leads to the sedimentation inside pit. It is also possible that in reality there is not much movable layer available in the south part (we have defined about 2 m of mobile sediment in this area). In this case, not much sediment would be available to be transported towards the deep pits. This has to be analyzed more carefully in future work (also in terms of how good new transport formulation as well as roughness definition work for this case).

- The extent and thickness of the active layers as well as non-erodible/fixed layers in Dordtsche Kil have been defined based on the analysis of the multi-beam data image and geotechnical survey result. The bed layer has been considered to be one fully mixed layer. In future study, the bed layer thickness for each fraction can be specified for the better prediction.

- In this study, the equilibrium boundary condition for suspended sediment transport has been used. It is also possible to impose the boundary conditions assigning the observed values for the better prediction of suspended load in all branches, particularly the silting of the Hollands Diep.

- The grid of the Dordtsche Kil has to be refined more for the better replication of the morphological behaviour.

For Appendix??

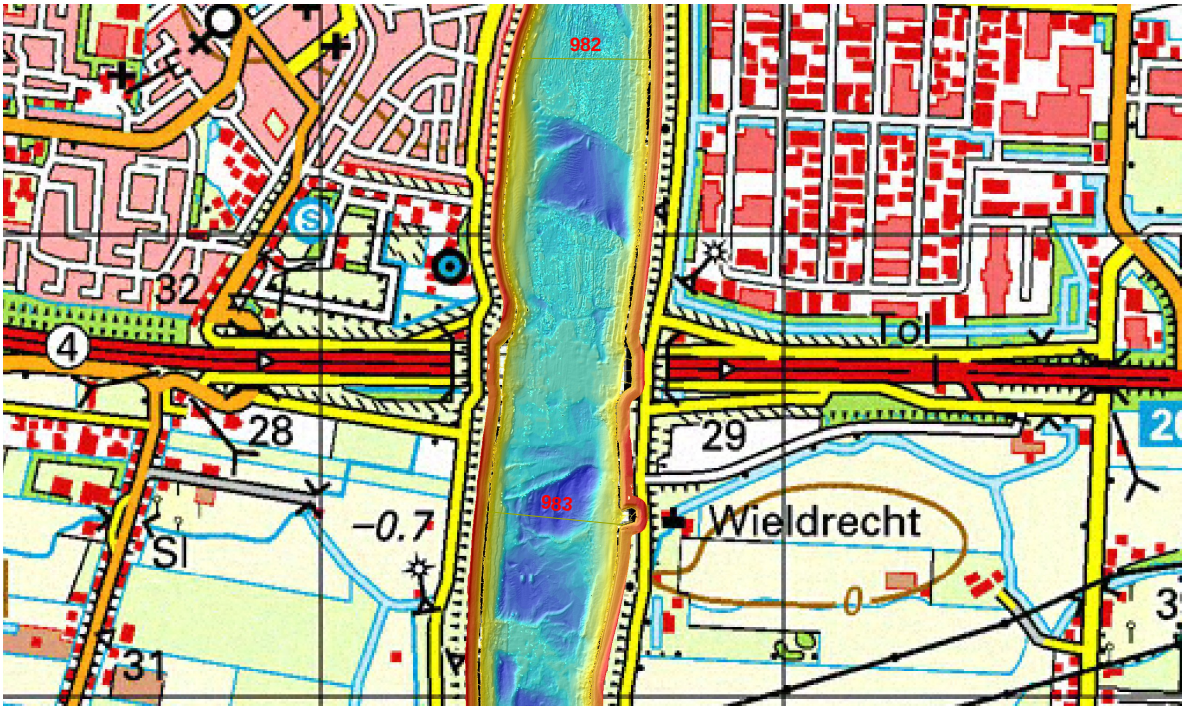
982
983
32
4
28
29
Tol
Wieldrecht
-0.7
Sl
31
0

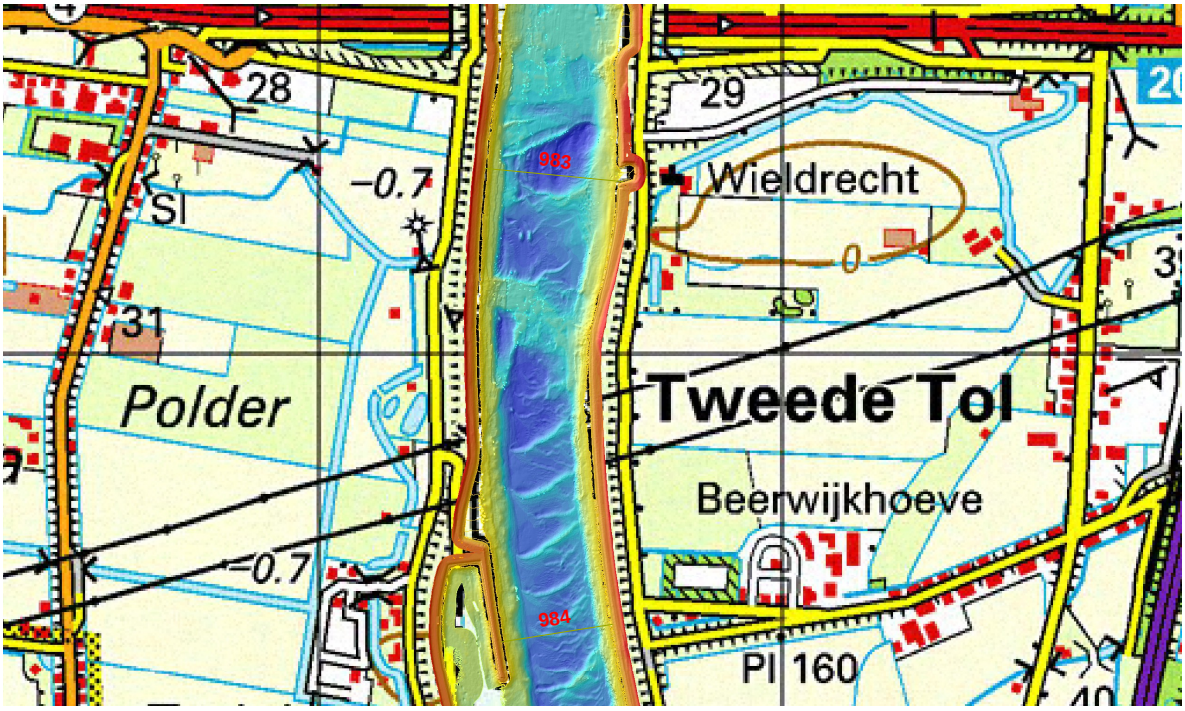
28
29
983
Wieldrecht
-0.7
Sl
31
0
Polder
Tweede Tol
Beerwijkhoeve
-0.7
984
Pl 160

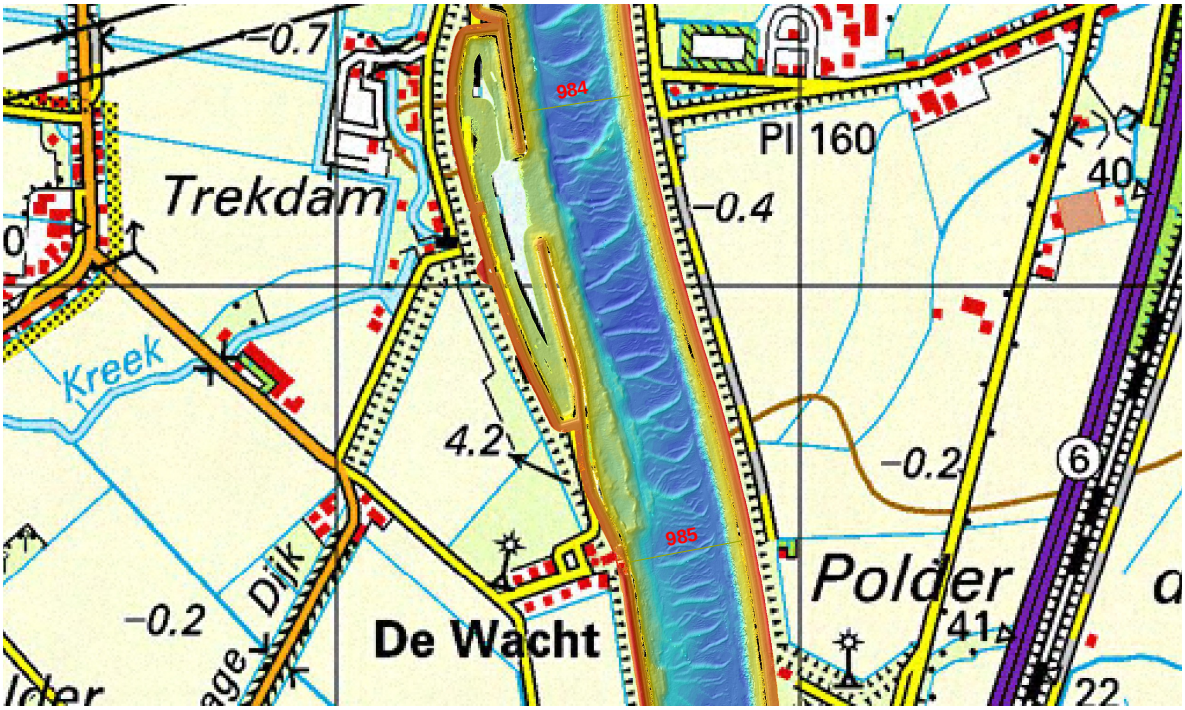
-0.7
984
Pl 160
40
Trekdam
-0.4
Kreek
4.2
-0.2
6
985
Polder
-0.2
Dijk
De Wacht
41
22

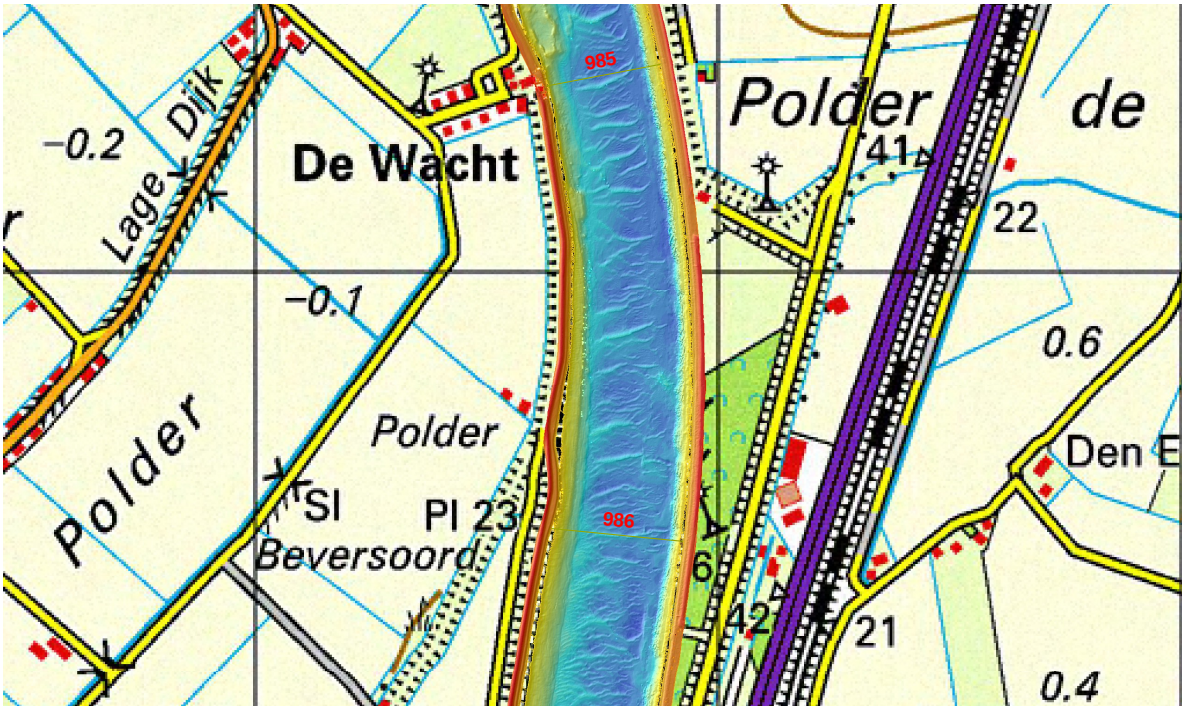
985
Polder
de
-0.2
Dijk
Lage
De Wacht
41
22
-0.1
0.6
Polder
Polder
Sl
Pl 23
Beversoord
986
6
42
21
0.4


Pl 23
Beversoord
986
6
42
21
0.4
5.0
0.3
Oude
Gorzen
polder
987
P
T
5.0
Pl 20
20
1.0

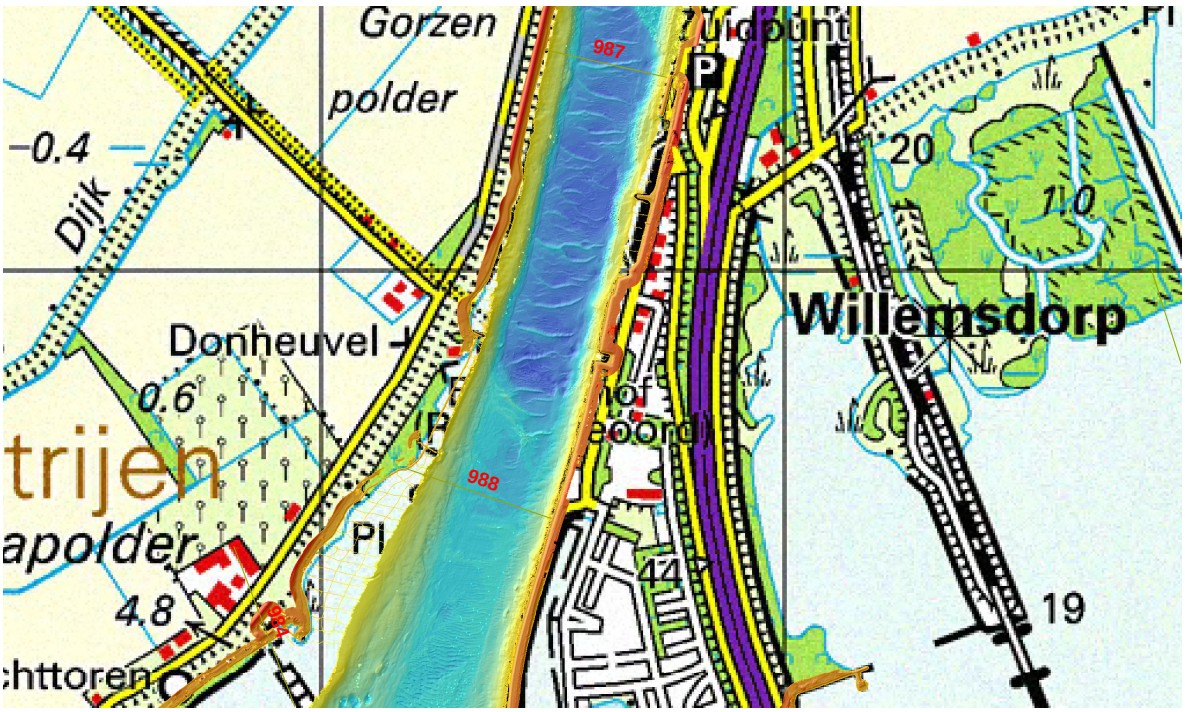
Gorzen
polder
987
P
20
1.0
0.4
Dijk
Donheuvel
0.6
Willemsdorp
988
Pl
4.8
19


988
984
44
2.0

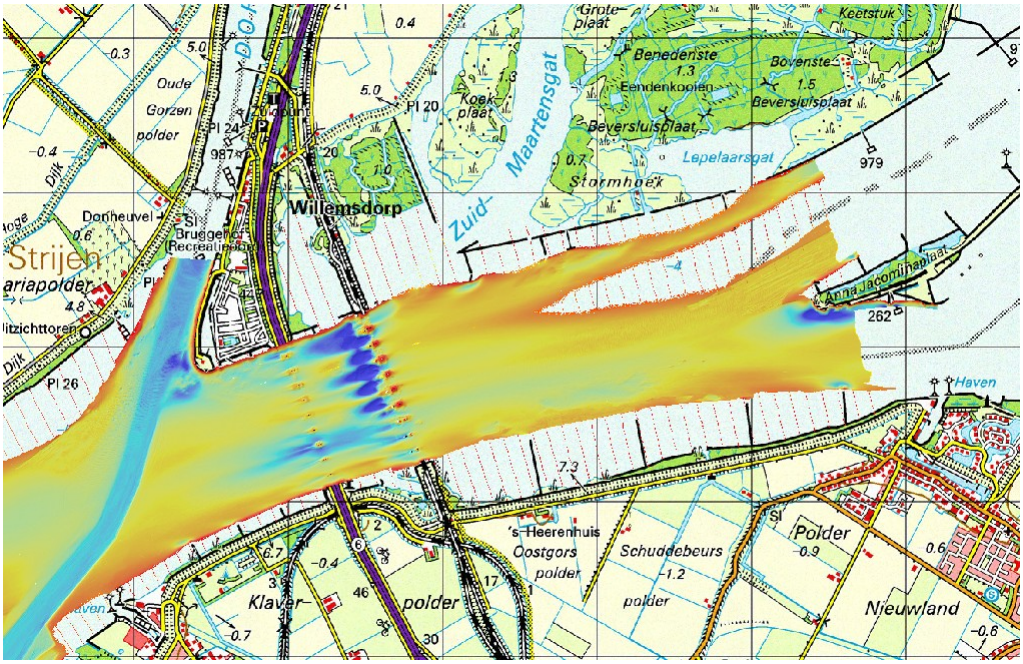
Grote plaat
Keetstuk
Benedenste
1.3
Bovenste
1.5
Eendenkooien
Beversluisplaat
Koek plaat
Pl 20
Maartensgat
Zuid-
Lepelaarsgat
Stormhoek
979
Willemsdorp
Oude Gorzen polder
Pl 24
Dorpheuvel
Strijen
Pl 26
Anna Jacominapolder
262
Haven
's Heerenhuis
Oostgors
polder
Schuddebeurs
polder
Polder
Klaver
polder
Nieuwland

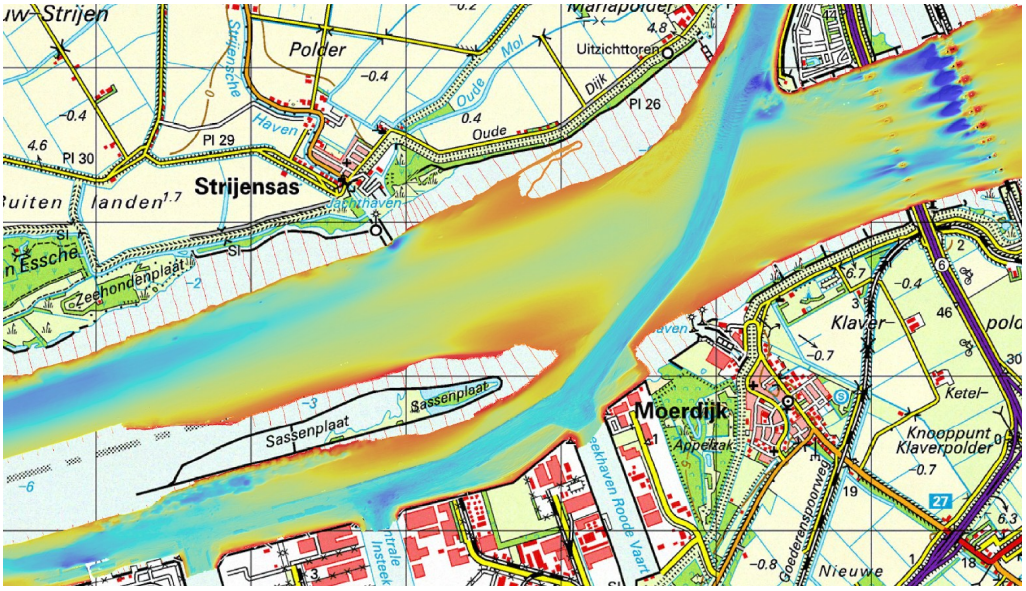
Strijen
Polder
Uitzichttoren
Pl 26
Pl 29
Pl 30
Strijensas
Zeehondenplaat
Sassenplaat
Moerdijk
Klaver-
Ketel-
Knooppunt
Klaverpolder
Nieuwe

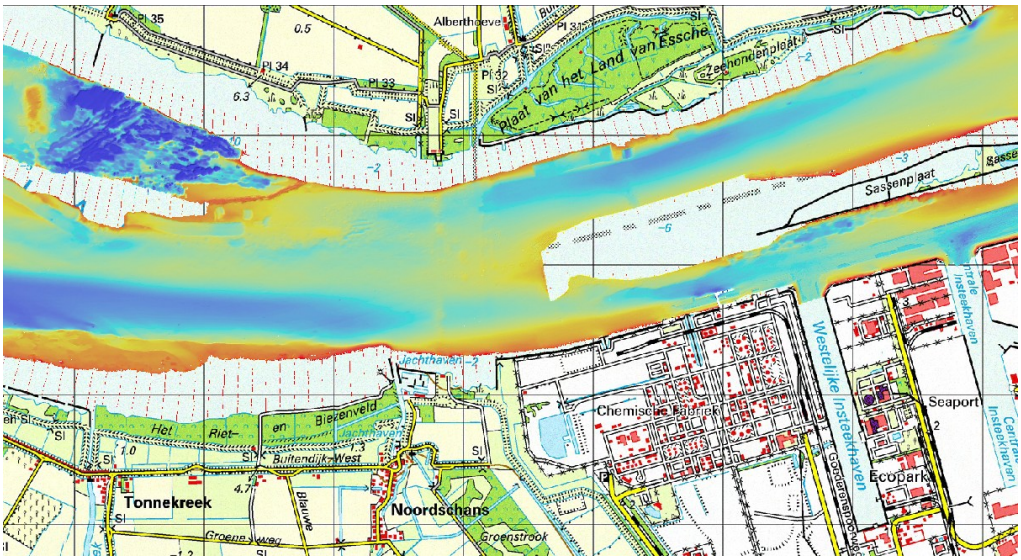
Albenthoeve
Pl 35
Pl 34
Pl 33
Pl 32
Plaat van het Land van Essche
Zeehondenplaat
Sassenplaat
Chemische Fabriek
Seaport
Ecopark
Westelijke Insteekhaven
Tonnekreek
Noordschans
Groenstrook

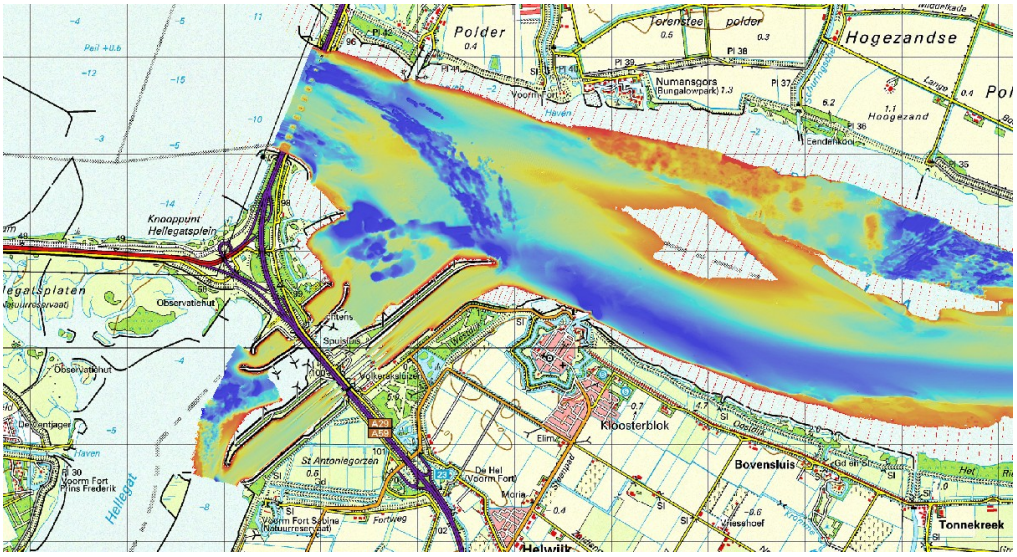

OTHER PICTURES: Oude Maas (by me!!!)

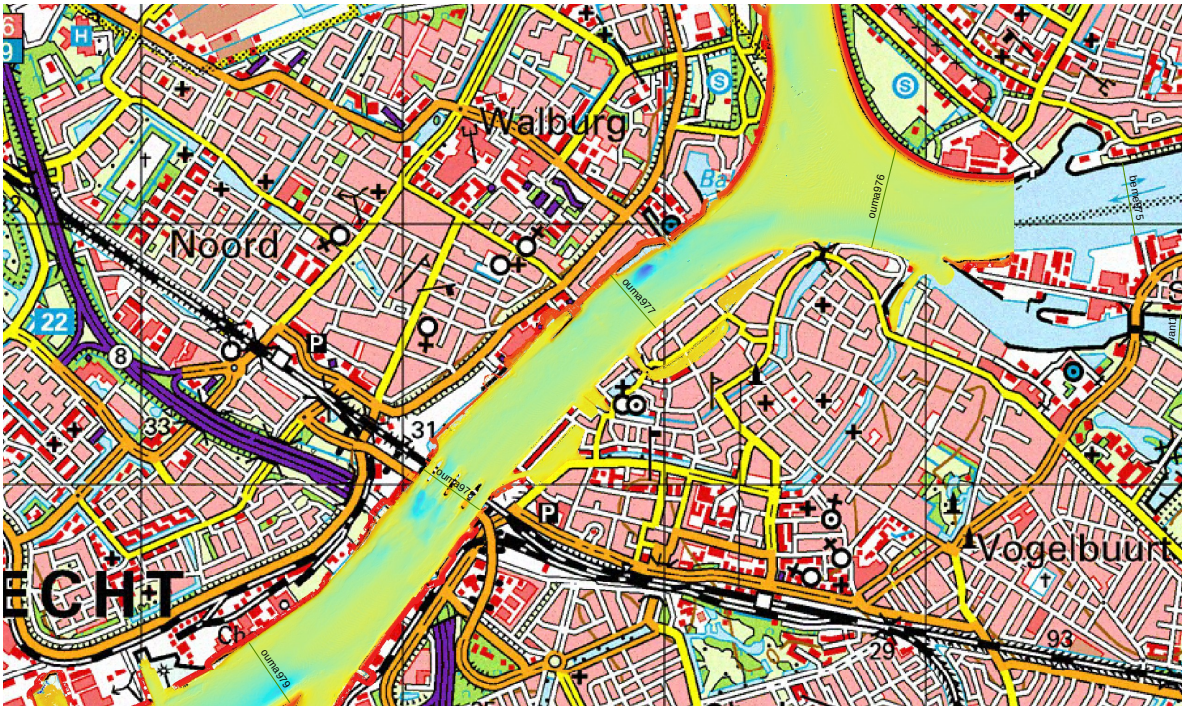

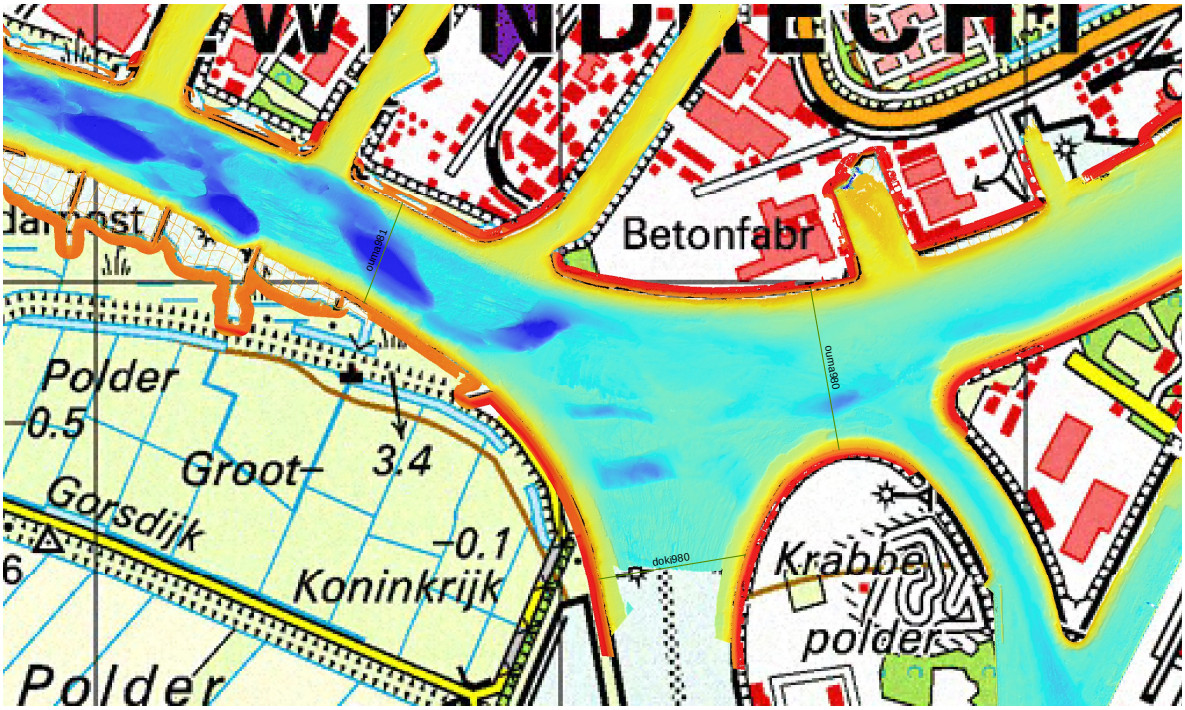
Betonfabr
ouma981
ouma980
Polder
-0.5
Groot-
3.4
Gorsdijk
-0.1
Koninkrijk
dok980
Krabbe
polder
Polder

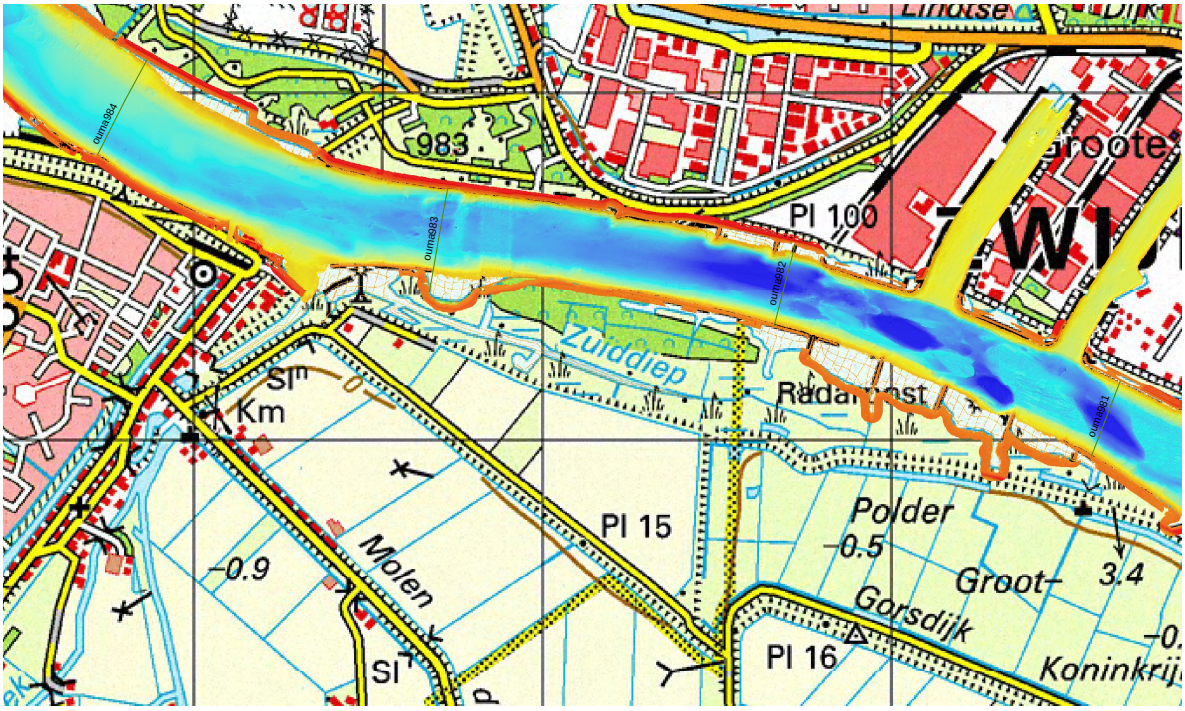
ouma984
983
ouma983
ouma982
Pl 100
Zuiddiep
Sl
Km
Pl 15
-0.9
Molen
Sl
Pl 16
Polder
-0.5
Groot-
3.4
Gorsdijk
Koninkrij

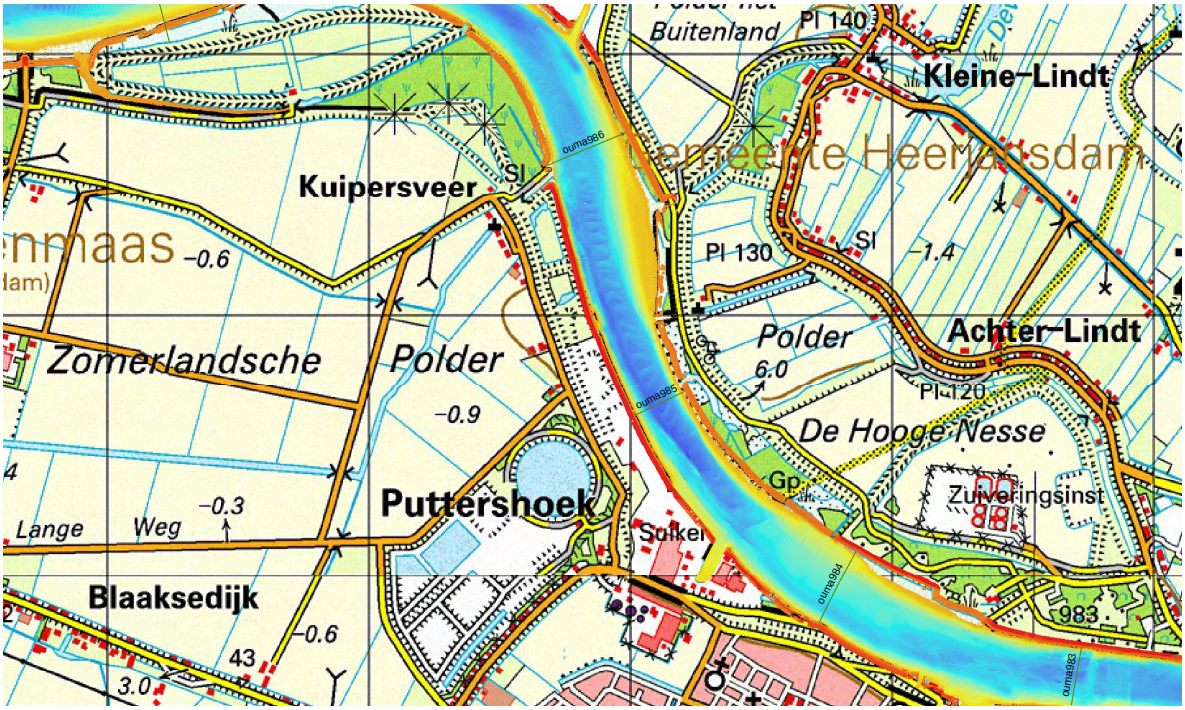
Buitenland
Pl 140
Kleine-Lindt
Kuipersveer
Sl
-0.6
Pl 130
-1.4
Polder
Achter-Lindt
6.0
Pl 120
Zomerlandsche
Polder
-0.9
De Hooge Nesse
Gp
Zuiveringsinst
Puttershoek
Sulkel
Lange
Weg
-0.3
Blaaksedijk
-0.6
43
3.0
983


Koedood
Molenpolder
Breeman
Buitenoord
Barendrecht
polder
Zuid
Portlandpolder
Golfterrein
Barendrechtse Veer
Pl 50
Heinenoord
West-Zomerlandsche
Polder
Kuipersveer
Gemeente Binnenmaas
(Gemeentehuis te Maasdam)
N217
Oud-
Reedijk
Heinenoord
Oost-
Zomerlandsche
Polder
Blaaksedijk
Westmaas
Nieuwland
N489
Lange
Weg
Puttershoek
Blaaksedijk
Moerkerken
Gemeente Binnenmaas
(Gemeentehuis te Maasdam)